UNIVERSITY OF CALIFORNIA

SANTA CRUZ

Single Molecule Studies of Telomere DNA

A dissertation submitted in partial satisfaction
of the requirements for the degree of

DOCTOR OF PHILOSOPHY

in

Chemistry

by

Xi Long

June 2014

The Dissertation of Xi Long is
approved:

_____

Professor Glenn L. Millhauser, Chair

_____

Professor Michael D. Stone, Advisor

_____

Professor Yat Li

_____

Tyrus Miller
Vice Provost and Dean of Graduate Studies

Table of Contents

List of Figures

List of Tables

Abstract

Single Molecule Studies of Telomere DNA

Xi Long

Since the discovery by Blackburn in 1978, the telomere has been the subject of intense research focus due to its close relationship with aging and cancer. Despite extensive research efforts for more than three decades, the structural properties of telomere remain elusive. In this dissertation, I used single molecule techniques to examine the physical properties of telomere. These studies have identified the kinetically trapped telomere G-quadruplex (GQ) structure, revealed the mechanical unfolding pathway of telomere GQ, and characterized the formation of the telomere displacement-loop (D-loop). Telomeres are specialize DNA sequence that prevent degradation and aberrant fusion of chromosome ends. Human telomere consists of 5-10 kb of duplex TTAGGG repeats follow by a 50 to 200 nucleotides of 3' single stranded overhang. The G-rich single stranded telomere has a propensity to fold into a structure known as GQ. In Chapter 2, single-molecule Förster resonance energy transfer (smFRET) was used for constructing the distribution of GQ conformations under physiological salt conditions. With circular dichroism, the kinetic trapped GQ conformation was discovered. In Chapter 3, smFRET and magnetic tweezers (MT) was used to dissect the folding property of telomere GQ. Under stretching force, the unfolding pathway of GQ was characterized by a short distance. In Chapter 4, the magnetic tweezers assay revealed that telomere is more resistant to torque-induced denaturation. The direct observation of telomere strand invasion suggested that the stretching force can influence the rate of the invasion and the formation of the telomere D-loop. The subsequent chapters detail the setup and experimental protocol for the MT-FRET, and describe how to use MT to manipulate DNA. These single molecule assays setup a foundation for investigating the interaction between the telomere and its associated proteins and serve as an experimental platform for telomere drug assessment. Ultimately, with these single molecule assays we will enhance our knowledge on how telomere regulates telomerase activity.

Acknowledgements

My deepest gratitude is to my adviser, Prof. Michael Stone, for his patience, encouragement and guidance in every step of my graduate study. It has been an honor to be his first Ph.D. student. He has helped me to discover my strengths and weaknesses as a scientist. His dedication and passion in science has inspired me to keep on learning.

I would like to extend my gratitude to my committee members, Prof. Glenn Millhauser and Prof. Yat Li for their valuable comments and helpful suggestions since the very beginning of my thesis work.

In addition, my sincere thanks to the members of Stone Research Group. The group provided me friendship, collaboration and good advice. They made my time at Santa Cruz fun and memorable.

Finally, I would like to thank Brian Gin, for his support, love and always being my biggest fan.

Chapter 1

General introduction

Telomeres, the repetitive DNA sequences found at the terminal ends of chromosomes, preserve the stability of eukaryotic chromosomes [1]. The foundation of human telomere structure is a stretch of double stranded telomere repeats of the sequence "TTAGGG" followed by a single stranded DNA tail at the 3'-end. This G-rich 3' terminal strand has the capacity to fold into a unique secondary structure called a G-quadruplex (GQ). Recent studies have revealed that GQ structures are found *in vivo* [2]. The existence of this structure creates an obstacle for recruiting the telomerase, an enzyme responsible for elongating telomeres, and DNA replication machinery [3,4]. To resolve these roadblocks, organisms rely on helicases, a class of enzymes that unwind GQs ([5-8].

The first solution structure of a human telomere GQ revealed a fundamental structural architecture in which guanine bases are hydrogen bonded in a planar quartet geometry [9]. Three consecutive intra-molecular G-quartets may interact via stacking interactions and are topologically linked by short intervening DNA loop sequences. In addition, telomere DNA GQ structures are stabilized by monovalent cations that may be site-specifically coordinated at the center of the planar G-quartet motif [9]. The specific identity of the monovalent cation used during telomere DNA GQ folding has a pronounced impact on the distribution of observed structures in a variety of model systems[10-16]. In the case of human telomere DNA, Na^+ ions promote the formation of the anti-parallel basket type GQ conformation, while K^+ ions induce folding of a mixture of GQ structures, including the parallel and anti-parallel conformations, as well as several hybrid topological forms [17,18]. Telomeres can also adopt a lariat-like structure in order to prevent DNA repair enzymes from recognizing its duplex and single stranded junction. This structure is known as a T-loop [19-21]. The formation of a T-loop is accomplished by a process called "strand invasion", which involves a single-stranded DNA tail wrap back, invading the nearby double stranded region of the telomere [22,23]. This process is enhance by a protein complex known as shelterin. Recent studies suggested that Telomeric Repeat-Binding Factor 2 (TRF2), a subunit of the shelterin complex, plays a key role in T-loop formation [21,24].

The major theme of the research within this thesis is understanding the properties of these telomere DNA structures. Most of the experiments were conducted at the single molecule level. One of the techniques used is single-molecule Förster resonance energy transfer (smFRET), which has been used for detecting conformational dynamics of biological molecules such as RNA, DNA, and proteins to within nanometer resolution.

In Chapter 2, I used smFRET to construct the distributions of telomere DNA GQ conformations generated by two different folding protocols: 1) An *in situ* refolding protocol commonly employed in single-molecule studies of GQ structure, 2) a slow cooling DNA annealing protocol typically used in the preparation of GQ samples for ensemble biophysical analyses. We discover that the choice of GQ folding protocol has a marked impact on the observed distributions of DNA conformations under otherwise identical buffer conditions. A detailed analysis of the kinetics of GQ folding over timescales ranging from minutes to hours revealed the distribution of GQ structures generated by *in situ* refolding gradually equilibrates to resemble the distribution generated by the slow cooling DNA annealing protocol. Interestingly, conditions of low ionic strength, which promote transient GQ unfolding, permit the fraction of folded DNA molecules to partition into a distribution that more closely approximates the thermodynamic folding equilibrium. These results are consistent with a model in which kinetic partitioning occurs during *in situ* folding at room temperature in the presence of K^+ ions, producing a long-lived non-equilibrium distribution of GQ structures in which the parallel conformation predominates on the timescale of minutes [25].

In Chapter 3, I analyzed the force-dependent equilibrium and rate constants for anti-parallel telomere GQ folding and unfolding, and have determined the location of the transition state barrier along the well-defined DNA-stretching reaction coordinate using a combined smFRET and magnetic tweezers instrument. The detailed description of this hybrid instrument is given in Chapter 5. The results reveal that the mechanical unfolding pathway of the anti-parallel telomere GQ is characterized by a short distance (<1 nm) to the transition state for the unfolding reaction. This mechanical unfolding response reflects a critical

contribution of long-range interactions to the global stability of the GQ fold, and suggests that telomere-associated proteins need only disrupt a few base pairs to destabilize this GQ structure. Comparison of the GQ unfolded state with a single-stranded polyT DNA revealed that the unfolded GQ exhibits a compacted non-native conformation reminiscent of a protein molten globule [26].

In Chapter 4, I described a magnetic tweezers assay to investigate the mechanism and stability of the T-loop. A detailed protocol on how to use magnetic tweezers to manipulate DNA is given in Chapter 6. We observe that duplex telomere DNA is more resistant to torque-induced denaturation than a non-telomere duplex control. The comparison of telomere DNA extension before and after denaturation revealed that the GQ can be stably folded in a duplex telomere. The direct observation of telomere strand invasion suggests that the stretching forces have influence on the rate of the invasion and the formation of the telomere displacement loop.

Based on these single molecule assays, we demonstrate that telomere DNA GQ folding kinetics, and not just thermodynamic stability, likely contributes to the physiological ensemble of GQ structures. The short distance between the folded GQ and its transition state suggests that long-range tertiary interactions are critical for GQ stability since only a small structural deformation is sufficient to destabilized the overall fold. This information is not only valuable for elucidating helicase action, but may also aid efforts to design small-molecules that target and stabilize GQ structures, towards disrupting telomere homeostasis. Duplex telomeres' high resisitance to torque denaturation suggests a high energy barrier to T-loop formation. Understanding the dynamics and structural changes of the duplex telomere during strand invasion provides insights into the mechanisms employed by the proteins associated with this process *in vivo*.

References

1. Palm W, de Lange T (2008) How shelterin protects mammalian telomeres. Annu Rev Genet 42: 301-334.
2. Biffi G, Tannahill D, McCafferty J, Balasubramanian S (2013) Quantitative visualization of DNA G-quadruplex structures in human cells. Nat Chem 5: 182-186.
3. Zaug AJ, Podell ER, Cech TR (2005) Human POT1 disrupts telomeric G-quadruplexes allowing telomerase extension in vitro. Proc Natl Acad Sci USA 102: 10864-10869.
4. Johnson JE, Cao K, Ryvkin P, Wang LS, Johnson FB (2010) Altered gene expression in the Werner and Bloom syndromes is associated with sequences having G-quadruplex forming potential. Nucleic Acids Res 38: 1114-1122.
5. Wu Y, Shin-ya K, Brosh RM, Jr. (2008) FANCJ helicase defective in Fanconia anemia and breast cancer unwinds G-quadruplex DNA to defend genomic stability. Mol Cell Biol 28: 4116-4128.
6. Huber MD, Lee DC, Maizels N (2002) G4 DNA unwinding by BLM and Sgs1p: substrate specificity and substrate-specific inhibition. Nucleic Acids Res 30: 3954-3961.
7. Vannier JB, Pavicic-Kaltenbrunner V, Petalcorin MI, Ding H, Boulton SJ (2012) RTEL1 dismantles T loops and counteracts telomeric G4-DNA to maintain telomere integrity. Cell 149: 795-806.
8. Paeschke K, Capra JA, Zakian VA (2011) DNA replication through G-quadruplex motifs is promoted by the Saccharomyces cerevisiae Pif1 DNA helicase. Cell 145: 678-691.
9. Wang Y, Patel DJ (1993) Solution structure of the human telomeric repeat d[AG3(T2AG3)3] G-tetraplex. Structure 1: 263-282.
10. Giraldo R, Rhodes D (1994) The yeast telomere-binding protein RAP1 binds to and promotes the formation of DNA quadruplexes in telomeric DNA. The EMBO journal 13: 2411-2420.

11. Patel PK, Hosur RV (1999) NMR observation of T-tetrads in a parallel stranded DNA quadruplex formed by Saccharomyces cerevisiae telomere repeats. Nucleic acids research 27: 2457-2464.

12. Oganesian L, Moon IK, Bryan TM, Jarstfer MB (2006) Extension of G-quadruplex DNA by ciliate telomerase. The EMBO journal 25: 1148-1159.

13. Haider S, Parkinson GN, Neidle S (2002) Crystal structure of the potassium form of an Oxytricha nova G-quadruplex. Journal of molecular biology 320: 189-200.

14. Schultze P, Macaya RF, Feigon J (1994) Three-dimensional solution structure of the thrombin-binding DNA aptamer d(GGTTGGTGTGGTTGG). Journal of molecular biology 235: 1532-1547.

15. Lustig AJ (1992) Hoogsteen G-G base pairing is dispensable for telomere healing in yeast. Nucleic acids research 20: 3021-3028.

16. Kang C, Zhang X, Ratliff R, Moyzis R, Rich A (1992) Crystal structure of four-stranded Oxytricha telomeric DNA. Nature 356: 126-131.

17. Dai J, Carver M, Yang D (2008) Polymorphism of human telomeric quadruplex structures. Biochimie 90: 1172-1183.

18. Sannohe Y, Sugiyama H (2010) Overview of formation of G-quadruplex structures. Current protocols in nucleic acid chemistry / edited by Serge L Beaucage [et al] Chapter 17: Unit 17 12 11-17.

19. Griffith JD, Comeau L, Rosenfield S, Stansel RM, Bianchi A, et al. (1999) Mammalian telomeres end in a large duplex loop. Cell 97: 503-514.

20. Nikitina T, Woodcock CL (2004) Closed chromatin loops at the ends of chromosomes. J Cell Biol 166: 161-165.

21. Doksani Y, Wu JY, de Lange T, Zhuang X (2013) Super-resolution fluorescence imaging of telomeres reveals TRF2-dependent T-loop formation. Cell 155: 345-356.

22. Stansel RM, de Lange T, Griffith JD (2001) T-loop assembly in vitro involves binding of TRF2 near the 3' telomeric overhang. EMBO J 20: 5532-5540.

23. Verdun RE, Karlseder J (2006) The DNA damage machinery and homologous recombination pathway act consecutively to protect human telomeres. Cell 127: 709-720.

24. Amiard S, Doudeau M, Pinte S, Poulet A, Lenain C, et al. (2007) A topological mechanism for TRF2-enhanced strand invasion. Nat Struct Mol Biol 14: 147-154.

25. Long X, Stone MD (2013) Kinetic partitioning modulates human telomere DNA G-quadruplex structural polymorphism. PLoS One 8: e83420.

26. Long X, Parks JW, Bagshaw CR, Stone MD (2013) Mechanical unfolding of human telomere G-quadruplex DNA probed by integrated fluorescence and magnetic tweezers spectroscopy. Nucleic Acids Res 41: 2746-2755.

Chapter 2

Kinetic partitioning modulates human telomere DNA G-quadruplex structural polymorphism

*Sections of this chapter are adapted from published material (Long and Stone, PLoS ONE 2013)

Introduction

The first solution structure of a human telomere G-quadruplex (GQ) revealed a fundamental structural architecture in which guanine bases are hydrogen bonded in a planar quartet geometry (Figure 2-1A) [1].Three consecutive intra-molecular G-quartets may interact via stacking interactions and are topologically linked by short intervening DNA loop sequences (Figure 2-1B). In addition, telomere DNA GQ structures are stabilized by monovalent cations that may be site-specifically coordinated at the center of the planar G-quartet motif [1]. The specific identity of the monovalent cation used during telomere DNA GQ folding has a pronounced impact on the distribution of observed structures in a variety of model systems [2-8]. In the case of human telomere DNA, Na^+ ions promote the formation of the anti-parallel basket type GQ conformation, while K^+ ions induce folding of a mixture of GQ structures, including the parallel and anti-parallel conformations, as well as several hybrid topological forms [9,10] (Figure 2-1C). Since K^+ is the predominant monovalent cation *in vivo,* much interest has focused on understanding telomere DNA GQ structural polymorphism induced by K^+ ions.

Human telomere DNA GQ structure has been studied by numerous techniques including NMR [1,11-14], X-ray crystallography [15], circular dichroism [16-19], UV melting [13,20,21], force spectroscopy [22-24], and Förster Resonance Energy Transfer (FRET) [25-28]. These studies revealed telomere DNA GQs are highly polymorphic, assuming a variety of topologically distinct structural forms, which may interconvert under certain experimental conditions. The dynamic properties of telomere DNA GQs motivated the use of single molecule FRET (smFRET) to provide a detailed description of GQ structural heterogeneity and folding [27-30]. However, many single molecule analyses of telomere DNA GQ structure employed sample preparation protocols that differ in potentially substantial ways from protocols utilized in prior ensemble biophysical studies. Therefore, in the present study we have used smFRET to systematically investigate the impact of different DNA folding protocols on the observed distribution of telomere DNA conformations. Our results demonstrate that

the distribution of telomere DNA conformations measured by smFRET is dramatically altered by changes in the DNA folding protocol under otherwise identical buffer conditions. By analyzing the kinetics of GQ DNA folding at room temperature over long timescales (from minutes to hours), as well as in varying ionic strengths, we provide evidence that kinetic partitioning produces a long-lived non-equilibrium distribution of GQ structures. These results not only highlight the importance of the specific folding protocol being used during biophysical analyses of GQ structure, but also suggest that kinetics of folding may dictate the distribution of telomere DNA GQs present *in vivo*.

Materials and Methods

Dye Labeleing of DNA oligonucleotides

All DNA fragments were purchased from Integrated DNA Technologies, Inc. (Table 2-1). The 3'amino modified, Tel22, Tel23, and Hybrid mutant oligonucleotides were labeled with mono-reactive Cy5 (GE Healthcare) and the internally amino modified biotinylated DNA handle was labeled with mono-reactive Cy3 (GE Healthcare). Dye labeled fragments were, EtOH precipitated and purified by reverse-phase chromatography on a C8 column (Agilent, Eclipse XDB-C8) on an AKTA purifier. Following HPLC purification samples were EtOH precipitated, and resuspended in ddH_2O. DNA concentrations were determined using a Nanodrop.

DNA annealing reactions

Cy5 labeled Tel22, Tel23 and Hybrid Mutant were annealed to Cy3 labeled biotinylated DNA handle by heating to 95 °C for 4 minutes followed by slow cooling to room temperature (over several hours) in the presence of a buffer (10 mM Tris-HCl pH 8) containing either 100 mM KCl or 100 mM NaCl.

Single molecule FRET measurements

Quartz slides (Finkenbeiner Inc.) were cleaned by sonicating for 20 minutes in 10% w/v Alconox, 20 minutes in ddH_2O, 20 minutes in acetone, 20 minutes 1M KOH, then 20 minutes in fresh 1M KOH. Slides are then rinsed with ddH2O and dried under nitrogen,

followed by flame cleaning with a propane torch for ~2 minutes. Sample chambers were prepared by sandwiching pieces of parafilm between the quartz slide and a plasma cleaned coverglass (Harrik Plasma Cleaner), cover glasses from TED Pella, Inc. (Prod.# 260146). Chambers were heated on a hot block (95^{o}C) for 1 minute to seal the parafilm to the glass. Channels (~10 uL total volume) were treated with 35 uL of 1 mg/mL of biotinylated BSA (Sigma Cat.#A8549) for 5 minutes, washed with 100 uL of T50 buffer (10 mM Tris-HCl pH 8, 50 mM NaCl), then incubated with 50uL of 0.2 mg/mL streptavidin (Invitrogen Cat.#S888), then washed with 100 uL of T50. Channels were then equilibrated with buffer matching the desired experimental condition (see main text). Next, 100 uL of 5-10 pM annealed biotinylated - DNA were deposited onto the streptavidin coated quartz slide in the desired buffer condition. After 5 minutes incubation, 100 uL of a buffer containing either 100 mM KCl or 100 mM NaCl was flushed to the slide to remove the unbound DNA. Data was collected in imaging buffer containing 10mM Tris pH 8, 100 mM KCl or NaCl, 0.4% (w/v) D-glucose, 0.1 mg/ml glucose oxidase (Sigma Cat.# G2133-250KU), 0.02 mg/ml catalase (CalBiochem Cat.#219001) and saturated with Trolox (Aldrich Cat.#23,881-3). Data was acquired using a green laser (532 nm, Laserglow, Inc.) and prism-type total internal reflection microscopy on an inverted Olympus IX71 microscope equipped with an Andor IXON (897) CCD camera with 100 ms integration time. For *in situ* refolding experiments, surface immobilized molecules incubated for 5 minutes in buffer containing no KCl or NaCl (10 mM Tris pH 8), followed by an incubation in the presence of 100 mM KCl for the indicated time. For experiments analyzing the *in situ* refolding distributions under varying KCl concentrations, folding incubation times were fixed at 10 minutes, and smFRET measurements were performed at the indicated salt concentrations in the presence of 50 mM Tris pH 8. smFRET histograms were recorded as described below.

smFRET analysis

Raw movie files were analyzed using in-house written software available upon request (IDL and Matlab). FRET is defined as the efficiency of energy transfer between

acceptor and donor dye, $I_A/(I_A+I_D)$. I_A is the acceptor intensity and I_D is the donor intensity. FRET histograms were compiled from the average FRET value obtained from each molecule over a 2 second observation time. The total data collection time for each smFRET histogram is approximately one minute. In each experiment a FRET = 0 population is observed, derived from molecules harboring only an active FRET donor dye. The origin of the FRET = 0 peak was confirmed by direct excitation of the acceptor molecules with a red laser (657 nm, Vortran Inc.). For clarity, these zero FRET peaks have been removed from the figures shown in the paper. To fit the smFRET distributions, data were binned (bin size was FRET = 0.03) and fit with multiple Gaussian functions using Origin. Based upon previous characterization of our system, the distribution widths were fixed at a value of 0.08 to avoid fitting artifacts. Fitting was evaluated using the adjusted R^2 value to determine the best fit model.

CD measurements

The DNA fragments (Tel 23 no duplex, and Hybrid mutant no duplex) used in the experiment were ordered from Integrated DNA Technologies,Inc. The CD spectra were measured by using an AVIV Model 62DS Circular Dichroism Spectrometer. The DNA sample was diluted in a buffer (10 mM Tris pH8) containing either 100 mM KCl or 100 mM NaCl, heated to 95 °C for 4 minutes followed by slow cooling to room temperature. 300 uL of 300 uM DNA solution was contained in a quartz cell of 1 mm optical path length and instrument scanning speed of 1mm per minute with 8 seconds response time. The spectra were averages of three repetitive scans between 200 and 340 nm at room temperature with buffer scan baseline subtraction and smoothed with a Savitsky-Golay filter [31].

Results

Distinct DNA folding protocols alter the observed distribution of GQ structures

To analyze telomere DNA GQ folding, we designed a smFRET construct comprised of the model telomere DNA sequence $TAGGG(T_2AG_3)_3$. This 23 nucleotide telomere DNA substrate (Tel23) was shown previously to adopt a variety of GQ topologies, including the parallel, anti-parallel, and several hybrid conformations [11,12] (Figure 2-1C). To mimic the

natural double-stranded/single-stranded telomere DNA junction, we designed the construct to have a single-stranded DNA G-rich tail that runs in the 5'→3' direction with respect to the phosphodiester backbone. We introduced a donor FRET dye (Cy3) on a biotinylated DNA handle, which is complementary to a 5' non-telomeric extension of the G-rich telomere DNA strand. In addition, we modified the 3' terminus of the G-rich strand with an acceptor FRET dye (Cy5) (Figure 2-1B). Single-molecule FRET labeled Tel23 molecules were surface immobilized via a biotin-streptavidin linkage and imaged using prism-type total internal reflection microscopy [32]. In our smFRET assay the conformational properties of telomere DNA are monitored as the efficiency of energy transfer between the donor and acceptor dye, and we define FRET = $I_A/(I_A+ I_D)$, where I_A and I_D are the background corrected intensities of the acceptor and donor dyes, respectively.

Our initial characterization of the Tel23 smFRET construct employed a DNA folding protocol used in previously reported NMR and CD spectroscopic analyses [12]. In this approach (hereafter referred to as *thermal annealing*), Tel23 molecules were heated to 95^{o}C for 4 minutes in the presence of 100 mM KCl and equimolar amounts of biotinylated DNA handle, then allowed to slowly equilibrate to room temperature over a period of several hours. These conditions are sufficient to melt out any pre-existing GQ structures [33] and promote the base paring of the biotin-labeled DNA handle. Following thermal annealing, Tel23 molecules were surface immobilized and imaged in buffer containing 100 mM KCl. The smFRET distributions constructed from Tel23 molecules thermally annealed and imaged in the presence of 100 mM KCl possessed a broad mid-FRET population centered at FRET = 0.44 and a second higher FRET population centered at FRET = 0.72 (Figure S1-1A). Moreover, thermal annealing of Tel23 molecules in the presence of 20 mM KCl yielded a similar FRET distribution (Figure S1-1), demonstrating the final equilibrium of folded GQ structures is independent of salt concentration.

Having characterized the structural distributions generated by thermal annealing of Tel23 molecules in KCl, we next studied Tel23 *in situ* refolding in KCl. Surface immobilized

Tel23 molecules initially folded by thermal annealing in 100 mM KCl were incubated in the absence of salt to promote DNA unfolding, producing a single unfolded FRET population centered at FRET = 0.23 (Figure S1-2) as previously described [29]. We then attempted to refold the telomere DNA molecules *in situ* by introducing buffer containing 100 mM KCl at room temperature and incubating for 10 minutes. Interestingly, the smFRET histogram generated by *in situ* KCl folding was markedly altered from the KCl thermal annealing experiments, exhibiting a predominant high FRET population centered at FRET = 0.72 and second population centered at FRET = 0.50 (compare Figure 2-2A with 2-2B). Taken together, these results demonstrate the distribution of structures generated by KCl thermal annealing of Tel23 is significantly altered during *in situ* KCl refolding at room temperature on the time scale of minutes.

***In situ* refolding induces kinetic trapping of GQ conformations**

One model to explain the differences observed for Tel23 molecules folded by either KCl *in situ* refolding or thermal annealing is that during *in situ* refolding the DNA becomes kinetically trapped in a higher energy GQ conformation, and if given sufficient time to equilibrate, the system would ultimately reach thermodynamic equilibrium. To test this notion, we performed a time course on KCl *in situ* refolded molecules from minutes to hours (Figure 2-3). Indeed, we found that over the course of several hours, the smFRET distributions of Tel23 molecules *in sit*u refolded in 100 mM KCl gradually converted to a distribution that more closely resembled the KCl thermal annealing result, characterized by a depletion of the high FRET peak and a corresponding increase in abundance of the mid FRET state (compare Figure 2-3 and Figure 2-3, bottom panel). Moreover, time course experiments performed at two lower KCl concentrations (20 mM and 60 mM), revealed the convergence of the smFRET distributions to the same states, albeit with slightly different kinetics (Figure S1-3). These results suggest that the KCl *in situ* refolding protocol kinetically traps the high FRET conformation which can, if given sufficient time, partition into the more energetically stable mid-FRET conformation.

Ionic strength alters the GQ folding landscape

We next analyzed the impact of KCl concentration on the observed smFRET distributions after 10 minutes of *in situ* refolding. As described above, previous reports demonstrated that conditions of low ionic strength promote GQ unfolding resulting in a low FRET population (Figure S1-2) [29]. Interestingly, we find that at low KCl concentration, where GQ unfolding is favored, the distribution of folded states more closely resembles the distribution obtained by thermal annealing at 100 mM KCl (Figure 2-4, top panel). In contrast, elevated KCl concentrations produce distributions of GQ structures with a larger fraction in the kinetically trapped (high-FRET) conformation (Figure 2-4, bottom panels). These experiments are consistent with previous studies of telomere DNA structural dynamics at low KCl concentrations, in which the unfolded conformation (low FRET state) was shown to be an obligatory intermediate during interconversion of distinct GQ topological isomers [27]. Therefore, the ability of the DNA to sample an unfolded conformation at low ionic strength increases the rate at which the folded fraction can attain the thermodynamically favored structural equilibrium.

The parallel GQ conformation is the kinetically trapped structure

We note that smFRET measurements alone do not provide sufficient resolution to unambiguously resolve all of the distinct GQ conformations anticipated to coexist for Tel23 folded in KCl. However, circular dichroism (CD) measurements on the telomere DNA constructs used in our smFRET measurements folded in the presence of either KCl or NaCl permit us to make preliminary correlations between particular GQ conformations and the FRET states observed in our experiments. A CD spectrum taken on Tel23 molecules prepared by KCl thermal annealing exhibited a positive peak at ~290 nm, a shoulder at ~265 nm, and a small negative peak at ~240 nm (Figure 2-5A, open circles). These CD signatures indicate a mixture of telomere DNA GQ topologies including anti-parallel, hybrid and parallel conformations, consistent with NMR studies of Tel23 molecules [34,35]. Our smFRET measurements of Tel23 prepared by KCl thermal annealing revealed the presence of at least

two distinct FRET states. Interestingly, treating the broad mid-FRET peak as two distinct populations, FRET = 0.42 and FRET = 0.50, yielded a substantially better fit as judged by adjusted R^2 values (Figure S1-4), suggesting the mid-FRET peak may represent a superimposition of two distinct FRET states. In contrast, smFRET analysis of a shorter telomere DNA substrate lacking the 5' terminal thymine, Tel22 ($AG_3(T_2AG_3)_3$), prepared by KCl thermal annealing yielded one predominant mid-FRET state (Figure S1-4). This observation is consistent with a previously reported NMR structure, which demonstrated a requirement for a Watson-Crick base pair between the 5' terminal thymine and an internal DNA loop to stabilize an alternative hybrid GQ conformation [12].

We next analyzed the conformational properties of Tel23 in the presence of 100 mM NaCl, a condition that promotes homogeneous folding of telomere DNA into the anti-parallel GQ conformation [1]. As anticipated, the CD spectrum of Tel23 thermally annealed in the presence of 100 mM NaCl yielded a strong positive peak at ~295 nm and a negative peak at ~265 nm, indicative of the anti-parallel conformation (Figure 2-5A, asterisks) [36]. When analyzed by smFRET, Tel23 molecules thermally annealed and imaged in 100 mM NaCl produced a distribution exhibiting a single predominant population centered on FRET=0.50 (Figure 2-5B). Based upon these results we conclude the single major population centered at FRET = 0.50 in our smFRET experiments corresponds to the anti-parallel GQ conformation.

To further dissect the heterogeneity of the smFRET distributions observed for Tel23 prepared by KCl thermal annealing, we next utilized a mutant telomere DNA construct that promotes the hybrid GQ conformation [12]. The CD spectrum for the hybrid mutant prepared by KCl thermal annealing was similar to Tel23 treated in the same manner, but possessed a more prominent positive peak at ~ 290 nm, a pronounced shoulder at ~ 265 nm, and a strong negative peak at ~240 nm (Figure 2-5A, closed circles). When analyzed by smFRET, the hybrid mutant folded under KCl thermal annealing conditions yielded a smFRET distribution possessing a predominant population in the mid-FRET range (Figure 2-5C). Thus, although Tel23 molecules folded by NaCl thermal annealing and the hybrid mutant prepared by KCl

thermal annealing yield FRET distributions with overlapping mid-FRET populations (compare Figure 2-5B and 2-5C), their respective CD spectra clearly indicate a difference in the predominant GQ conformation (Figure 2-5A). Thus, we suggest the hybrid and anti-parallel GQ conformations are both characterized by a mid-FRET state, while the high FRET kinetically trapped state we observe in our experiments represents the parallel conformation. In further support of these assignments, a qualitative analysis of the atomic resolution structures for each of these telomere GQ conformations indicates that the DNA termini are in much closer proximity in the parallel conformation when compared with both the anti-parallel and hybrid structures (Figure S1-5).

Discussion

In summary, we have used smFRET to directly demonstrate the distribution of telomere DNA GQ structures generated during KCl *in situ* refolding on the timescale of minutes is demonstrably altered from the identical molecules prepared by KCl thermal annealing. Since thermally annealed and *in situ* refolded Tel23 molecules were imaged under identical buffer conditions (100 mM KCl), we conclude that *in situ* refolding gives rise to kinetic partitioning of GQ conformations. A combination of smFRET and CD measurements on several model telomere DNA constructs in the presence of KCl or NaCl provided insight into which GQ conformations correspond to the observed FRET states. Since we cannot conclusively differentiate between the two overlapping mid-FRET conformations, which we suggest represent a mixture of the hybrid and anti-parallel GQ folds, we interpret our results in terms of a simple three state model: low-FRET (unfolded), mid-FRET (anti-parallel and/or hybrid GQ), and high-FRET (parallel GQ) (Figure 2-6). Kinetic partitioning of GQ folds can be understood by assuming there is a large energy barrier between each of the folded and unfolded GQ states. Thus, high temperature or low ionic strength conditions serve to reduce the height of the barriers separating these states, and in turn facilitate a more rapid attainment of the thermodynamically favored GQ conformations. Additional experiments will be required to investigate the contribution of kinetic partitioning during telomere DNA GQ

folding *in vivo,* as well as the potential impact of GQ resolving enzymes on the observed distributions of GQ conformations

Table 2-1

DNA oligonucleotides used in this study

Tel22	5'GCGTGGCACCGGTAATAGGAAAATGGAGAAGGGTTAGGGTTAGGGTTAGGG (Amino C3) -3'
Tel23	5'GCGTGGCACCGGTAATAGGAAAATGGAGATAGGGTTAGGGTTAGGGTTAGGG (Amino C3) -3'
Hybrid mutant	5'GCGTGGCACCGGTAATAGGAAAATGGAGATTGGGTTAGGGTTAGGGTTAGGGA (Amino C3)-3'
DNA handle	5' TCTCCAT(Amino C6 T)TTCCTATTACCGGTGCCACGC-Biotin 3'
Tel23 no duplex	5' TAGGGTTAGGGTTAGGGTTAGGG 3'
Hybrid mutant no duplex	5' TTGGGTTAGGGTTAGGGTTAGGGA 3'

Figure 2-1

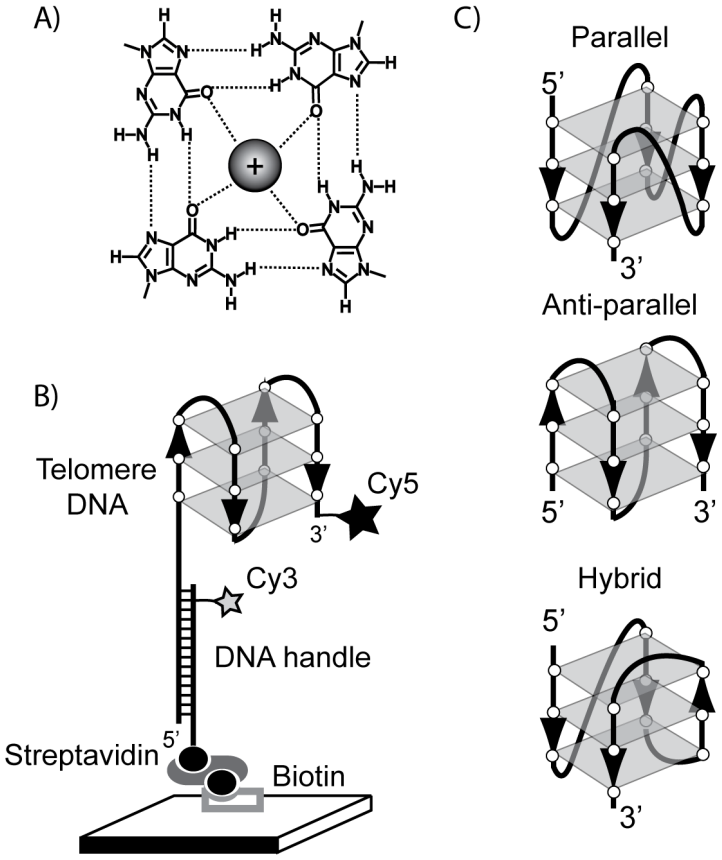

(A) Planar telomere DNA G-quartet structure with coordinated monovalent cation. (B) Experimental setup for telomere DNA GQ single molecule FRET measurements. Grey rectangles represent planar G-quartets and backbone polarity (5'→3') is indicated by black arrowheads. Molecules are immobilized on a microscope slide and FRET is measured as the energy transfer between the donor (Cy3) and acceptor (Cy5) dye. (C) Human telomere G-quadruplex structures formed by Tel23 sequence.

Figure 2-2

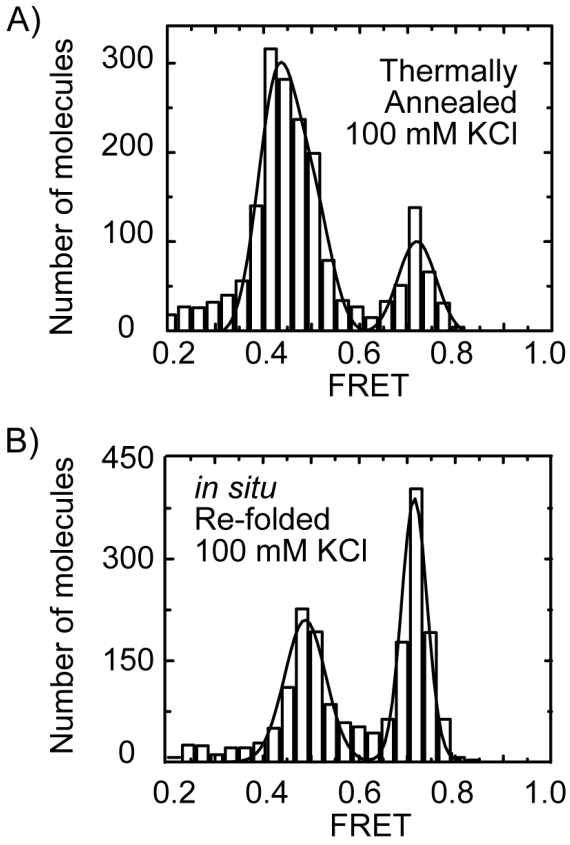

Single-molecule FRET histograms for telomere DNA GQ constructs. Gaussian fits to the data are shown in red. (A)Tel23 thermally annealed in 100 mM KCl. (B) Bar plot of the percentage of each of the observed FRET states for Tel23 thermally annealed in 100mM KCl. Error bars represent the standard deviation of the experiment performed in triplicate. (C) Tel23 *in situ* refolded in 100 mM KCl. (D) Bar plot of the percentage of each of the observed FRET states for Tel23 *in situ* refolded in 100 mM KCl. Error bars represent the standard deviation of the experiment performed in triplicate.

Figure 2-3

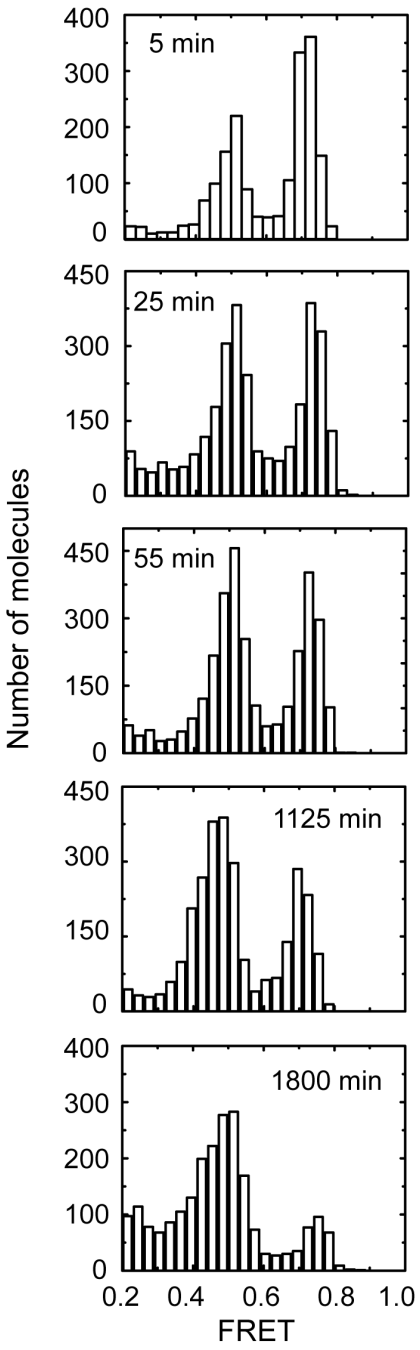

Single-molecule FRET histograms of Tel23 *in situ* refolded in 100 mM KCl for the indicated period of time.

Figure 2-4

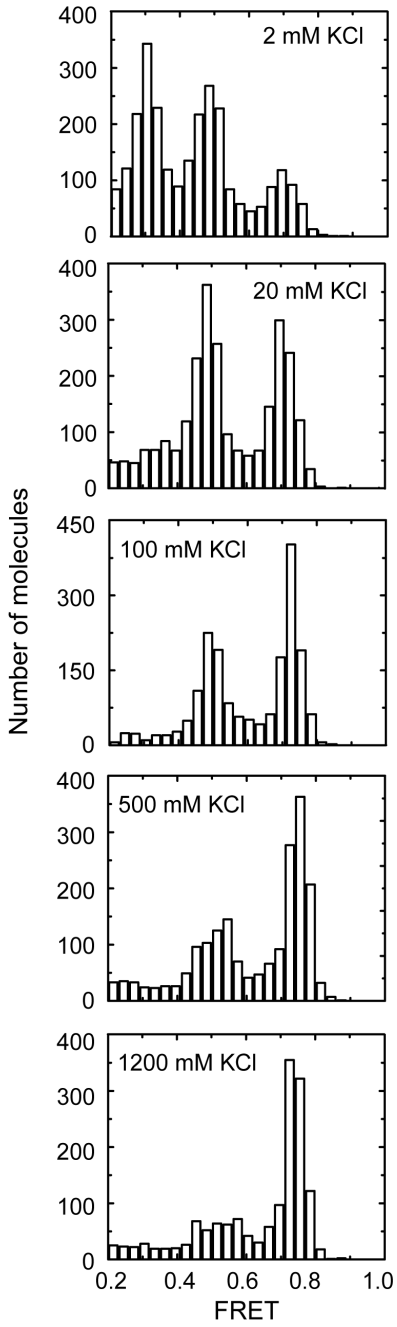

Single-molecule FRET histograms of Tel23 *in situ* refolded at the indicated KCl concentrations.

Figure 2-5

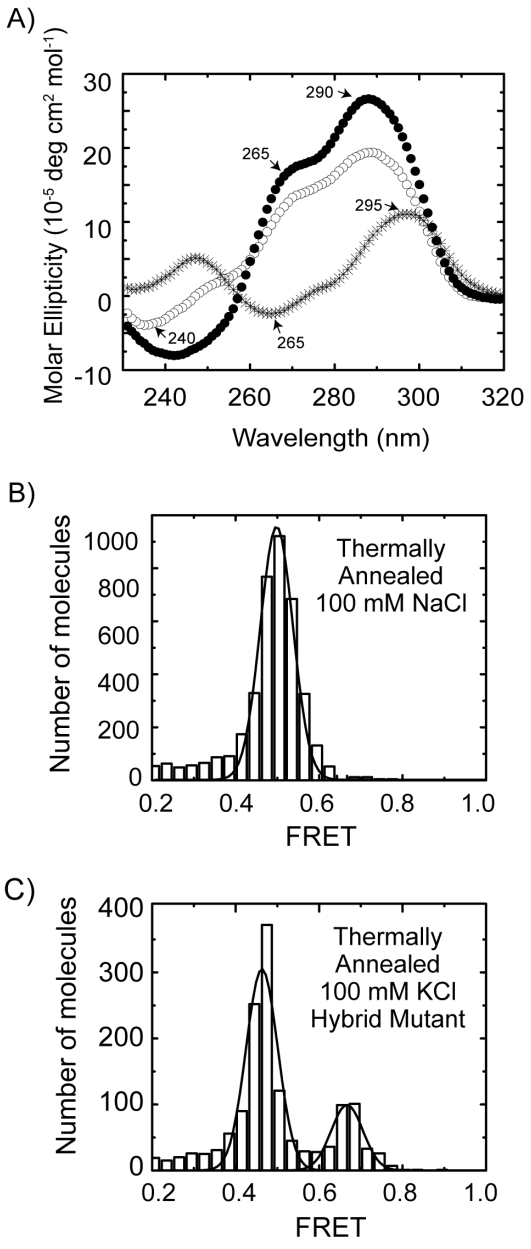

(A) CD spectra of Tel23 thermally annealed in 100 mM KCl (open circles), Tel23 in 100 mM NaCl (asterisks), and Hybrid Mutant in 100 mM KCl (closed circles). (B) Tel23 thermally annealed in 100 mM NaCl with Gaussian fits to the data (C) Hybrid Mutant thermally annealed in 100 mM KCl with Gaussian fits to the data.

Figure 2-6

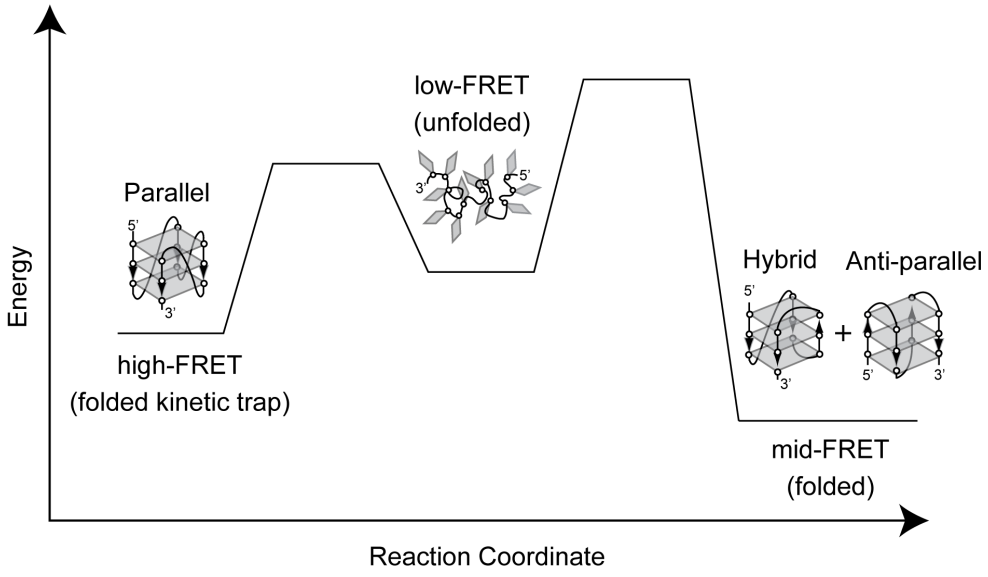

A qualitative energy landscape model for kinetic partitioning during telomere DNA GQ folding. A lower energy barrier between the low-FRET (unfolded) and the high-FRET (folded) state creates a kinetic trap during the early stages of folding. To escape the kinetic trap, the molecule must unfold and then re-fold into one of the more energetically stable mid-FRET (folded) states. This process is facilitated during thermal annealing by higher temperatures, or during *in situ* folding by low ionic strength or prolonged incubation times.

References

1. Wang Y, Patel DJ (1993) Solution structure of the human telomeric repeat d[AG3(T2AG3)3] G-tetraplex. Structure 1: 263-282.
2. Giraldo R, Suzuki M, Chapman L, Rhodes D (1994) Promotion of parallel DNA quadruplexes by a yeast telomere binding protein: a circular dichroism study. Proceedings of the National Academy of Sciences of the United States of America 91: 7658-7662.
3. Patel PK, Hosur RV (1999) NMR observation of T-tetrads in a parallel stranded DNA quadruplex formed by Saccharomyces cerevisiae telomere repeats. Nucleic acids research 27: 2457-2464.
4. Oganesian L, Moon IK, Bryan TM, Jarstfer MB (2006) Extension of G-quadruplex DNA by ciliate telomerase. The EMBO journal 25: 1148-1159.
5. Haider S, Parkinson GN, Neidle S (2002) Crystal structure of the potassium form of an Oxytricha nova G-quadruplex. Journal of molecular biology 320: 189-200.
6. Schultze P, Macaya RF, Feigon J (1994) Three-dimensional solution structure of the thrombin-binding DNA aptamer d(GGTTGGTGTGGTTGG). Journal of molecular biology 235: 1532-1547.
7. Lustig AJ (1992) Hoogsteen G-G base pairing is dispensable for telomere healing in yeast. Nucleic acids research 20: 3021-3028.
8. Kang C, Zhang X, Ratliff R, Moyzis R, Rich A (1992) Crystal structure of four-stranded Oxytricha telomeric DNA. Nature 356: 126-131.
9. Dai J, Carver M, Yang D (2008) Polymorphism of human telomeric quadruplex structures. Biochimie 90: 1172-1183.
10. Sannohe Y, Sugiyama H (2010) Overview of formation of G-quadruplex structures. Current protocols in nucleic acid chemistry / edited by Serge L Beaucage [et al] Chapter 17: Unit 17 12 11-17.

11. Ambrus A, Chen D, Dai J, Bialis T, Jones RA, et al. (2006) Human telomeric sequence forms a hybrid-type intramolecular G-quadruplex structure with mixed parallel/antiparallel strands in potassium solution. Nucleic acids research 34: 2723-2735.

12. Luu KN, Phan AT, Kuryavyi V, Lacroix L, Patel DJ (2006) Structure of the human telomere in K+ solution: an intramolecular (3 + 1) G-quadruplex scaffold. J Am Chem Soc 128: 9963-9970.

13. Phan AT, Kuryavyi V, Luu KN, Patel DJ (2007) Structure of two intramolecular G-quadruplexes formed by natural human telomere sequences in K+ solution. Nucleic acids research 35: 6517-6525.

14. Lim KW, Amrane S, Bouaziz S, Xu W, Mu Y, et al. (2009) Structure of the human telomere in K+ solution: a stable basket-type G-quadruplex with only two G-tetrad layers. Journal of the American Chemical Society 131: 4301-4309.

15. Parkinson GN, Lee MPH, Neidle S (2002) Crystal structure of parallel quadruplexes from human telomeric DNA. Nature 417: 876-880.

16. Gray RD, Li J, Chaires JB (2009) Energetics and kinetics of a conformational switch in G-quadruplex DNA. The journal of physical chemistry B 113: 2676-2683.

17. Renciuk D, Kejnovska I, Skolakova P, Bednarova K, Motlova J, et al. (2009) Arrangements of human telomere DNA quadruplex in physiologically relevant K+ solutions. Nucleic acids research 37: 6625-6634.

18. Balagurumoorthy P, Brahmachari SK (1994) Structure and stability of human telomeric sequence. The Journal of biological chemistry 269: 21858-21869.

19. Chang CC, Chien CW, Lin YH, Kang CC, Chang TC (2007) Investigation of spectral conversion of d(TTAGGG)4 and d(TTAGGG)13 upon potassium titration by a G-quadruplex recognizer BMVC molecule. Nucleic acids research 35: 2846-2860.

20. Mergny JL, Phan AT, Lacroix L (1998) Following G-quartet formation by UV-spectroscopy. FEBS letters 435: 74-78.

21. Antonacci C, Chaires JB, Sheardy RD (2007) Biophysical characterization of the human telomeric (TTAGGG)4 repeat in a potassium solution. Biochemistry 46: 4654-4660.

22. Koirala D, Dhakal S, Ashbridge B, Sannohe Y, Rodriguez R, et al. (2011) A single-molecule platform for investigation of interactions between G-quadruplexes and small-molecule ligands. Nat Chem 3: 782-787.

23. Long X, Parks JW, Bagshaw CR, Stone MD (2013) Mechanical unfolding of human telomere G-quadruplex DNA probed by integrated fluorescence and magnetic tweezers spectroscopy. Nucleic acids research 41: 2746-2755.

24. Li W, Hou XM, Wang PY, Xi XG, Li M (2013) Direct measurement of sequential folding pathway and energy landscape of human telomeric G-quadruplex structures. Journal of the American Chemical Society 135: 6423-6426.

25. Mergny JL, Maurizot JC (2001) Fluorescence resonance energy transfer as a probe for G-quartet formation by a telomeric repeat. Chembiochem : a European journal of chemical biology 2: 124-132.

26. Green JJ, Ying L, Klenerman D, Balasubramanian S (2003) Kinetics of unfolding the human telomeric DNA quadruplex using a PNA trap. Journal of the American Chemical Society 125: 3763-3767.

27. Lee JY, Okumus B, Kim DS, Ha T (2005) Extreme conformational diversity in human telomeric DNA. Proc Natl Acad Sci USA 102: 18938-18943.

28. Ying L, Green JJ, Li H, Klenerman D, Balasubramanian S (2003) Studies on the structure and dynamics of the human telomeric G quadruplex by single-molecule fluorescence resonance energy transfer. Proc Natl Acad Sci USA 100: 14629-14634.

29. Jena PV, Shirude PS, Okumus B, Laxmi-Reddy K, Godde F, et al. (2009) G-quadruplex DNA bound by a synthetic ligand is highly dynamic. J Am Chem Soc 131: 12522-12523.

30. Alberti P, Mergny JL (2003) DNA duplex-quadruplex exchange as the basis for a nanomolecular machine. Proceedings of the National Academy of Sciences of the United States of America 100: 1569-1573.

31. Savitzky A, Golay, M.J.E. (1964) Smoothing and Differentiation of Data by Simplified Least Squares Procedures. Anal Chem 36: 1627-1639.

32. Roy R, Hohng S, Ha T (2008) A practical guide to single-molecule FRET. Nat Meth 5: 507-516.

33. Tran PL, Mergny JL, Alberti P (2011) Stability of telomeric G-quadruplexes. Nucleic acids research 39: 3282-3294.

34. Viglasky V, Tluckova K, Bauer L (2011) The first derivative of a function of circular dichroism spectra: biophysical study of human telomeric G-quadruplex. European biophysics journal : EBJ 40: 29-37.

35. Gray DM, Wen JD, Gray CW, Repges R, Repges C, et al. (2008) Measured and calculated CD spectra of G-quartets stacked with the same or opposite polarities. Chirality 20: 431-440.

36. Dapic V, Abdomerovic V, Marrington R, Peberdy J, Rodger A, et al. (2003) Biophysical and biological properties of quadruplex oligodeoxyribonucleotides. Nucleic acids research 31: 2097-2107.

Chapter 3

Mechanical unfolding of human telomere G-quadruplex DNA probed by Integrated Fluorescence and Magnetic Tweezers Spectroscopy

*Sections of this chapter are adapted from published material (Long et al., NAR 2013)

Introduction

Model RNA and DNA hairpins have been extensively characterized by optical trapping methods, providing a detailed view of the folding energy landscapes of these fundamental nucleic acid structures [1-5]. However, the ability to achieve high spatial resolution using force spectroscopy relies upon the application of relatively large stretching forces (>10 pN) to suppress the measurement noise introduced by the long, flexible DNA handles used to attach the structure of interest to micron-scale beads held in the optical trap. Recently, a study of the force-dependent structural dynamics of single Holliday junctions was reported, which paired an optical trap to apply precisely calibrated stretching forces with single molecule Förster resonance energy transfer (smFRET) to monitor DNA structural dynamics [6]. This fluorescence-force method provided a powerful tool for probing sub-nanometer scale structural rearrangements within single Holliday junctions at very low stretching forces (< 1pN) over short periods of time. In addition, several groups have reported measurements which combine smFRET with a magnetic tweezers apparatus [7,8]. The use of magnets to apply mechanical loads to individual DNA molecules has several potential advantages over optical traps. For example, the combination of a high power optical trapping laser with single molecule fluorescence is technically difficult to implement, typically requiring interlacing of the FRET excitation and optical trapping beams in order to avoid rapid photo-damage of the FRET probes by the high power trapping laser [9,10]. Moreover, the sensitivity of optical traps to mechanical drift makes the application of low stretching forces (< 1 pN) over extended periods of time far more challenging than with a simple magnetic tweezers system. Here we describe an integrated fluorescence and magnetic tweezers microscope capable of measuring nanometer scale structural transitions in single DNA molecules at low stretching forces. We demonstrate the utility of this approach by analyzing the mechanical unfolding pathway of a model human telomere DNA substrate.

Telomeres are specialized chromatin structures that protect linear ends of eukaryotic chromosomes from aberrant DNA processing by DNA damage repair machinery [11]. The

foundation of human telomere structure is a long stretch of double-stranded DNA comprised of a hexa-nucleotide DNA repeat sequence (T_2AG_3). In addition, all telomeres terminate with a 3' single-stranded G-rich DNA tail which has the capacity to fold into a unique secondary structure called a G-quadruplex (GQ). Human telomere DNA GQs are proposed to play a central role in telomere homeostasis and small molecule ligands that selectively bind and stabilize telomere DNA GQs have shown promise as anti-cancer drugs [12,13]. Thus, intensive efforts have been made to better understand the structure and function of telomere DNA GQs.The first solution structure of a human telomere GQ revaled a fundamental structural architecture in which guanine bases are hydrogen bonded in a planar quartet geometry and may coordinate a single centrally located monovalent metal ion (Figure 3-1A, top left) [14].Three adjacent intra-molecular G-quartets may interact via stacking interactions and are topologically linked by short intervening DNA loop sequences (Figure 3-1A, bottom left). Moreover, the folding properties of telomere DNA GQs vary with the presence of different monovalent cations. Na^+ ions predominantly promote the formation of an anti-parallel GQ conformation[14], whereas GQ DNA crystals formed in the presence of K^+ ions revealed a distinct parallel GQ folding topology[15]. More recent solution studies have demonstrated that multiple GQ topologies coexist in the presence of K^+, including the anti-parallel, parallel, and several hybrid forms [16-19].

The structural and dynamic properties of telomere DNA GQs have been studied using smFRET [20-22]. These experiments revealed that a particular GQ topological fold must transit through an obligatory unfolded intermediate in order to isomerize into a distinct GQ fold. More recently, the rupture force distribution of single telomere DNA GQs has been analyzed using atomic force microscopy and optical trapping, providing a direct measurement of telomere DNA GQ mechanical stability [23-26]; however, these force spectroscopy studies did not analyze the force dependence of telomere DNA GQ folding/unfolding at equilibrium. Here, we report a detailed analysis of the force-dependence of telomere DNA GQ folding and unfolding at equilibrium under Na^+ folding conditions. Our results demonstrate that the

structural equilibrium between the unfolded and Na^+-induced telomere DNA GQ structure is highly sensitive to forces between ~1-8 pN. Analysis of the force-dependent rate constants for folding and unfolding provide a direct measurement of the position of the transition state barrier for telomere DNA GQ unfolding along the DNA stretching reaction coordinate. Interestingly, in contrast to other DNA secondary structures characterized by force spectroscopy, we find telomere DNA GQs exhibit a very short distance (< 1 nm) to the transition state barrier for unfolding. This unfolding behavior indicates telomere DNA GQ structure is significantly stabilized by long range contacts, and once these contacts are disrupted the entire GQ fold readily dissolves.

Materials and Methods

DNA Oligonucleotides

All DNA oligonucleotides were purchased from Integrated DNA Technologies, Inc. The sequences of all DNAs used in the study are listed in Table 3-1.

Dye labeling of DNA oligonucleotides

The biotin DNA Handle was labeled at the amino modification on C6 of T3 with mono-reactive Cy5 (GE Healthcare) and the EcoRI DNA Handle was labeled at the amino modification on C6 of T16 with mono-reactive Cy3 (GE Healthcare). Dye labeled fragments were EtOH precipitated and purified by reverse-phase chromatography using a C8 column (Agilent, Eclipse XDB-C8) on an AKTA purifier. Following HPLC purification samples were EtOH precipitated, and resuspended in ddH_2O. DNA concentrations were determined using a Nanodrop.

DNA annealing reactions

The biotinylated,Cy5-labeled, and Cy3-labeled strands were annealed to either the Tel24 abasic, 15R60/T8 hairpin abasic, or polyT abasic containing sequence by heating to 95 °C for 4 minutes followed by slow cooling to room temperature (over several hours) in the presence of a buffer (50mM Tris-HCl pH 8) containing either 100mM NaCl or 100mM KCl.

DNA molecule for integrated fluorescence and magnetic tweezers measurements

DNA molecules were constructed by ligation of three precursor DNA fragments: the annealed biotinylated smFRET fragment, a digoxigenin modified DNA linker fragment, and lambda DNA handle. The preparation of desired Cy5 and Cy3 labeled DNA insert is described above. The digoxigenin-labeled DNA linker is synthesized by PCR reaction with a pUC19 template using primers flanking the multiple cloning site. PCR reaction were set up using a dNTP mixture containing a 1:4 molar ratio of Digoxigenin-11-dUTP (Roche) : dTTP and digested with BamHI. The 15721 base pair lambda DNA handle was prepared by BamHI and EcoRI enzymatic digestion and agarose gel purification. Ligation reactions were set up with a 1:1:1 molar ratio of the desired Cy5 and Cy3 labeled DNA insert harboring an EcoRI sticky end, the purified EcoRI/BamHI lambda DNA handle, and the BamHI digoxigenin modified DNA linker fragment. Ligation reactions were run overnight at 16^{o}C in the presence of T4 DNA ligase (NEB). The final ligation product was heat inactivated at 65^{o} C to ensure the T4 DNA ligase did not remain associated with the DNA.

Single molecule FRET measurements in the absence of force

For these experiments, quartz slides (Finkenbeiner Inc.) were cleaned by sonicating for 20 minutes in 10% w/v Alconox, 20 minutes in ddH_2O, 20 minutes in acetone, 20 minutes 1M KOH, then 20 minutes in fresh 1M KOH. Slides are then rinsed with ddH2O and dried under nitrogen, followed by flame cleaning with a propane torch for ~2 minutes. Sample chambers were prepared by sandwiching pieces of parafilm between the quartz slide and a plasma cleaned coverglass (Harrik Plasma Cleaner), cover glasses from TED Pella, Inc. (Prod.# 260146). Chambers were heated on a hot block (95^{o}C) for 1 minute to seal the parafilm to the glass. Channels (~10 uL total volume) were treated with 35 uL of 1 mg/mL of biotinylated BSA (Sigma Cat.#A8549) for 5 minutes, washed with 100 uL of T50 buffer (10mM Tris-HCl pH 8, 50mM NaCl), then incubated with 50uL of 0.2 mg/mL streptavidin (Invitrogen Cat. #S888), then washed with 100 uL of T50. Channels were then equilibrated with buffer matching the desired experimental condition (see main text).

Next, 100 uL of 5-10 pM annealed fluorescent and biotin-labeled smFRET DNA was deposited onto the streptavidin coated quartz slide in the desired buffer condition. After 5 minutes incubation, desired buffer was flushed to the slide to remove the unbound DNA. Data was collected in imaging buffer containing 50mM Tris pH 8, 100 mM KCl or NaCl, 0.4% (w/v) D-glucose, 0.1 mg/ml glucose oxidase (Sigma Cat.# G2133-250KU), 0.02 mg/ml catalase (CalBiochem Cat.#219001) and saturated with Trolox (Aldrich Cat.#23,881-3). Data was acquired using a green laser (532 nm, Laserglow, Inc.) and prism-type total internal reflection microscopy on an inverted Olympus IX71 microscope equipped with an Andor IXON (897) CCD camera with 100 ms integration time.

Single molecule FRET analysis

Raw movie files were analyzed using in house written software available upon request (IDL and Matlab). FRET is defined as the efficiency of energy transfer between acceptor and donor dye, $I_A/(I_A+I_D)$. I_A is the acceptor intensity and I_D is the donor intensity. FRET histograms were compiled by combining data from ~ 100 individual single molecule trajectories.The Hidden Markov modeling was performed using the HaMMy[27] software program. First, dye intensity traces used in the HaMMy analysis were normalized after photo-bleaching, then the period prior to photo-bleaching was cropped to be used in the analysis. Since individual traces did not typically possess a sufficient number of transitions to produce a reliable HMM fit, we opted to stitch all of the normalized and cropped trajectories into a single trace using in house written Matlab software. This compiled trace was then fit using the HaMMy software. The idealized FRET trace that was produced by the HaMMy fitting was then parsed back into individual traces using in house Matlab software to prevent the inclusion of artificial FRET transitions at the trace stitch points. The individual HaMMy fits were then used to generate a transition density plot using in house written Matlab software. To fit the smFRET distributions, data were binned (bin size was FRET = 0.03) and fit with multiple Gaussian functions using Origin software. For dwell time analysis, idealized traces produced by fitting the single molecule trajectories using the HaMMy software package were

used to calculate the average lifetime of the folded or unfolded states. The smFRET histograms for the Na^+ and K^+ titrations, as well as in the presence of Mg^{2+}, were constructed by averaging the observed FRET for each molecule over two seconds (20 frames at 100 msec integration time) and binning the data with a bin size of FRET = 0.03.

Integrated FRET and Magnetic Tweezers measurements

The DNA tethers for FRET-Magnetic Tweezers measurements were attached to anti-dig coated magnetic beads. Anti-digoxigenin beads were made using EDC coupling chemistry (Pierce CAS# 22980) using carboxylated magnetic beads (Dynal, either 1μm (Invitrogen Cat.#650.11) or 2.8 μm (Invitrogen Cat.#143.05D) diameter. After 10 minutes incubation at 4^oC, the DNA-magnetic bead mixture was washed to remove the excess DNA fragments prior to being deposited onto the streptavidin coated coverglass (#1.5, Ted Pella) prepared using the same cleaning procedure described above. After 30 minutes incubation in room temperature to allow the DNA-magnetic bead complexes to settle to the surface, 100uL of 50mM Tris with 100mM Na^+ (for GQ experiments) or 200mM K^+ (for control DNA hairpin experiments) was flowed onto the slide by gravity to remove the unattached DNA linked magnetic beads.

To calibrate the stretching forces being applied to each DNA tether, forces were measured across a wide range of positions of the magnet assembly held above the sample chamber. Force measurements were determined using the expression $F = Lk_BT/\langle x^2 \rangle$, where F is the force in pico-Newtons (pN), L is the DNA tether length at a particular magnet height, k_BT is thermal energy (4.1pN*nm) at room temperature, and $\langle x^2 \rangle$ is the variance in the bead position in x-axis. The DNA tether length was measured by calibrating the diffraction ring pattern of the magnetic bead using a piezo-controlled objective positioning device (Mad City Labs) as previously described [28]. Separate calibrations were made for the 1μm and 2.8μm magnetic beads. The force was found to decrease exponentially as the distance of the magnets was increased from the sample chamber as described[28]. The magnet height vs. Force plots were fit with single exponential decay functions and the parameters from these

fits were then used to calculate the forces applied to subsequent experimental setups using the same size bead. The bead manufacturer estimates a deviation in the radius (r) of the beads on the order of 1-2%, and the force scales with the volume of the bead (r^3), thus we estimate the systematic error of our force measurements based upon an imperfect calibration to be on the order of 10%.

Data was collected in imaging buffer containing 100mM Na^+ or 200mM K^+ salt, 0.4% (w/v) D-glucose, 0.1 mg/ml glucose oxidase (Sigma Cat.# G2133-250KU), 0.02 mg/ml catalase (CalBiochem Cat.#219001) and saturated with Trolox (Aldrich Cat.#23,881-3). Data was acquired using objective-type total internal reflection microscopy with a green laser (532 nm, Laserglow, Inc.) on an Olympus IX71 microscope equipped with an Andor IXON (860) CCD camera. 100ms integration time was used for telomere DNA GQ and polyT measurements and 33 ms integration time was used for hairpin measurement. The stretching force applied to individual DNA tethers was altered by changing the linear position of a pair of rare earth magnets mounted on a computer controlled translation stage above the sample. The DNA extension and applied stretching force were determined by visualizing the magnetic bead with a blue LED (Thorlabs) mounted above the magnet assembly as described previously [28]. Prior to collecting smFRET data, the length of each DNA tether was monitored in real time as a function of applied twist to ensure that there was only a single DNA molecule attached between the bead and the surface. Molecules whose extension changed as a function of twist represented DNA braids and were not used in the measurements.

Raw movie files were first analyzed using in house written software (Labview and Matlab), and then fit with the HaMMy[27] software to generate idealized FRET traces used for dwell time analysis. Single molecule FRET histograms generated from combined FRET-magnetic tweezers data were compiled from all molecules analyzed at a particular force set point. Traces were first normalized for photo-bleaching and then cropped prior to the photo-bleaching event for HaMMy analysis. We focused our analysis on the equilibrium between

the predominant mid-FRET (folded) and the low-FRET (unfolded) state. To this end, for our analysis we used the idealized FRET traces generated by the HaMMy [27] fitting to remove the minority of time spent in the alternative high-FRET (folded) state. For dwell time analysis, idealized traces produced by fitting the smFRET trajectories using the HaMMy software package were used to calculate the average lifetime of the folded or unfolded states at each of the indicated forces.

Results

Single molecule FRET analysis of telomere DNA GQ structure in the absence of force

The experimental geometry utilized in the present study of the force-dependent folding/unfolding of telomere DNA GQ structure includes attachment of duplex DNA handles to each end of a single GQ forming sequence (Figure 3-1A, right). A similar design has been employed in recent optical trapping experiments [24-26], but it has not been analyzed using smFRET; therefore, we first set out to characterize the structure and dynamics of our model human single stranded telomere DNA construct (Tel24, $(TTAGGG)_4$) embedded within a duplex DNA molecule. For these experiments the Tel24 sequence was flanked by non-telomeric DNA extensions which were hybridized to their respective complementary DNA strands harboring either a FRET donor (Cy3) or acceptor (Cy5) dye (Figure 3-1A, right). To minimize the possibility of the adjacent duplex altering the folding properties of the GQ forming sequence, abasic sites were introduced between the Tel24 and the non-telomere sequence. Experiments investigating the structure of Tel24 in the absence of force were conducted on a prism-type total internal reflection fluorescence (TIRF) microscope [29]. Throughout this study we define FRET = $I_A/(I_A + I_D)$, where I_A and I_D are the background corrected intensities of the acceptor and donor dyes, respectively.

We first measured the folding properties of Tel24 over a wide range of NaCl concentrations (Figure S2-1). As the NaCl concentration was gradually increased to 100 mM, we observed the emergence of a predominant FRET population centered at FRET = 0.54, a second population centered at FRET = 0.33, and a minor population centered at FRET = 0.70

(Figure 3-1B). Analysis of single molecule trajectories revealed the Tel24 construct is in a dynamic equilibrium between each of these three FRET states (Figure 3-1C). Conversion of the predominant mid-FRET state to the high-FRET state required formation of the transient low-FRET state, as has been previously reported [21]. Single molecule trajectories were fit to a Hidden Markov model which yielded idealized FRET trajectories (Figure 3-1C) [27]. The idealized traces were used to generate transition density plots which clearly indicated the majority of FRET transitions (70%, n = 2426/3475 transitions) occurred between the mid-FRET and the low-FRET states (Figure 3-1D). The ratio of time spent in the unfolded folded (FRET = 0.33) and the predominant folded (FRET = 0.54) states yielded a K_{eq} = 0.25, corresponding to a ΔG_{unfold} = 0.81 kcal mol^{-1}, a value that is in good agreement with previously reported calorimetric studies of Tel24 unfolding in NaCl [30]. Dwell time analysis yielded rate constants of 0.87 s^{-1} and 0.29 s^{-1} for the folding and unfolding reactions, respectively, giving a K_{eq} = 0.33 in reasonable agreement with the value obtained by fitting the smFRET histograms. NMR and CD spectroscopy experiments on telomere DNA substrates in the presence of NaCl have demonstrated the strong preference of single stranded telomere DNA to form the anti-parrallel GQ conformation under this folding condition [14,31]. Thus, while smFRET data alone are not sufficient to conclusively determine which GQ structure is present, it is likely the predominant FRET = 0.54 conformation observed in the presence of 100 mM Na^+ represents the anti-parallel conformation and the FRET = 0.33 state represents the unfolded conformation.

In contrast to the Na^+ folding condition, the presence of KCl produced a considerably broader distribution of FRET states, with increasing concentrations of K^+ stabilizing several distinct high FRET GQ conformations (Supplementary Figure S2-2). The smFRET distribution for Tel24 folded in 100 mM KCl is well fit by two Gaussian functions, with populations centered at FRET = 0.61 and FRET = 0.76. Consistent with this result, analysis of single molecule trajectories in the presence of 100 mM KCl revealed two distinct long-lived FRET states, which occasionally inter-converted via the obligatory low FRET intermediate

(Supplementary Figure S2-3). In addition, the presence of Mg^{2+} in the K^+ folding reaction appeared to have a slightly stabilizing effect on GQ structure, but did not significantly alter the smFRET histograms in the presence of 100 mM K^+ (Supplementary Figure S2-4). Taken together, our smFRET results are in good agreement with previous findings that demonstrated Na^+ ions promote homogeneous folding of telomere DNA GQs, while K^+ ions induced a more complex distribution of FRET states that are more thermodynamically stable than the Na^+-induced fold. Based upon these results, we conclude that the presence of duplex DNA flanking the Tel24 sequence does not significantly alter telomere DNA GQ folding and stability.

Integrated Fluorescence and Magnetic Tweezers Spectroscopy

Previously reported force spectroscopy experiments using optical traps achieved sub-nanometer spatial resolution by applying relatively large stretching forces (>20 pN) to the system of study [32,33]. Since many biologically important structural transitions in nucleic acids and proteins are induced by much smaller forces, we have developed a simple method for measuring sub-nanometer structural rearrangements within individual DNA molecules held under a wide range of stretching forces (0.1 – 50pN). In our integrated fluorescence and magnetic tweezers system, a single Tel24 sequence is embedded within a duplex DNA molecule specifically attached between a microscope slide and a magnetic bead (Figure 3-2A). The length of the DNA handle attached to the microscope slide was 29 base pairs (~10 nm), while the length of the DNA handle attached to the bead was made considerably longer (15.7 kb, 5.4 mm contour length) to prevent background signal introduced by the large magnetic bead entering the evanescent field produced near the surface of the glass slide by total internal reflection of the excitation laser. The DNA construct is further modified with FRET donor (Cy3) and acceptor (Cy5) dyes on the DNA handles flanking the Tel24 sequence, as well as abasic sites between the duplex DNA handles and the Tel24 sequence. Stretching force was applied to the tethered DNA molecule with a pair of permanent rare-earth magnets mounted on a computer-controlled translation stage. Integrated fluorescence

and magnetic tweezers experiments employed objective-type TIRF which is readily compatible with the presence of the magnet assembly held above the sample chamber. We note that due to slight differences in the optical components in the microscopes, smFRET values made by objective-type TIRF vary slightly from those measured using the prism-type TIRF setup described in Figure 3-1 (ie. mid-FRET (folded state) is 0.64 in low force objective-type TIRF experiments vs. 0.54 in prism-type TIRF microscope under zero force); however, this variation does not impact our assignment of the mid-FRET and low-FRET states to the folded and unfolded telomere DNA GQ conformations, respectively.

In Figure 3-2B, representative smFRET trajectories are plotted at three different stretching forces for a single telomere DNA GQ in the presence of 100 mM NaCl. It is evident that at low forces (0.7 pN) the molecule spends the majority of the time in the high FRET (folded) state consistent with our zero force measurements described above. In contrast, a higher force (5.1 pN) substantially shifts the telomere DNA GQ folding equilibrium toward the low FRET (unfolded) state. Notably, the application of small degrees of tension appeared to substantially reduce the number of transitions into the minority high-FRET (FRET = 0.70) conformation when compared to experiments performed in the absence of force; thus, we focused our analysis on the structural equilibrium between the low-FRET (unfolded) and predominant mid-FRET (folded) conformation. These data qualitatively demonstrate the capacity of our technique to detect nanometer scale structural transitions within single telomere DNA GQs at low forces. However, to determine whether this approach can be used to extract quantitative information about force-induced structural transitions in DNA, we next performed control experiments on a model DNA hairpin construct (Supplementary Figure S2-5). Data taken on the model DNA hairpin was analyzed as a simple two state system separated by a single energetic barrier, yielding an unfolding force $F_{1/2}$ = 12.1 pN (defined as the force at which the hairpin folded and unfolded states are equally populated) and a distance between the folded and unfolded state, Δx = 16.2 nm. Furthermore, analysis of the force-dependent rate constants for folding and unfolding placed the transition state barrier 8.9

nm from the folded state and 6.1 nm from the unfolded state. These results are in good quantitative agreement with previously reported optical-trapping measurements on the same model DNA hairpin [2], demonstrating the ability of our integrated fluorescence and magnetic tweezers system to extract quantitative information about DNA folding processes.

Force dependence of telomere DNA GQ folding and unfolding

We next characterized in greater detail the force-dependence of the telomere DNA GQ folding/unfolding equilibrium. For these experiments, we performed force titrations for 75 individual telomere DNA GQ molecules (for each force a minimum of five different molecules were analyzed), and compiled the results into FRET histograms (Figure 3-3A, see Supplementary Figure S2-6 for complete data set). Analysis of the amount of time spent in the mid-FRET (folded) state vs. the low-FRET (unfolded) state as a function of force provided a direct measurement of the effect of stretching force on the telomere DNA GQ folding equilibrium. We fit each histogram with two Gaussian functions and calculated K_{eq} for the unfolding reaction as the area under the low-FRET peak divided by the area under the mid-FRET peak. From the slope of the plot of ln(Keq) as a function of stretching force, we determined the unfolding distance Δx = 2.7 nm and $F_{1/2}$ = 2.5 pN (Figure 3-3B).

We observed that the centers of the Tel24 low-FRET (unfolded) and mid-FRET (folded) populations shifted toward lower values as the applied stretching force was increased (Figure 3-3A). The two different Tel24 conformations fall within significantly different regions of the FRET response curve; thus, the magnitude of the force-induced ΔFRET for the low-FRET population reflects a substantially larger change in distance between the FRET probes than the ΔFRET of the mid-FRET population (Supplementary Figure S2-7). The low-FRET Tel24 conformation, previously identified as an obligatory folding intermediate during inter-conversion between distinct topological isomers [21], was suggested to reflect an unfolded DNA conformation that would be expected to respond to stretching force by gradually increasing its end-to-end distance, as observed in our experiments. To further explore the structural properties of this obligatory unfolded

intermediate, we compared the force response of the low-FRET (unfolded) telomere DNA GQ conformation to a 24 nucleotide polyT DNA strand, which has been utilized as a model for unstructured single stranded DNA in previous smFRET experiments [34]. We find that under low stretching force conditions, the unfolded conformation of the Tel24 construct is significantly more compact (higher FRET) than the polyT construct (Figure 3-4). This result demonstrates the G-rich Tel24 unfolded state experiences an attractive force, perhaps derived from increased stacking interactions between purine bases or transient H-bonding, which promotes telomere DNA GQ folding. Interestingly, the elastic properties of the unfolded Tel24 and polyT constructs converge within the force range (~8 pN) that completely inhibits telomere DNA GQ folding within the 100 msec time resolution of these measurements (Supplementary Figure S2-6). We note that the gradual increase in extension of the unfolded Tel24 state with increasing force is not consistent with the presence of any long-lived structured GQ folding intermediates such as a DNA hairpin or triplex structure. These structured intermediates have been previously suggested to occur during telomere DNA GQ folding [35-37], but may be too transient to detect in our experiments.

The force-dependence of the rate constants for telomere DNA GQ folding and unfolding can also be analyzed from our single molecule trajectories. Making the simplifying assumptions that along the reaction coordinate defined by the DNA stretching axis, the position of the energy barrier is independent of the stretching force and the positions of the folded and unfolded energy wells are not substantially altered by the applied force, we modeled the lifetime of the folded state, τ_{folded}, as given by $\tau_{folded}(F) = \tau_{folded,0}*\exp(F\Delta x^{\ddagger}_{folded}/k_BT)$, where $\tau_{folded,0}$ is the folded lifetime at zero force, $\Delta x^{\ddagger}_{folded}$ is the distance from the folded to the transition state, k_B is Boltzman's constant, and T is temperature. Similarly, the lifetime of the unfolded state as a function of force can be expressed as $\tau_{unfolded}(F) = \tau_{unfolded,0}*\exp(F\Delta x^{\ddagger}_{unfolded}/k_BT)$. Fitting these expressions to a plot of the average lifetimes of the folded or unfolded states as a function of force yielded $\Delta x^{\ddagger}_{unfolded}$ =

2.1 nm, $\Delta x^{\ddagger}_{folded}$ = 0.6 nm, $\tau_{folded,0}$ =4.1 sec, and $\tau_{folded,0}$ = 0.76 sec (Figure 5A). The results of our kinetic analysis are in good agreement with the Δx value derived from the equilibrium data ($\Delta x = \Delta x^{\ddagger}_{folded} + \Delta x^{\ddagger}_{unfolded}$ = 2.7nm). In addition, the extrapolated zero force rate constants of k_{fold} = 1.3 s^{-1} and k_{unfold} = 0.24 s^{-1} are in good agreement with our smFRET measurements in the absence of force (see above). The short distance (0.6 nm) from the folded state to the transition state barrier suggests the telomere DNA GQ structure is stabilized by long-range contacts, and that disruption of just a few of the terminal base pairing contacts is sufficient to promote the unfolding of GQ structure (Figure 3-5B).

Discussion

Here, we describe an integrated fluorescence and magnetic tweezers technique that combines objective-type total internal reflection microscopy with a 'classical' magnetic tweezers setup [28,38]. Although several groups have described combined fluorescence-force instruments using optical traps to apply stretching forces [6,9], these tools remain inaccessible to non-specialists, due to the technical challenges associated with aligning and calibrating these advanced optical trapping systems. Furthermore, the integration of a high-power trapping laser with single molecule fluorescence detection has the potential to negatively impact the photo-physical stability of the fluorescence probes, thereby limiting the duration of the FRET measurement. By comparison, the technique described in the present study is a simple instrument to construct and maintain, and should therefore be a generally accessible tool for a wide range of biochemists and structural biologists. Moreover, the use of permanent magnets to apply stretching forces obviates concerns of photo-damage induced by a high power trapping laser and provides a means to stably apply low forces for arbitrarily long periods of time. Indeed, smFRET trajectories acquired using our approach routinely last for tens of minutes, facilitating measurement of a single molecule under a variety of experimental conditions. An additional advantage of hybrid force-fluorescence methods using magnetic tweezers is the ability to monitor torque-induced structural transitions by smFRET,

as has recently been reported in studies of the torque-induced B-DNA to Z-DNA transition [7]. We expect the capability of integrated fluorescence and magnetic tweezers systems to detect nanometer scale structural rearrangements under conditions of low tensions and torques will be broadly applicable to a wide range of macromolecular folding studies.

In the present work, we have analyzed the force-dependent folding of a model human telomere DNA G-quadruplex (GQ) in the presence of Na^+. We find that the dynamic equilibrium between the Na^+-induced GQ folded and unfolded states is extremely sensitive to applied stretching forces between ~1-8 pN. By analyzing the effect of stretching force on the rate constants for telomere DNA GQ folding and unfolding, we have directly measured the position of the transition state barrier for GQ unfolding along the well defined DNA stretching reaction coordinate. Interestingly, we find the distance between the telomere DNA GQ folded state and the transition state barrier for unfolding is quite short (~0.6 nm). Our finding is consistent with a recent report that used dynamic force spectroscopy (DFS) to reconstruct the distribution of rupture forces for a DNA GQ formed by a sequence upstream of the human insulin gene promoter [26]. Fitting the DFS results to theoretical models which predict the distribution of rupture forces assuming a single transition state barrier suggested the barrier for folding is within ~1nm of the GQ folded state, in close accord with our present results. However, as with previous optical trapping experiments which analyzed the mechanical stability of GQ DNA [24,25], the DFS measurements did not directly observe a reversible folding/unfolding equilibrium in the low force regime as reported here. At present, it is unclear why the low force 'hopping' behavior we report for the telomere DNA GQ in the present study is not observed in the optical trapping experiments, but the discrepancy may be due to differences in the sequences being used or challenges associated with detecting small extension changes at low stretching forces in an optical tweezers instrument.

Force spectroscopy experiments with RNA and DNA hairpins revealed the transition state barrier for unfolding lies closer to the unfolded state than the folded state [1,2]. This long distance to the transition state barrier for unfolding is expected for compliant structures

whose folding stability is derived primarily from local interactions (ie. zipping of adjacent base pairs within a DNA hairpin). However, a short distance to the transition state barrier for unfolding, as measured here for the telomere DNA GQ, is indicative of a more brittle structure whose stability is reliant upon critical contributions of long-range interactions. This result can be explained within the framework of the NMR structure for the Na^+- induced anti-parallel GQ fold[14], wherein guanine bases separated by as many as 20 nucleotides must be brought together within a planar G-quartet configuration. Thus, disruption of just a few H-bonding interactions by mechanically pulling on the terminal bases of the telomere DNA GQ structure is sufficient to effectively destabilize the entire fold (Figure 3-5B), a finding that has direct implications on the molecular mechanisms of telomere-associated proteins and enzymes which must resolve DNA GQs during telomere maintenance. Telomere DNA GQs are typically classified as DNA secondary structure; however, our studies reveal these unique DNA folds share important structural properties with RNA and protein tertiary structures, which have also been characterized by sub-nanometer distances to the transition state barrier for unfolding[1,39-41]. Finally, understanding the critical contribution of long-range interactions in promoting telomere GQ folding stability should aid efforts in designing small molecule drugs that target and stabilize GQ structure in order to disrupt telomere homeostasis.

Table 3-1

DNA oligonucleotides used in this study

Tel24 Abasic	5’ GCGTGGCACCGGTAATAGGAAAATGGAGA(abasic spacer)$(TTAGGG)_4$(abasic spacer)CAGCTACGTGCAC-3’
polyT Abasic	5’ GCGTGGCACCGGTAATAGGAAAATGGAGA(abasic spacer) T_{24} (abasic spacer)CAGCTACGTGCAC-3’
15R60/T8 Hairpin Abasic	5’ GCGTGGCACCGGTAATAGGAAAATGGAGA(abasic spacer)GAGTCCTGGATCCTGTTTTTTTTCAGGATCCAGG ACTC(abasic spacer)CAGCTACGTGCAC-3’
Biotin DNA Handle T3 Amino	5’ TCT(AminoC6)CCATTTTCCTATTACCGGTGCCACGC-Biotin 3’
DNA Handle T16 Amino with EcoRI overhang	5’ Phosphate-AATTGTGCACGTAGCT(Amino C6)G 3’
PCR Primer I for Synthesized Digoxigenin labeled DNA Linker	5’ ACATTTCCCCGAAAAGTGCCA 3’
PCR Primer II for Synthesized Digoxigenin labeled DNA Linker	5’ GTTTCGCCACCTCTGACTTGA 3’

Figure 3-1

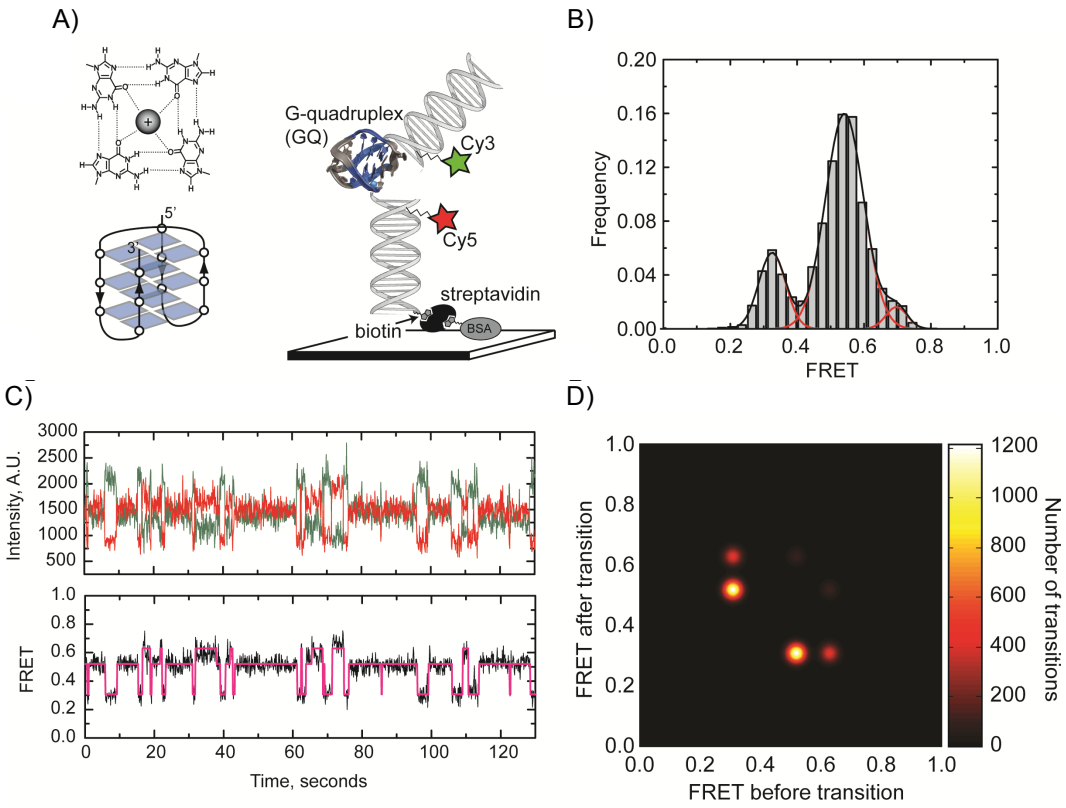

Single molecule FRET analysis of Na^+-induced telomere DNA G-quadruplex folding in the absence of force. (A) (top left) Diagram of a single G-quartet with a monovalent metal ion coordinated at its center. (bottom left) Schematic illustration of the anti-parallel G-quadruplex folding topology. (right) smFRET experimental setup. (B) Single molecule FRET histogram derived from data collected on >100 molecules is fit with three Gaussian functions centered at FRET = 0.33, 0.54, and 0.70. (C) A representative smFRET trajectory for Tel24 in the presence of 100 mM NaCl. (top) Individual donor (green) and acceptor (red) dye intensities, and (bottom) calculated FRET ratio are plotted as a function of time. FRET trajectories were fit with a Hidden Markov model yielding idealized FRET traces (magenta). (D) Idealized FRET traces from HMM fitting were used to generate a transition density plot indicating the frequency of each observed transition. Color bar on right indicates the number of transitions.

Figure 3-2

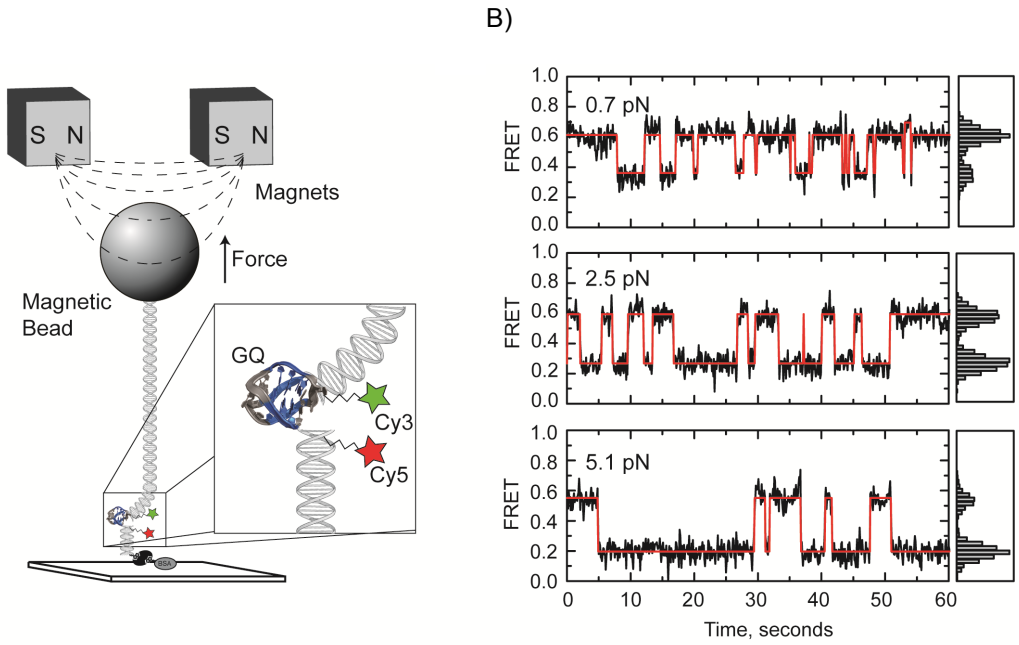

Force biases the telomere DNA G-quadruplex folding/unfolding equilibrium. (A) Schematic diagram of the experimental setup for integrated fluorescence and magnetic tweezers measurements. A FRET-labeled Tel24 molecule is flanked by a short biotinylated duplex DNA handle on one side, and a second longer duplex DNA handle with terminal digoxigenin modifications on the other side. Individual Tel24 constructs were attached between a streptavidin coated microscope slide and an anti-digoxigenin coated magnetic bead in a magnetic tweezers setup and imaged using objective-type total internal reflection microscopy. Variable stretching force was applied to individual Tel24 molecules by translating a pair of rare earth magnets held above the sample chamber. (B) Representative smFRET trajectories of a single Tel24 molecule held under three different forces (0.7, 2.5, and 5.1 pN). Histogram of the FRET values obtained at each force set point are shown on the right side of the FRET trajectories.

Figure 3-3

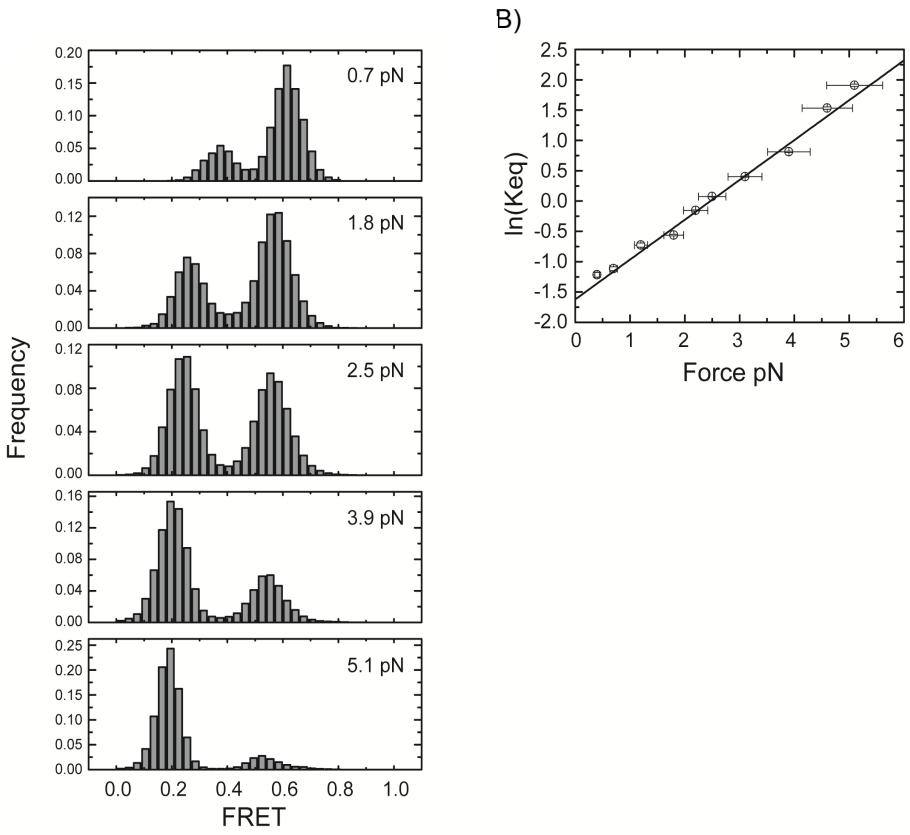

Telomere DNA G-quadruplex folding equilibrium as a function of applied force. (A) Compiled single molecule FRET histograms from data taken on 75 individual Tel24 molecules. For each force, a minimum of five different molecules were analyzed. Data for five representative forces ranging from 0.7 to 5.1 pN are shown. (see Supplementary Figure S2-6 for complete data set). (B) Plot of the $\ln(K_{eq})$ vs. Force. For each force set point at which folding/unfolding transitions were detected, smFRET histograms were fit with two Gaussian functions and Keq for unfolding was calculated as the area under the low FRET (unfolded) state divided by the area under the high FRET (folded) state. Plot was fit with the expression $\ln(K_{eq}) = F\Delta x/k_BT - \Delta G^o/k_BT$, yielding an unfolding distance, Δx = 2.7 nm and a $F_{1/2}$ = 2.5 pN. Y-axis error bars are estimates of the standard error of the mean determined by bootstrapping analysis of smFRET data and x-axis error bars reflect an ~10% systematic error in determination of stretching force.

Figure 3-4

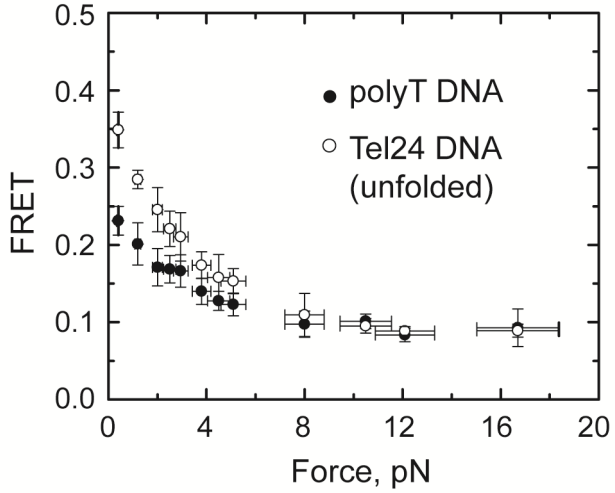

Force response of Tel24 low FRET (unfolded) state and polyT DNA (open circles). The average FRET values of the Tel24 low FRET (unfolded) state (open circles) and a 24 nucleotide polyT DNA construct (closed circles) are plotted as a function of force. Y-axis error bars are the standard deviation of the average FRET value measured for at least 5 individual molecules at each force set point and x-axis error bars reflect ~10% systematic error in the calibration of the applied stretching force.

Figure 3-5

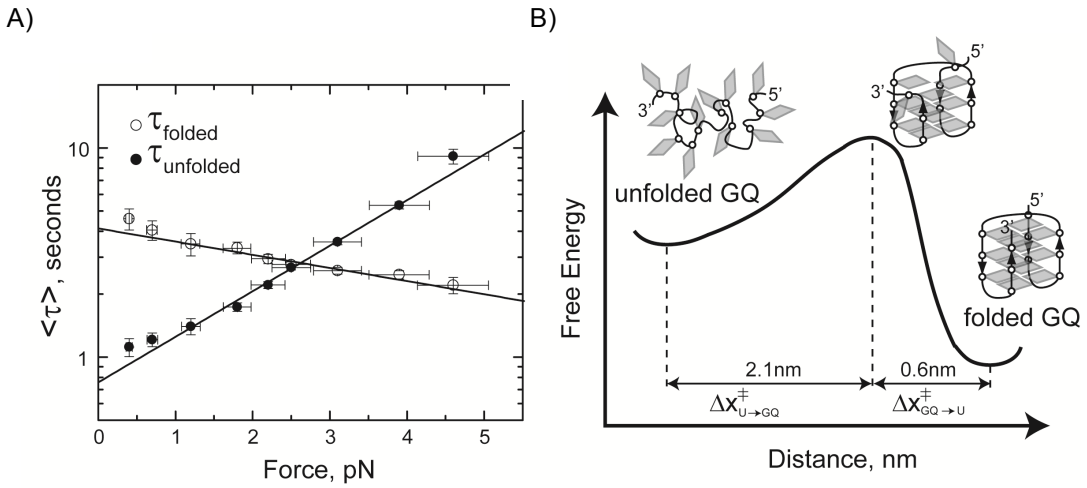

Force-dependent rate constants of telomere DNA G-quadruplex folding and unfolding. (A) Average lifetimes (τ) of the folded (high FRET) and unfolded (low FRET) states are plotted as a function of force. Plots are fit with exponential functions described in the main text, yielding $\Delta x^{\ddagger}_{unfolded}$ = 2.1 nm and $\Delta x^{\ddagger}_{folded}$ = 0.6 nm. (B) A schematic folding energy landscape for Tel24 in the presence of 100 mM NaCl. Cartoon model for the folded, transition state, and unfolded structures are superimposed on the folding energy landscape. The short distance between the transition state barrier and the folded conformation suggests just a few base pairs are disrupted in the transition state structure.

References

1. Liphardt J, Onoa B, Smith SB, Tinoco I, Jr., Bustamante C (2001) Reversible unfolding of single RNA molecules by mechanical force. Science 292: 733-737.

2. Woodside MT, Behnke-Parks WM, Larizadeh K, Travers K, Herschlag D, et al. (2006) Nanomechanical measurements of the sequence-dependent folding landscapes of single nucleic acid hairpins. Proc Natl Acad Sci U S A 103: 6190-6195.

3. Harlepp S, Marchal T, Robert J, Leger JF, Xayaphoummine A, et al. (2003) Probing complex RNA structures by mechanical force. Eur Phys J E Soft Matter 12: 605-615.

4. Li PT, Collin D, Smith SB, Bustamante C, Tinoco I, Jr. (2006) Probing the mechanical folding kinetics of TAR RNA by hopping, force-jump, and force-ramp methods. Biophys J 90: 250-260.

5. Onoa B, Dumont S, Liphardt J, Smith SB, Tinoco I, Jr., et al. (2003) Identifying kinetic barriers to mechanical unfolding of the T. thermophila ribozyme. Science 299: 1892-1895.

6. Hohng S, Zhou R, Nahas MK, Yu J, Schulten K, et al. (2007) Fluorescence-force spectroscopy maps two-dimensional reaction landscape of the holliday junction. Science 318: 279-283.

7. Lee M, Kim SH, Hong SC (2010) Minute negative superhelicity is sufficient to induce the B-Z transition in the presence of low tension. Proc Natl Acad Sci U S A 107: 4985-4990.

8. Shroff H, Reinhard BM, Siu M, Agarwal H, Spakowitz A, et al. (2005) Biocompatible force sensor with optical readout and dimensions of 6 nm3. Nano Lett 5: 1509-1514.

9. Brau RR, Tarsa PB, Ferrer JM, Lee P, Lang MJ (2006) Interlaced optical force-fluorescence measurements for single molecule biophysics. Biophys J 91: 1069-1077.

10. Tarsa PB, Brau RR, Barch M, Ferrer JM, Freyzon Y, et al. (2007) Detecting force-induced molecular transitions with fluorescence resonant energy transfer. Angew Chem Int Ed Engl 46: 1999-2001.

11. Palm W, de Lange T (2008) How shelterin protects mammalian telomeres. Annu Rev Genet 42: 301-334.

12. Oganesian L, Bryan TM (2007) Physiological relevance of telomeric G-quadruplex formation: a potential drug target. Bioessays 29: 155-165.

13. Rezler EM, Bearss DJ, Hurley LH (2002) Telomeres and telomerases as drug targets. Curr Opin Pharmacol 2: 415-423.

14. Wang Y, Patel DJ (1993) Solution structure of the human telomeric repeat d[AG3(T2AG3)3] G-tetraplex. Structure 1: 263-282.

15. Parkinson GN, Lee MP, Neidle S (2002) Crystal structure of parallel quadruplexes from human telomeric DNA. Nature 417: 876-880.

16. Ambrus A, Chen D, Dai J, Bialis T, Jones RA, et al. (2006) Human telomeric sequence forms a hybrid-type intramolecular G-quadruplex structure with mixed parallel/antiparallel strands in potassium solution. Nucleic Acids Res 34: 2723-2735.

17. Dai J, Carver M, Yang D (2008) Polymorphism of human telomeric quadruplex structures. Biochimie 90: 1172-1183.

18. Li J, Correia JJ, Wang L, Trent JO, Chaires JB (2005) Not so crystal clear: the structure of the human telomere G-quadruplex in solution differs from that present in a crystal. Nucleic Acids Res 33: 4649-4659.

19. Luu KN, Phan AT, Kuryavyi V, Lacroix L, Patel DJ (2006) Structure of the human telomere in K+ solution: an intramolecular (3 + 1) G-quadruplex scaffold. J Am Chem Soc 128: 9963-9970.

20. Jena PV, Shirude PS, Okumus B, Laxmi-Reddy K, Godde F, et al. (2009) G-quadruplex DNA bound by a synthetic ligand is highly dynamic. J Am Chem Soc 131: 12522-12523.

21. Lee JY, Okumus B, Kim DS, Ha T (2005) Extreme conformational diversity in human telomeric DNA. Proc Natl Acad Sci U S A 102: 18938-18943.

22. Ying L, Green JJ, Li H, Klenerman D, Balasubramanian S (2003) Studies on the structure and dynamics of the human telomeric G quadruplex by single-molecule fluorescence resonance energy transfer. Proc Natl Acad Sci U S A 100: 14629-14634.

23. Lynch S, Baker H, Byker SG, Zhou D, Sinniah K (2009) Single molecule force spectroscopy on G-quadruplex DNA. Chemistry 15: 8113-8116.

24. Koirala D, Dhakal S, Ashbridge B, Sannohe Y, Rodriguez R, et al. (2011) A single-molecule platform for investigation of interactions between G-quadruplexes and small-molecule ligands. Nat Chem 3: 782-787.

25. Yu Z, Koirala D, Cui Y, Easterling LF, Zhao Y, et al. (2012) Click chemistry assisted single-molecule fingerprinting reveals a 3D biomolecular folding funnel. J Am Chem Soc 134: 12338-12341.

26. de Messieres M, Chang JC, Brawn-Cinani B, La Porta A (2012) Single-molecule study of g-quadruplex disruption using dynamic force spectroscopy. Phys Rev Lett 109: 058101.

27. McKinney SA, Joo C, Ha T (2006) Analysis of single-molecule FRET trajectories using hidden Markov modeling. Biophys J 91: 1941-1951.

28. Lipfert J, Hao X, Dekker NH (2009) Quantitative modeling and optimization of magnetic tweezers. Biophys J 96: 5040-5049.

29. Roy R, Hohng S, Ha T (2008) A practical guide to single-molecule FRET. Nat Methods 5: 507-516.

30. Lane AN, Chaires JB, Gray RD, Trent JO (2008) Stability and kinetics of G-quadruplex structures. Nucleic Acids Res 36: 5482-5515.

31. Rezler EM, Seenisamy J, Bashyam S, Kim MY, White E, et al. (2005) Telomestatin and diseleno sapphyrin bind selectively to two different forms of the human telomeric G-quadruplex structure. J Am Chem Soc 127: 9439-9447.

32. Abbondanzieri EA, Greenleaf WJ, Shaevitz JW, Landick R, Block SM (2005) Direct observation of base-pair stepping by RNA polymerase. Nature 438: 460-465.

33. Moffitt JR, Chemla YR, Smith SB, Bustamante C (2008) Recent advances in optical tweezers. Annu Rev Biochem 77: 205-228.

34. Murphy MC, Rasnik I, Cheng W, Lohman TM, Ha T (2004) Probing single-stranded DNA conformational flexibility using fluorescence spectroscopy. Biophys J 86: 2530-2537.

35. Gray RD, Li J, Chaires JB (2009) Energetics and kinetics of a conformational switch in G-quadruplex DNA. J Phys Chem B 113: 2676-2683.

36. Mashimo T, Yagi H, Sannohe Y, Rajendran A, Sugiyama H (2010) Folding pathways of human telomeric type-1 and type-2 G-quadruplex structures. J Am Chem Soc 132: 14910-14918.

37. Zhang Z, Dai J, Veliath E, Jones RA, Yang D (2010) Structure of a two-G-tetrad intramolecular G-quadruplex formed by a variant human telomeric sequence in K+ solution: insights into the interconversion of human telomeric G-quadruplex structures. Nucleic Acids Res 38: 1009-1021.

38. Strick TR, Allemand JF, Bensimon D, Croquette V (1998) Behavior of supercoiled DNA. Biophys J 74: 2016-2028.

39. Carrion-Vazquez M, Li H, Lu H, Marszalek PE, Oberhauser AF, et al. (2003) The mechanical stability of ubiquitin is linkage dependent. Nat Struct Biol 10: 738-743.

40. Li PT, Bustamante C, Tinoco I, Jr. (2006) Unusual mechanical stability of a minimal RNA kissing complex. Proc Natl Acad Sci U S A 103: 15847-15852.

41. Williams PM, Fowler SB, Best RB, Toca-Herrera JL, Scott KA, et al. (2003) Hidden complexity in the mechanical properties of titin. Nature 422: 446-449.

Chapter 4

Investigation of duplex telomere DNA stability and D-loop formation by magnetic tweezers

Introduction

The telomere is a repetitive DNA sequence located at the end of chromosomes. It consists of 5-10kb of duplex TTAGGG and ends with a 50-200nt single stranded 3‘ end. This specialized DNA sequence facilitates the protection of genetic information.To protect the chrosome end, telomeres adopt a lariat-like structure known as T-loop, which can prevent the DNA repair machinery from recognizing the duplex and single stranded telomere junction [1,2,3]. The T-loop is not only a structure that is distinct from a damaged DNA site, it also provides the natural ending for the chromosome. The formation of a T-loop is not intuitive, it requires the G-rich single-stranded telomere tail to fold back and undergo base pairing to the duplex CCCTAA to generate a displacement loop (D-loop) (Figure 4-1A) [4,5]. In addition to secure the T-loop structure, the telomere D-loop has implications for homologous recombination on the Alternative Lengthening of Telomere (ALT), which is a mechanism involved in telomere length maintenance in 15% of cancers [6].

The telomere DNA invasion process and formation of a D-loop is accomplished by a protein complex known as shelterin. Recent studies suggested that Telomeric Repeat-Binding Factor 2 (TRF2), a subunit of the shelterin complex, plays a key role in stabilizing or promoting the D-loop formation by unwinding the duplex telomere and allowing the single stranded telomere to invade [7].

Despite intense research efforts to characterize the single stranded telomere DNA, information on the physical properties of duplex telomere remain elusive. In this study, we have used magnetic tweezers (MT) to characterize the mechanical properties of duplex telomeres. Our results demonstrate the duplex telomere is more resistant to torque denaturation. The comparison of telomere DNA extension before and after denaturation revealed that the GQ can be stably folded in a duplex telomere. The direct observation on strand invasion suggests that the stretching force can influence the rate of the invasion and the formation of the telomere displacement loop.

Materials and Methods

Telomere molecule for magnetic tweezers measurements

In these experiments, the telomere DNA molecule is prepared by a DNA segment excised from pRST5 plasmid, which contains 96 repeats TTAGGG (human telomere sequence). Construction of this molecule requires ligating five precursor DNA fragments: a biotin modified DNA linker, a digoxigenin modified DNA linker, two telomere DNA handles and a center telomere fragment. The biotin and digoxigenin modified DNA linkers are synthesized by PCR reactions with a pUC19 template using primers flanking the multiple cloning site. PCR reactions were set up using a dNTP mixture containing a 1:4 molar ratio of either digoxigenin-11-dUTP or biotin-11-dUTP: dTTP. The biotin modified DNA linker was digested with HindIII and the digoxigenin modified DNA linker was digested with BamHI. One of the telomere DNA handles was prepared by digesting pRST5 plasmid with BamHI and BbSI. The other handle was prepared by digesting pRST5 plasmid with HindII and BsmBI. The center telomere fragment was generated by digesting pRST5 plasmid with BbSI and BsmBI. Ligation reactions were set up with eight-fold excess of the center telomere fragment. The mixture was run overnight at 16°C in the presence of T4 DNA ligase (NEB). The final ligation product was heat inactivated at 65°C to ensure the T4 DNA ligase did not remain associated with the DNA. The final construction was anchored between a glass surface coated with anti-digoxigenin and a magnetic bead coated with streptavidin.

Experimental Setup

A detailed description of the MT experimental setup is described in chapter 5. A pair of magnets located above the sample chamber was used to manipulate the DNA. The extension of the DNA was monitored under various stretching forces and torques (Figure 4-1B). Data was acquired using an objective-type total internal reflection microscope equipped with an Andor IXON (860) CCD camera. 100ms integration time was used for data collections.

For the torque induced G-quadruplex formation experiment, we first negatively supercoiled the telomere DNA molecule at low force (F=0.5pN). After stretching at high force (F=4pN), the molecule was relaxed back down to low force. The DNA extension was monitored throughout the process using in-house-written software (LabView). Data was collected in an imaging buffer containing 10mM Tris (pH=7.4), 0.2% BSA and either 150mM K or 150mM Li.

For the telomere strand invasion experiment, 15 μM of single stranded invasion probes T3C $(CCTAA)_3$ were introduced to the negatively supercoiled telomere. We inferred invasion events based on the change in DNA extension. Data was collected in imaging buffer containing 10mM Tris (pH=7.4), 0.2% BSA and 150mM K.

Results and discussion

Force extension curve

To understand the physical properties of duplex telomere DNA, we first analyze the force extension curve of a duplex telomere DNA molecule. In this measurement, we monitor the extension of the DNA as a function of stretching force. Our experimental data show that the telomere DNA behaves like an ideal polymer chain under low stretching forces. Fitting the data with WLC model yields a persistence length of 45nm under our buffer condition. Based on this result, we conclude that the telomere DNA has similar stiffness as the non-telomere DNA [8].

Rotation extension curve

Next, we study the response of duplex telomere DNA to supercoiling. In this experiment, we compare the extension of non-telomere to telomere DNA as a function of torque (Figure 4-2). At low force, the introduction of negative and positive twist change the DNA extension linearly. The applied torsional stress is being converted to plectonemic structures. In contrast, at high force, the formation of plectonemic structures are inhibited in the negative supercoiling regime. In here, the negative supercoiling is transferred to twist and eventually cause the separation of the double helix. Subsequently, the DNA molecule regains

its full length extension. It is interesting to note that the control molecule is able to regain its full extension at 1pN, which indicates that the control molecule is denatured at this force (Figure 4-2A). However, at 1pN, the duplex telomere DNA extension decreases as rotation is continually applied to the molecule, which suggests that duplex telomere DNA is not denatured and it relies on forming plectonemic structures to relieve the superhelical stress in the molecule (Figure 4-2B). Based on this observation, we conclude that higher force is required to denature duplex telomere DNA.

Torque induced GQ formation

Previous studies have suggested that the G-rich single stranded telomere 3' end has the propensity to fold into a non-canonical structure known as a G-quadruplex (GQ). A GQ consists of a stack of G-quartets, which is generated by Hoogsteen base pairing. The GQ is further stabilized by a monovalent cation such as K^+ (Figure 4-1B) [9,10,11,12]. The GQ within the single stranded telomere has been studied intensively [13,14,15,16,17,18]. However, information on the GQ found in the duplex telomere remains elusive.

We next set out to test whether torque can induce GQ formation in the duplex telomere. For these experiments, the duplex DNA is negatively supercoiled at low stretching force (F=0.5pN), where plectonemic structures are generated. Then, the negatively supercoiled DNA is denatured through high-force stretch (F=4pN). We compare the DNA extension before and after denaturation (Figure 4-4A). In the control DNA molecule, the DNA fully recovers to its original state after being stretched, which indicates that there is no formation of a stable structure during denaturation. The molecule is able to re-generate the plectonemic structure. Interestingly, the duplex telomere DNA is not able to recover its original extension after being stretched in K^+, which suggests that there is a stable structure generated during denaturation (Figure 4-4B, black dots). The formation of this structure prevents the separated strands from re-associating. It locally unwinds the molecule and causes compensatory positive supercoils to cancel the negative twist, subsequently increasing the extension of duplex telomere DNA. We measure the pro-stretching DNA

extension as a function of rotation. Fitting the data with a linear regression line, we determined that the DNA extension increases 5nm per rotation (Figure S3-1).

One explanation is that the GQ structures are generated when the telomere strands are dissociated. To test our hypothesis, we repeat the experiments on the same molecule but exchanged the buffer from 150mM K^+ to 150mM Li^+, where GQ structures can't be stably folded. Indeed, the duplex telomere DNA in Li^+ is able to recover its original extension after being negatively supercoiled and stretched (Figure 4-5). This result suggests that no stable DNA structure is formed in Li^+, which further supports our model that GQ structures affect the change of DNA extension in K^+.

It is important to note that a small subset of data show that extension of DNA is different in Li^+ buffer, but the change of extension is not uniform (Figure 4-4B, red dots). This result suggests that there are DNA structures being produced after denaturation in low frequency. Since the GQ structure is prohibited under Li^+, the other DNA structure, rather than the GQ, must cause the change in DNA extension. To further differentiate this structure from the GQ structure, we compare the post stretching rotation extension curve of the molecule in K^+ and Li^+ buffers. Prior to stretching, the duplex telomere yields a symmetrical rotation extension curve as described earlier (Figure 4-6, black squares). If the molecule extension does not change after being stretched, the post extension rotation curve will be identical, which is similar to the data collected in Li^+ buffer (Figure S3-2). In K^+ buffer, the rewinding of the molecule to zero twist shows no change in the position of the relaxed state, which suggests that the molecule has regained its native topology (Figure 4-6A, 3-6B). However, in Li^+ buffer, the position of the relaxed state is less clear. The molecule was not able to recover to its native state until it was rewound in the positive supercoiled regime (Figure 4-6C). This phenomenon is more pronounced if the molecule is held at a lower force. The rotation extension curve is shifted toward negative twist (Figure 4-6D).

The differences in mechanical rotation properties of the structure generated in the Li^+ and K^+ buffers support the hypothesis that the structure formed in the Li^+ buffer is not a GQ.

One explanation for the change in DNA extension in Li^+ is slippage. During the re-association process, the repetitive telomere DNA aligns in a frame shifted configuration. The miss-pairing DNA creates stable denaturation bubbles and prevents regeneration of plectonemic structure, resulting in DNA extension. The heterogeneity of DNA extension is mostly due to the size variation of the DNA bubble created by slippage.

Strand invasion

Having characterized the duplex telomere DNA alone, we next set out to analyze the telomere D-loop formation. In this assay, the duplex DNA molecule is negatively supercoiled at low force. We stop applying rotation to the molecule once it reaches the minimum detectable extension. Then, the invading strand is introduced to the negatively supercoiled DNA for invasion. When the invading strand hybridizes with the duplex telomere, it unwinds the helix locally. This causes the other part of the molecule to generate compensatory positive twist, which cancels the negative plectonemic supercoils, resulting in an increase of DNA extension (Figure 4-7A). Figure 4-7B shows the process of a duplex telomere DNA being invaded by 18nt primers (T3C). Step-like behavior in the process represented an individual invasion event. The dwell time of individual invasion events represents the waiting time for the next invading strand to hybridize with the duplex telomere and generate a D-loop. The average waiting time for strand invasion allows us to calculate the rate constant for D-loop formation.

Next, we investigate how stretching forces influence the D-loop formation. Figure 4-8 shows the representative invasion traces at force=0.58, 0.68, 0.79 and 0.97pN. Increasing the stretching force alters the rate of invasion. The molecules experience force-dependent lag time, followed by a series of invasion events. At high forces, there is not a large discrepancy in dwell time for an individual invasion event. However, at low forces, the molecule can experience some long invasion steps.

It is not a surprise that the molecule has lag time before the initial invasion because the force affects helix stability. This dictates the ratio between the denatured-DNA and B-

DNA in the molecule. At higher force, more denaturation bubbles are created for hybrization, therefore the invasion time is faster. It is interesting to note that after the first step, some of the dwell time for invasion at low force shares similar invasion waiting time as the one at high force (Figure 4-9). This suggests there is a nucleation effect on the invasion process. The long pauses at low force probably indicate 1) a limited denaturation spot for invasion 2) a decreased boundary effect [19,20].

Conclusion

In summary, we used MT to directly examine the mechanical properties of the duplex telomere. Since the persistence length of the duplex telomere is similar to the non-telomere molecule, we conclude that the telomere DNA has similar stiffness as the other duplex DNA. By comparing the rotation extension curve, we discovered that the duplex telomere is more resistant to torque-induced denaturation. In addition, we demonstrated that by denaturing the duplex telomere, we can promote GQ formation and detect the telomere slippage. Furthermore, the preliminary results of the strand invasion suggest the rate of the invasion can be influenced by the stretching forces. Additional experiments will be required for analysis of torque-dependence on the rate constant for invasion. This information can be used to estimate the distance to the transition state for telomere D-loop formation along the DNA roation reaction coordinate.

This set of experiments allows us to study the intrinsic properties of individual duplex telomere DNA under physiological conditions. It lays a foundation to investigate the impact of telomere-associated proteins on the telomere. This will further our understanding of telomere replication.

Figure 4-1

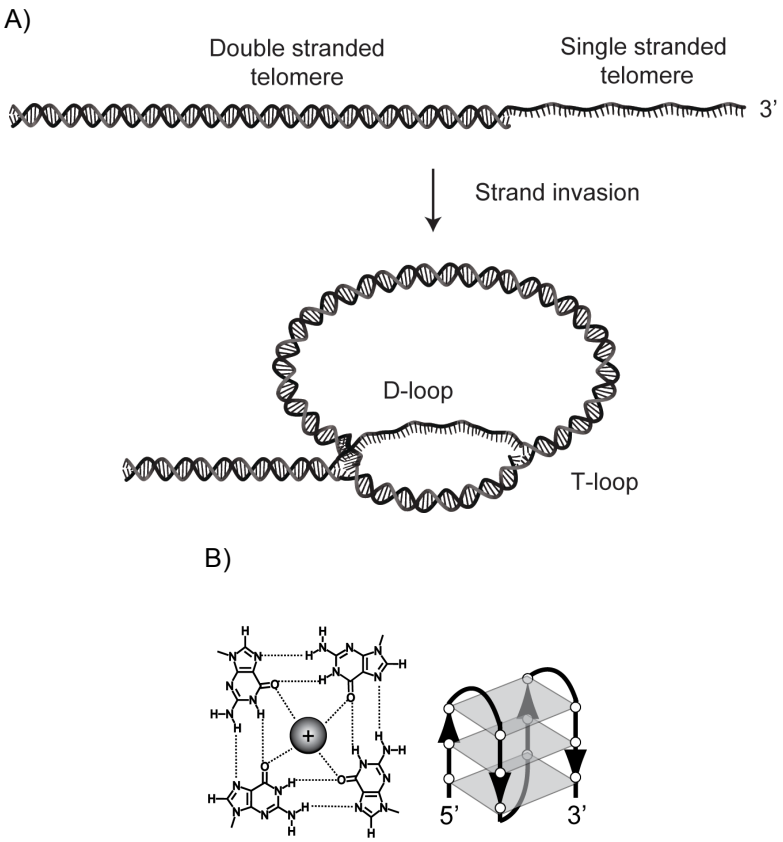

(A) The human telomere is comprised of double stranded DNA but terminates with a 3' single stranded DNA tail. Telomeres can form a lasso-like loop structure known as a T-loop. The formation of this structure requires invasion of the 3' single stranded telomere tail into the duplex telomere. (B) The G-rich telomere can fold into a secondary structure known as a G-quadruplex (GQ). The GQ consists of a stack of planar tetrads generated by Hoogsteen base pairing of four guanines. Monovalent cations, such as K^+, can further stabilize the GQ by coordinating in the center of the planar tetrad.

Figure 4-2

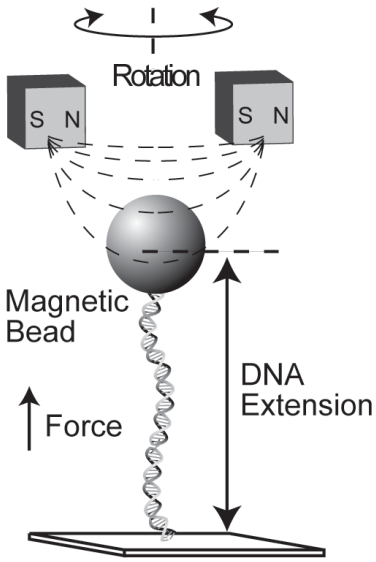

Schematic diagram of the MT experimental setup. A telomere DNA molecule is torsionally constrained at one end to a glass surface and at the other end to a magnetic bead. A pair of magnets controls the stretching force applied to the molecule, and the number of rotations imposed on the magnetic bead regulates the supercoil of the molecule. The DNA extension determines the responses of the molecule under various stretching forces and rotations.

Figure 4-3

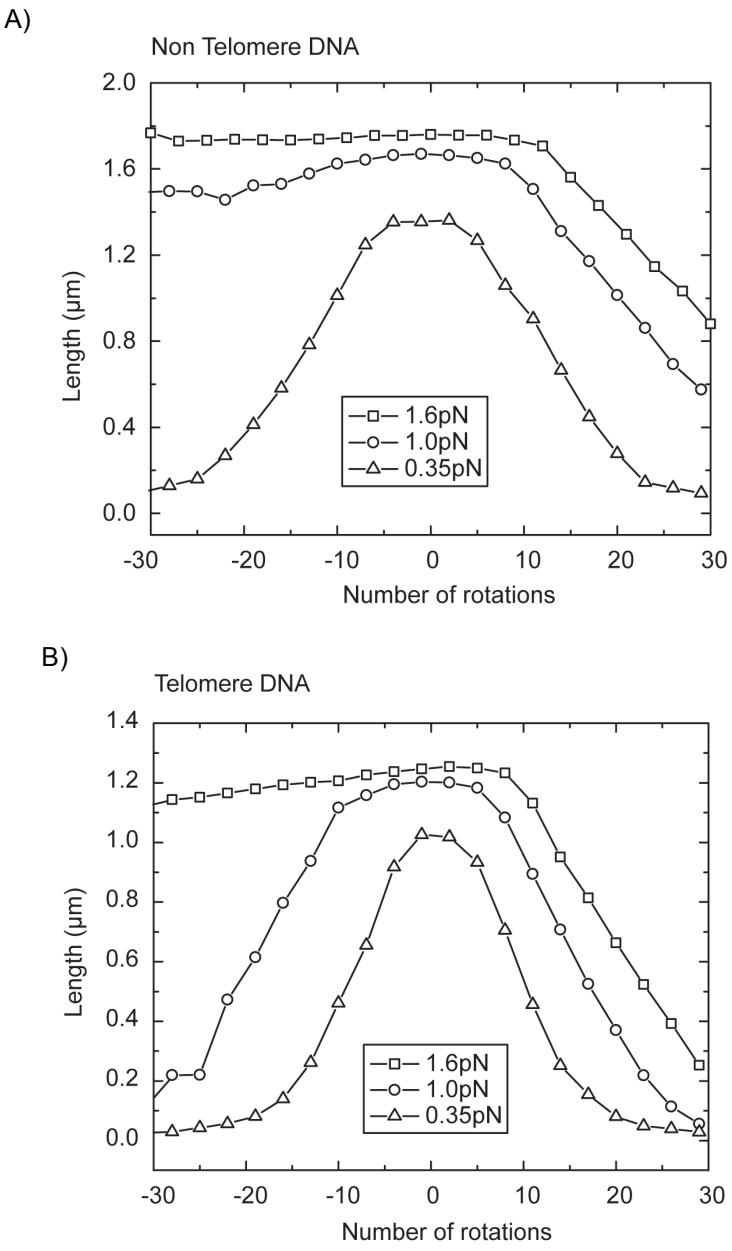

Rotation extension curves of (A) non-telomere DNA and (B) telomere DNA under stretching force 0.35pN, 1.0pN and 1.6pN.

Figure 4-4

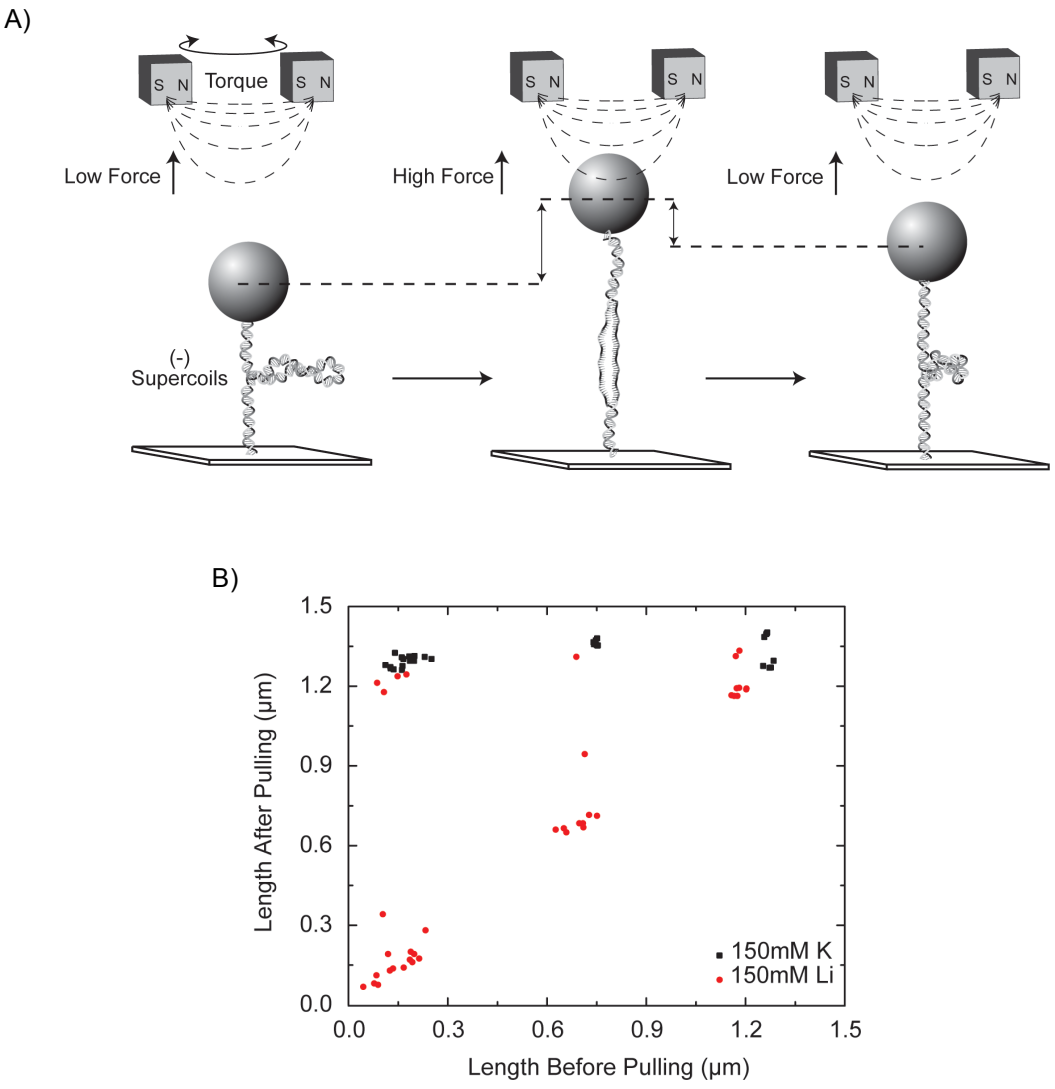

(A) Experimental scheme of torque induced G-quadruplex formation. A negatively supercoiled telomere is stretched at high force. In this experiment, DNA extension is compared before and after stretch. (B) Correlation plot of telomere DNA extension before and after stretching in 150 mM K^+ and 150 mM Li^+ buffers.

Figure 4-5

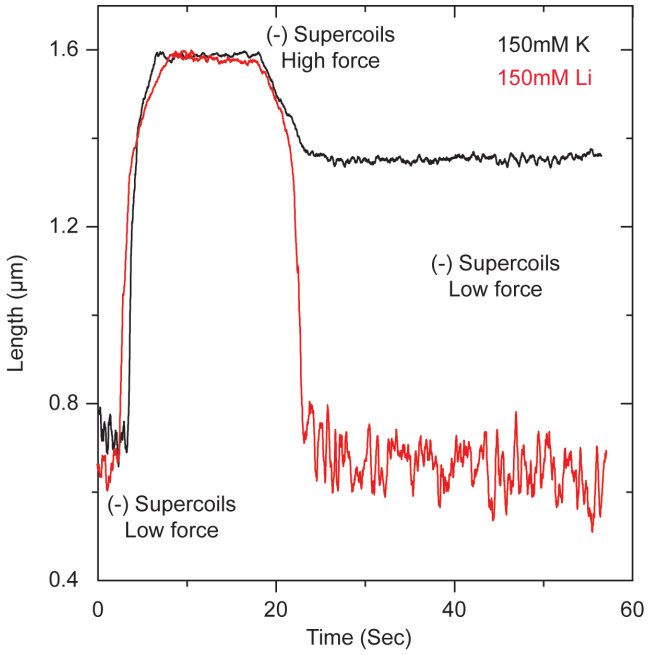

A trajectory of a negatively supercoiled telomere DNA displays a change of extension after the molecule is stretched at high force in 150mM K^+ (black line). Similar measurements were performed under 150mM Li^+. The telomere DNA was able to recover its extension prior to stretch (red line).

Figure 4-6

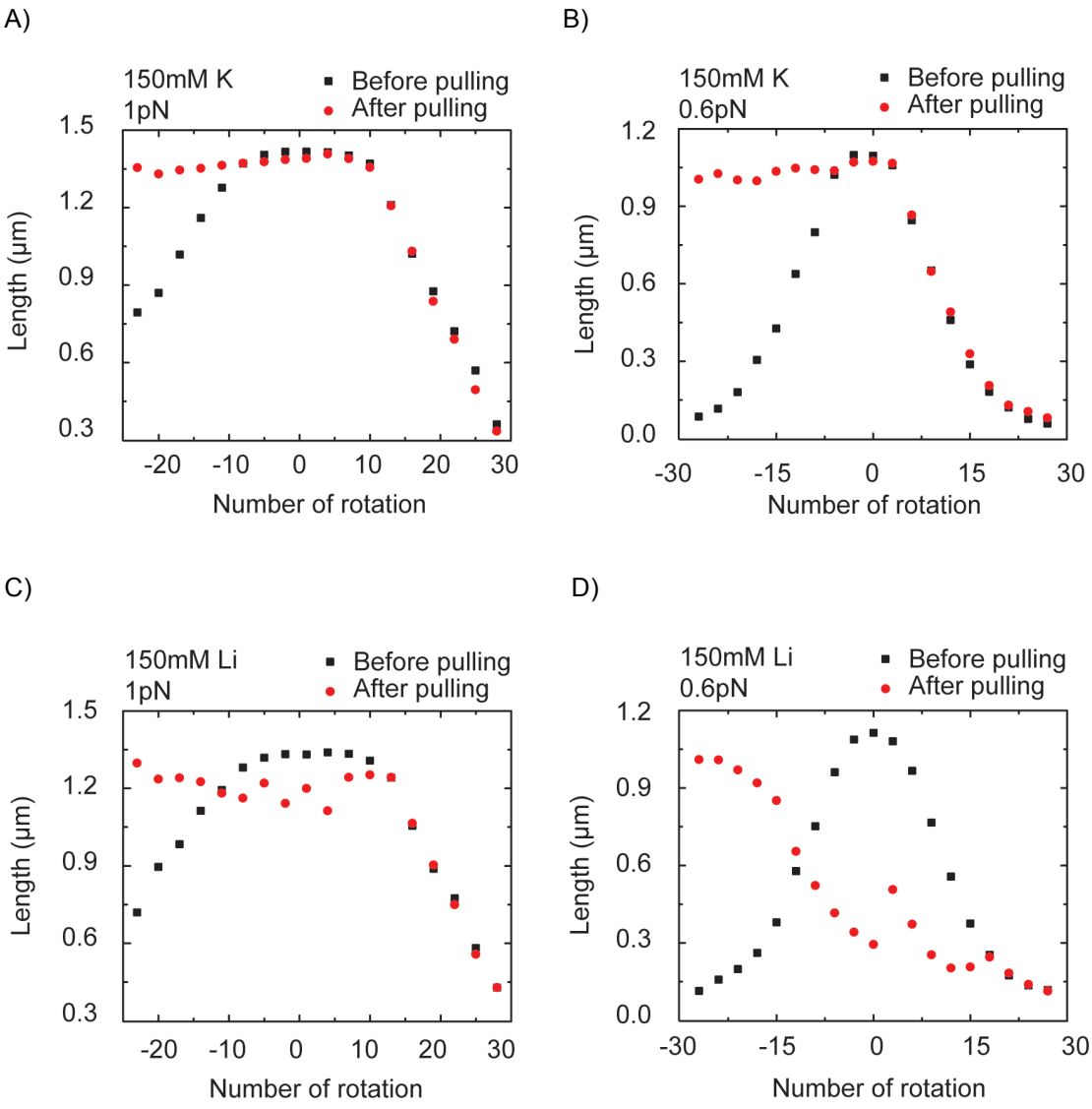

Rotation extension of telomere DNA before and after stretching in 150mM K^+ and 150mM Li^+ buffers at 0.6pN and 1pN.

Figure 4-7

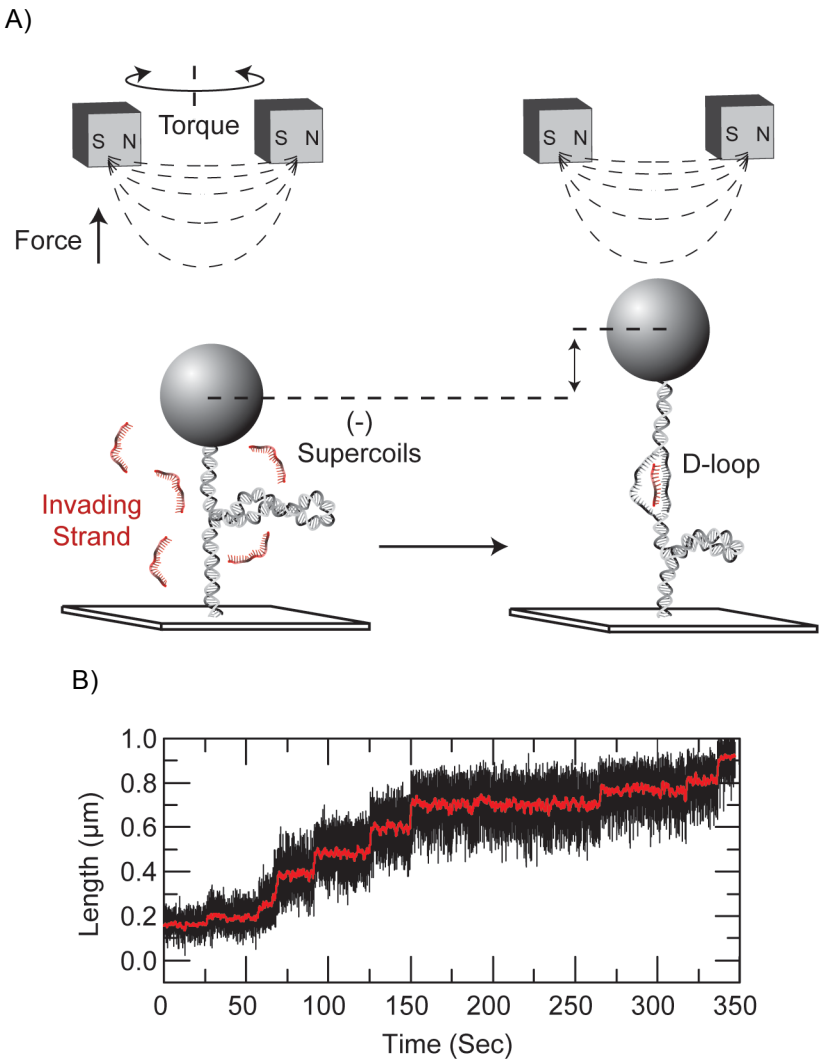

(A) Experimental setup of strand invasion assay. A telomere DNA is torsionally constrained and mechanically stretched. The invading strands are introduced to the telomere under negative supercoiling. Once the telomere DNA is invaded, its length changes. (B) A single molecule trajectory displays the individual invasion of an 18 nt invading strand on a telomere molecule.

Figure 4-8

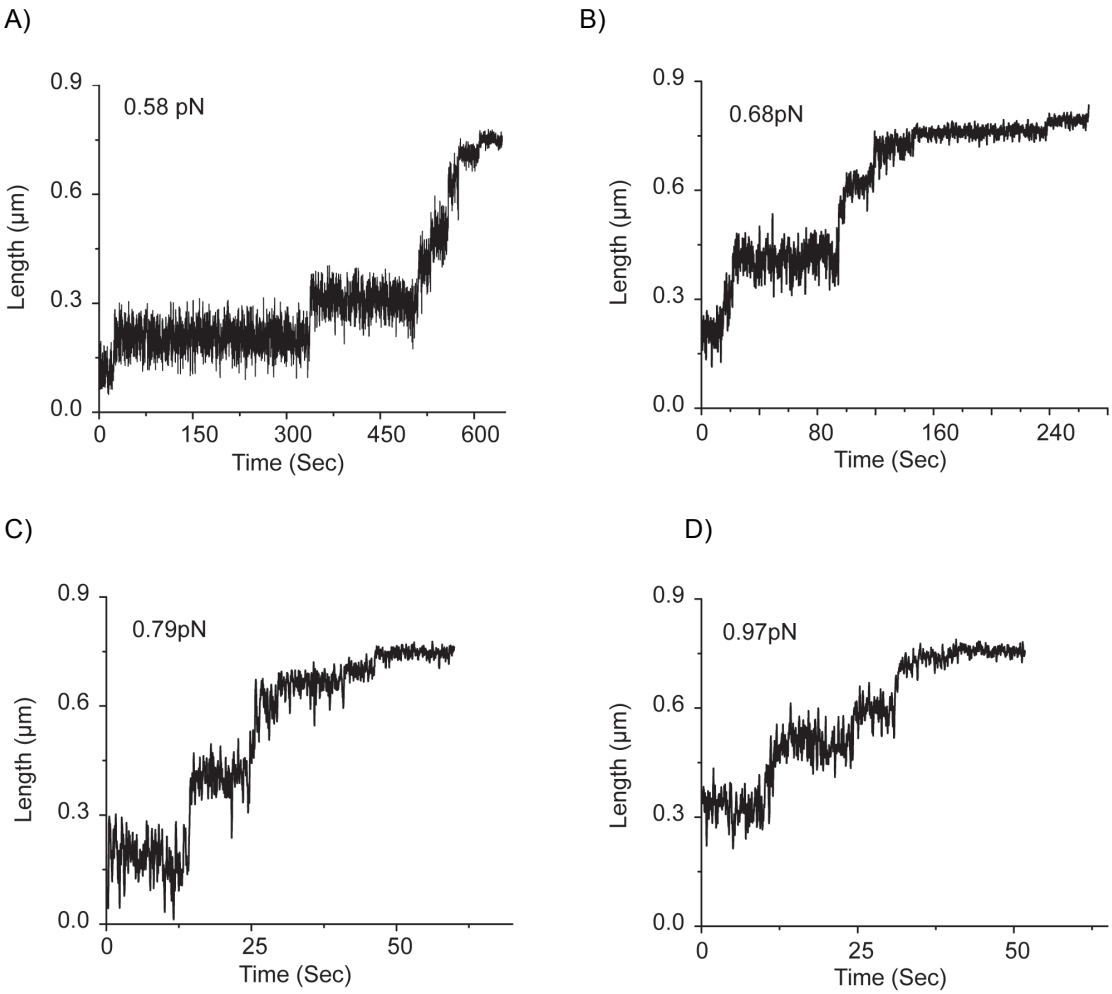

Single molecule traces of individual invasions of an 18nt invading strand at 0.58pN, 0.68pN, 0.79pN and 0.97pN. These trajectories show the last 15 seconds of the initial invasion step.

Figure 4-9

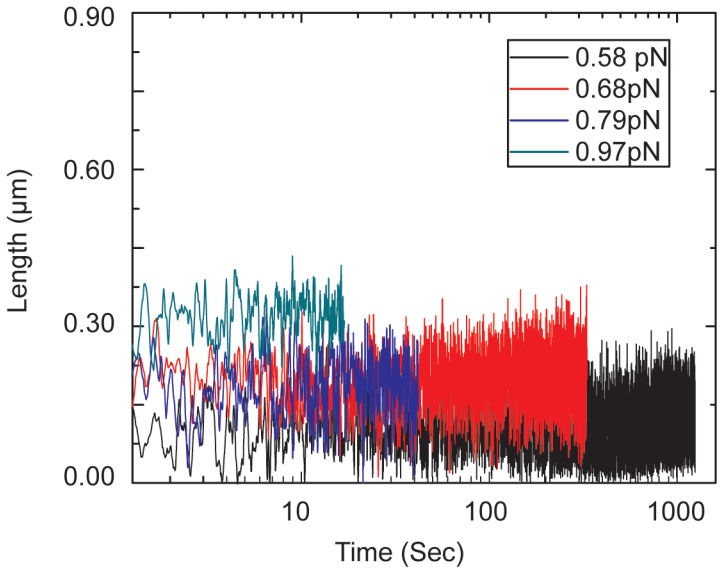

Single molecule trajectories display the first invasion step of an 18nt invading strand at 0.58pN, 0.68pN, 0.79pN and 0.97pN.

References

1. Griffith JD, Comeau L, Rosenfield S, Stansel RM, Bianchi A, et al. (1999) Mammalian telomeres end in a large duplex loop. Cell 97: 503-514.
2. Nikitina T, Woodcock CL (2004) Closed chromatin loops at the ends of chromosomes. J Cell Biol 166: 161-165.
3. Doksani Y, Wu JY, de Lange T, Zhuang X Super-resolution fluorescence imaging of telomeres reveals TRF2-dependent T-loop formation. Cell 155: 345-356.
4. Stansel RM, de Lange T, Griffith JD (2001) T-loop assembly in vitro involves binding of TRF2 near the 3' telomeric overhang. EMBO J 20: 5532-5540.
5. Verdun RE, Karlseder J (2006) The DNA damage machinery and homologous recombination pathway act consecutively to protect human telomeres. Cell 127: 709-720.
6. Cesare AJ, Reddel RR Alternative lengthening of telomeres: models, mechanisms and implications. Nat Rev Genet 11: 319-330.
7. Amiard S, Doudeau M, Pinte S, Poulet A, Lenain C, et al. (2007) A topological mechanism for TRF2-enhanced strand invasion. Nat Struct Mol Biol 14: 147-154.
8. Smith SB, Finzi L, Bustamante C (1992) Direct mechanical measurements of the elasticity of single DNA molecules by using magnetic beads. Science 258: 1122-1126.
9. Wang Y, Patel DJ (1993) Solution structure of the human telomeric repeat d[AG3(T2AG3)3] G-tetraplex. Structure 1: 263-282.
10. Parkinson GN, Lee MPH, Neidle S (2002) Crystal structure of parallel quadruplexes from human telomeric DNA. Nature 417: 876-880.
11. Ambrus A, Chen D, Dai J, Bialis T, Jones RA, et al. (2006) Human telomeric sequence forms a hybrid-type intramolecular G-quadruplex structure with mixed parallel/antiparallel strands in potassium solution. Nucleic acids research 34: 2723-2735.

12. Luu KN, Phan AT, Kuryavyi V, Lacroix L, Patel DJ (2006) Structure of the human telomere in K+ solution: an intramolecular (3 + 1) G-quadruplex scaffold. J Am Chem Soc 128: 9963-9970.

13. Jena PV, Shirude PS, Okumus B, Laxmi-Reddy K, Godde F, et al. (2009) G-quadruplex DNA bound by a synthetic ligand is highly dynamic. J Am Chem Soc 131: 12522-12523.

14. Lee JY, Okumus B, Kim DS, Ha T (2005) Extreme conformational diversity in human telomeric DNA. Proc Natl Acad Sci USA 102: 18938-18943.

15. Ying L, Green JJ, Li H, Klenerman D, Balasubramanian S (2003) Studies on the structure and dynamics of the human telomeric G quadruplex by single-molecule fluorescence resonance energy transfer. Proc Natl Acad Sci USA 100: 14629-14634.

16. Green JJ, Ying L, Klenerman D, Balasubramanian S (2003) Kinetics of unfolding the human telomeric DNA quadruplex using a PNA trap. Journal of the American Chemical Society 125: 3763-3767.

17. Dai J, Carver M, Yang D (2008) Polymorphism of human telomeric quadruplex structures. Biochimie 90: 1172-1183.

18. Chaires JB Human telomeric G-quadruplex: thermodynamic and kinetic studies of telomeric quadruplex stability. FEBS J 277: 1098-1106.

19. Oberstrass FC, Fernandes LE, Bryant Z Torque measurements reveal sequence-specific cooperative transitions in supercoiled DNA. Proc Natl Acad Sci U S A 109: 6106-6111.

20. Oberstrass FC, Fernandes LE, Lebel P, Bryant Z Torque spectroscopy of DNA: base-pair stability, boundary effects, backbending, and breathing dynamics. Phys Rev Lett 110: 178103.

Chapter 5

Integrated magnetic tweezers and single-molecule FRET for investigating the mechanical properties of nucleic acid structure

Introduction

Mechanical force is a critical modulator of molecular, cellular, and organismal function [1-3]. For example, DNA experiences a wide array of mechanical perturbations during the processes of replication, RNA transcription, and chromatin compaction. Thus, to fully appreciate the structure and function of DNA within its native cellular context, it is necessary to understand how the genetic material responds to mechanically induced bending, twisting, and stretching forces. Over the past several decades, force spectroscopic methods have revolutionized the manner in which DNA biophysics experiments are conducted, permitting the direct manipulation and analysis of single DNA molecules[3-6]. Optical trapping (OT) and magnetic tweezers (MT) have emerged as the preferred methods of choice for analyzing the response of nucleic acids to precisely calibrated stretching forces and torques [7-10], and each of these techniques posses certain advantages and limitations. For example, a well-aligned and vibration-isolated OT system can achieve a remarkable degree of spatial resolution, capable of detecting molecular displacements with angstrom resolution [11-13]. Although MT instruments cannot achieve such high spatial resolution, this approach offers several distinct advantages. First, a MT system is particularly well-suited for the stable application of very low stretching forces over long periods of time and provides a facile means to introduce precise degrees of twist into a single DNA molecule [14-17]. Moreover, the MT instrumentation is substantially simpler to construct and operate than an optical trap and has therefore been widely applied to diverse biological systems in a large number of laboratories.

One challenge that arises in both OT and MT based experiments is that the achievable spatial resolution is directly linked to the level of stretching force being applied to the system. This limitation arises due to the relatively long, flexible DNA handles typically used to hold the system of interest in the trap during measurement. The compliance of the flexible DNA handles introduces noise in the measurement, which can only be suppressed by large stretching forces that serve to stiffen the system and improve the signal-to-noise ratio

[5,11,12]. To overcome this challenge, several research groups have reported hybrid force-fluorescence spectroscopy methods, which decouple the application of stretching force from the measurement of conformational rearrangements within a structure of interest (SOI) [18-24]. In these systems, nanometer-scale conformational changes in a SOI are typically detected by single-molecule Förster resonance energy transfer (smFRET), a method that monitors in real-time the distance-dependent efficiency of energy transfer between a donor dye and a nearby acceptor dye.

Hybrid force-fluorescence techniques based on both OT and MT systems have been reported [19,21,22,25]; however, the integration of MT with smFRET has certain practical advantages. First, unlike MT systems which employ permanent magnets to apply stretching forces and torques, OT methods require the use of a high-power trapping laser which has the potential to induce photo-damage of the smFRET probes. Although this challenge can be overcome by inter-lacing the trapping laser with the smFRET excitation source using high frequency shutters or acousto-optical modulators (AOM) [26], implementing such a system remains an expensive and technically challenging endeavor. In contrast, a MT system is ideally-suited for integration with standard objective-type total internal reflection fluorescence (TIRF) microscopy [27] without concerns of induced photo-damage by a trapping laser. In addition, the relative simplicity of the magnetic tweezers and the possibility of setting up this assay utilizing a commercially available TIRF microscope should enable biochemistry laboratories to establish this assay ‘in house’ for studies of their particular system of expertise, rather than exclusively relying on collaborative efforts with groups that specialize in single-molecule biophysical techniques.

We have recently investigated the mechanical unfolding pathway of a human telomere DNA G-quadruplex (GQ) using the integrated magnetic tweezers and smFRET (MT-smFRET) assay [28]. Using this approach, we analyzed the force-dependent equilibrium and rate constants for telomere DNA GQ folding and unfolding, and determined the location of the transition state barrier along the DNA-stretching reaction coordinate. These studies provided

unique insights into the folding properties of telomere DNA GQ structures, have implications for the mechanisms of DNA binding proteins that resolve GQ structure during telomere maintenance, and demonstrate the general utility of the integrated MT-smFRET assay. Here, we describe in detail the method used in our studies of telomere DNA GQ structure. We note that although we describe the MT-smFRET system in the context of analyzing a specific DNA structure, this method can be readily adapted to studies of other biological macromolecules such as RNA and proteins.

Experimental Design

Preparation of sample chambers and antibody coated magnetic beads

As with all MT experiments, DNA molecules to be studied must be specifically attached between a microscope coverglass and a magnetic bead. Sample chambers are prepared by sandwiching two pieces of parafilm between a standard glass microscope slide and coverglass (Figure 5-1A). To prevent non-specific sticking of DNA and beads, the microscope slide is cleaned using a plasma-cleaner. Since this surface is not the side of the sample chamber that is imaged during the experiment, we do not perform any additional cleaning steps on the microscope slide. In contrast, the coverglass is extensively cleaned by a series of alternating sonication treatments in a strong base and acetone to reduce fluorescence background. Once assembled, sample chambers are heated on a hot block to melt and adhere the parafilm to the glass. The flow channels are treated with biotinylated bovine serum albumin (BSA), washed to remove the excess biotin-BSA, and then incubated with streptavidin (Figure 5-1B) Following the streptavidin incubation, flow channels are washed again in a suitable buffer (ie. 10mM Tris pH=8, 100 mM NaCl), and stored in a humidity chamber to prevent evaporation.

A wide variety of functionalized magnetic beads can be purchased from several different vendors. For the majority of our experiments, we have used either 1 micron or 2.8 micron diameter Dynal beads. The magnetic beads used in our experiments are coated with a polyclonal anti-digoxigenin antibody. Since these beads are not commercially available, we

couple the antibody to carboxyl-functionalized beads using a water-soluble carbodiimide crosslinker, and resuspend the beads in a buffer containing sodium azide for long-term storage.

Construction of smFRET-labeled DNA molecules for MT-FRET analysis

The molecules employed in a hybrid MT-smFRET experiment are minimally comprised of three separate fragments: (i) a segment that harbors the SOI, together with appropriately placed smFRET probes and a biotin modification for surface immobilization; (ii) a relatively long DNA handle to space the large magnetic bead away from the imaging surface; and (iii) a linker DNA fragment that contains digoxigenin-modified dUTP to be immobilized on the anti-digoxigenin coated magnetic bead (Figure 5-2). For experiments aiming to study torque-induced structural changes in DNA, it is necessary to topologically constrain the DNA molecule between the coverglass and the magnetic bead. Therefore, one must separate the SOI into an independent fragment and include an additional linker DNA fragment containing biotin-modified dUTP.

To prepare our SOI segment (telomere DNA GQ), we anneal three separate oligonucleotides: (i) a biotin-modified DNA strand with an acceptor FRET dye; (ii) a second DNA strand with an donor FRET dye and an engineered single-stranded DNA overhang that creates an EcoRI sticky end; and (iii) an unlabeled DNA fragment harboring a telomere DNA GQ forming sequence flanked by sequence that is complementary to each of the dye labeled strands (Figure 5-2A, left). The DNA oligonucleotides are generated synthetically (IDT) with site-specific amino modifications and we perform the specific dye coupling reaction in the lab, followed by reverse phase HPLC purification. Equimolar concentrations of each of the three DNA strands are mixed together in an annealing reaction that is heated and then slow cooled over a period of several hours. The efficiency of the annealing reaction can be determined using native polyacrylamide gel electrophoresis and a fluorescence gel scanner (Figure 5-2A, right).

The digoxigenin-modified linker DNA fragment is generated by performing a polymerase chain reaction (PCR) across the multiple cloning site (MCS) of pUC19 plasmid DNA in the presence of digoxigenin-11-dUTP (Figure 5-2B, left). Primers were designed to amplify a 1 kilobase DNA fragment with a selected endonuclease restriction site positioned approximately in the middle of the fragment. In this way, the digoxigenin-modified PCR product can be cut with BamHI to yield a ~ 500 basepair DNA linker fragment to be ligated onto one end of the DNA handle. The presence of modified-dUTP in the DNA reduces the cleavage efficiency of the BamHI restriction endonuclease; therefore, it is important to run a diagnostic agarose gel to determine the efficiency of DNA cleavage (Figure 5-2B, right).

The large magnetic bead introduces a substantial amount of background fluorescence if it is not sufficiently spaced away from the imaging surface in the TIRF microscope. We therefore used a large DNA fragment generated by cleaving commercially available lambda DNA with the EcoRI and BamHI restriction endonucleases. Using a low percentage agarose gel, we purify the 15,721 basepair (~ 5.3 microns contour length) DNA lambda fragment for use in our MT-smFRET DNA molecule ligation reaction (Figure 5-2C).

Ligation reactions were set up with a 1:1:1 molar ratio of the biotinylated smFRET-labeled SOI segment harboring an EcoRI sticky end, the purified EcoRI/BamHI lambda DNA handle, and the BamHI digested digoxigenin-modified DNA linker fragment (Figure 5-2D, left). Ligation reactions were run overnight at 16^{o}C in the presence of T4 DNA ligase and used directly in MT-smFRET measurements. The efficiency of the ligation reaction was determined by running a diagnostic agarose gel, and comparing an ethidium bromide stained image with a fluorescence scan for the smFRET dyes (Figure 5-2D, right).

Sample Immobilization

As can be seen in the diagnostic gel shown in Figure 5-2D, the ligation reactions used to generate the MT-smFRET DNA molecules are not 100% efficient. We therefore optimized our method of immobilizing the molecules on the sample chamber surface to minimize the presence of unwanted side products or unreacted material from the ligation

reactions (Figure 5-3). First, an empirically determined dilution of the ligation reaction is incubated with anti-digoxigenin coated magnetic beads that have been pre-blocked with BSA to avoid nonspecific sticking of the DNA (Figure 5-3A). The beads are next washed during a mangetic bead pull-down step to remove any DNA fragments that were not ligated to an anti-digoxigenin DNA linker fragment (Figure 5-3B). The washed beads bound with DNA are next introduced onto the streptavidin coated coverglass (see Fig. 1) and permitted to settle to the surface by gravity over a period of ~ 20 minutes. Following this incubation period, unbound beads are gently washed out of the sample chamber using gravity controlled buffer flow to prevent excessive force that might rip the beads off of the surface. In this way, our immobilization strategy greatly enriches for those beads that are specifically bound to the streptavidin coverglass and the anti-digoxigenin coated magnetic bead (Figure 5-3C).

Calibration of MT-applied forces

In a MT experiment, the force being applied to the DNA molecule tethered between the coverglass and the magnetic bead can be directly extracted by measuring the length of the DNA tether and the amplitude of beads lateral fluctuations in the x-y plane (Figure 5-4A). The methods used for tracking the height of the tethered bead from the surface (z-position), as well as tracking the x- and y-positions of the bead in real-time have been described [17], and will therefore not be described in detail in this protocol. In the context of the integrated MT-smFRET experiment it is desirable to determine a precise calibration of the stretching force applied as a function of a well-controlled distance between the top of the sample chamber and the magnet assembly (Figure 5-4B). In this way, the force can be directly estimated from the magnet height across a large number of DNA tethers without performing individual force calibrations on each molecule. One critical assumption made by this approach is that the magnetic beads used in the experiments are highly uniform, both in their shape and size, as well with respect to their iron content. In this regard, we have found the 1 micron (MyOne) beads from Dynal to be sufficiently uniform so as to provide force estimates with an error of ~ 10% between different beads. This level of accuracy is sufficient for most

low force experiments (< 5 pico-Newtons, pN). Moreover, the precision of the calibrated forces can be assessed by fitting DNA force-extension curves with the well-established worm like chain model for DNA elasticity (Figure 5-4C) [29,30]. In contrast, when larger forces (> 10 pN) are required, the 2.8 micron magnetic beads must be employed. For these experiments, we find the size distribution of the beads to be too large to use a general calibration, and therefore forces are calibrated on each DNA molecule following each MT-smFRET measurement.

Design and construction of a hybrid MT-smFRET microscope

The MT-smFRET instrument layout is illustrated in Figure 5-5. The instrument is built on a standard objective-type total internal reflection fluorescence (TIRF) microscope equipped with an electron multiplying charged coupled device (EMCCD) with single-molecule detection sensitivity. The excitation lasers are coupled through the back port of the microscope and guided to the sample through an oil-immersion (NA 1.4) objective. The same objective is used to collect the fluorescence emission from the sample, which is then split by imaging optics into FRET donor and acceptor channels, before being imaged onto the EMCCD camera. The microscope objective is mounted onto a piezo-controlled stepping device, which is critical for calibrating the z-position of the magnetic bead during force calibrations. In addition to the EMCCD camera, we use a lower magnification CCD camera mounted to a sideport of the microscope to screen for molecules of the correct length using a video monitor. We note that although we have chosen to build our TIRF microscope ourselves, there are a large number of commercially available systems that would be suitable for the MT-smFRET assay described in this protocol. In a TIRF microscope, the excitation illumination penetrates ~100-200 nanometers into the sample chamber, thereby suppressing fluorescence background and providing a highly favorable signal-to-noise ratio for single-molecule imaging applications.

The use of objective-type TIRF microscopy provides an ideal geometry for integrating a MT system, which must be built above the sample chamber. The magnetic tweezers

apparatus consists of a pair of rare earth magnets mounted onto a set of computer controlled translation and rotation stages. This automated motor assembly is used to change the linear position and angular displacement of the magnets to apply specific degrees of tension and twist, respectively, to individual DNA molecules. When necessary, we directly image the magnetic bead using a blue LED light source mounted on top of the magnet assembly. There have been a variety of MT systems described, using different translation stages and motors to drive the magnet positioning system. For our instrument, we have designed a custom magnet holder that mounts directly onto a brushless rotation stage with a built in digital encoder, which provides a vibration free mechanism of rotating the magnets at arbitrary speeds with high angular precision. Moreover, we have built the MT assembly, including magnets, computer-controlled stages, and light source, into a single stand-alone component that can be easily mounted to fit any inverted light microscope.

The hybrid MT-smFRET microscope is controlled by a series of LabView programs that allow the user to adjust the camera settings for data acquisition, control and monitor the stages for magnet positioning, as well as to perform the necessary bead tracking and piezo-driven objective stepping required during force calibrations. All LabView programs are available upon request; however, we note that the programs are designed to interface with the specific hardware used in our system.

Zero force control smFRET experiments

In force spectroscopy experiments, the behavior of the SOI under zero force conditions is often determined by extrapolating the experimentally determined force-dependent behavior to zero force. In our MT-smFRET measurements, we have the unique capacity to directly measure the zero-force condition by analyzing the behavior of the SOI in the absence of the long DNA handle and bead (Figure 5-6A). In addition to providing a direct measurement of the zero-force behavior of a SOI, these control experiments help to rapidly identify the suitable salt and buffer conditions for the MT-smFRET assay, as well as to

characterize the expected FRET states for the folded and unfolded conformation of our SOI (telomere DNA GQ) (Figure 5-6B and 5-6C).

MT-smFRET measurement

As with all MT assays, the experiment begins with a large number of candidate molecules tethered between the coverglass and a magnetic bead. A MT-smFRET measurement starts by first identifying a DNA molecule of the appropriate length. This process is greatly facilitated by the use of a low magnification CCD camera that is connected to an external video monitor, but can also be achieved using the eye pieces of the microscope. Once a candidate molecule is found, it is centered on the eye-piece which is aligned with the EMCCD camera used for the MT-smFRET measurement. At this point a series of quality control checks is performed on the molecule before data collection can begin. First, we use the rotation stage to rapidly introduce ~200 turns into the DNA molecule. Since the molecules in our experiment are not torsionally constrained, the length of the DNA tether should not change as turns are introduced. If the length does change, then this indicates the bead is tethered to the surface by more than one DNA molecule and cannot be used for data collection. If the length of the DNA tether is not affected by rotating the magnets, we next determine whether the molecule has an active pair of FRET dyes. Although our microscope uses a dual band dichroic filter, which nominally blocks the blue LED light, when the EMCCD camera is set up for single-molecule imaging the small amount of blue light that leaks through the filter can be readily imaged in the donor channel of our imaging optics (Figure 5-5). In this way the bead can be centered on the middle of the viewing area. Next, the blue LED is switched off and the red laser is turned on to check for an active acceptor (Cy5) dye that is located directly below the magnetic bead. This step also provides an opportunity to focus the objective on the surface of the coverglass. If an active acceptor dye is observed, then the red laser is switch off and the green laser is turned on to directly excite the smFRET donor (Cy3) dye. Data is then acquired at the user-determined frame rate (typically 10-30 frames per second) and desired stretching force (Figure 5-7) until irreversible

photo-bleaching of one of the smFRET dyes is observed. Raw movie files are subsequently analyzed using a separate set of LabView programs to extract background corrected time series of FRET values for each experiment. Data analysis LabView programs are available upon request.

Reagents and Equipment

Reagents

- 1-Ethyl-3-(3-dimethylaminopropyl)carbodiimide (EDC; Thermo Scientific, cat. no. 77149)
- 2-(*N*-morpholino)ethanesulfonic acid (MES; Sigma, cat. no. M3671)
- +/- 6-hydroxy-2,5,7,8-tetramethylchroman-2-carboxylic acid (Trolox; Aldrich, cat. no. 238813)
- 10 x Phosphate-buffered saline (PBS; Mediatech, cat. no. 46-013-CM)
- NE Buffer 3 (New England Biolabs, cat. no. B7003S)
- Acetone (Fisher Scientific, cat. no. A929SK-4)
- Acetonitrile (Fisher Scientific, cat. no. A998-4)
- Agarose (Thermo Scientific, cat. no. 17852)
- Alconox (VWR International, cat. no. 21835-032)
- Anti-digoxigenin (Roche, cat. no. 11333089001)
- BamHI (New England Biolabs, cat. no. R0136M)
- Biotinylated BSA (Sigma, cat. no. A8549)
- Biotinylated DNA oligonucleotide (5’ TCT(AminoC6)CCATTTTCCTATTACCGGTGCCACGC-Biotin 3’; Integrated DNA Technologies)
- Bovine serum albumin (BSA; New England Biolabs, cat. no. B9001S)
- Carboxylated magnetic bead (Invitrogen, cat.no. 650.11)
- Catalase (CalBiochem, cat. no. 219001)

- DNA ligase (New England Biolabs, cat. no. M0202S)
- Digoxigenin-11-dUTP (Roche, cat. no. 11558706910)
- EcoRI (New England Biolabs, cat. no. R0101M)
- EcoRI DNA oligonuclecleotide (5' Phosphate-AATTGTGCACGTAGCT(Amino C6)G 3'; Integrated DNA Technologies)
- Ethanol (EtOH; Gold Shield)
- Ethanolamine (Sigma, cat. no. 398136)
- Structure of interest (SOI) oligonucleotide (5' GCGTGGCACCGGTAATAGGAAAATGGAGA abasic spacer $(TTAGGG)_4$ abasic spacer CAGCTACGTGCAC-3'; Integrated DNA Technologies)
- Glacial acetic acid (Fisher Scientific, cat. no. A38-500)
- Glucose oxidase (Sigma, cat. no. G2133)
- Lambda DNA (New England Biolabs, cat. no. N3011S)
- Cy3 monoreactive dye packs (GE Healthcare, cat. no. PA23001)
- Cy5 monoreactive dye packs (GE Healthcare, cat. no. PA25001)
- Nitrogen gas (Praxair Gas)
- QIAEX II Gel Extraction Kit (Qiagen, cat. no. 20051)
- QIAquick PCR Purification Kit (Qiagen, cat. no. 28106)
- Sodium Acetate (NaOAc; Sigma, cat. no. 25022)
- Sodium Azide (MP Biomedicals, cat. no. 102891)
- Sodium bicarbonate ($NaHCO_3$; Fisher Scientific, cat. no. S233)
- Sodium chloride (NaCl; Fisher Scientific, cat. no. S641-212)
- Sodium hydroxide (NaOH; Fisher Scientific, cat. no. BP359-500)
- Streptavidin (Invitrogen, cat. no. S888)
- Taq DNA polymerase with standard Taq buffer (New England Biolabs, cat. no. M0273S)

- Triethanolamine (TEA; Fisher Scientific, cat. no. W635-07)
- Tris-HCl (Fisher Scientific, cat. no. BP153)
- dNTP (New England Biolabs, cat. no. N0446S)
- pUC19 (New England Biolabs, cat. no. N3041S)
- pUC 19 primer I (5' ACATTTCCCCGAAAAGTGCCA 3'; Integrated DNA Technologies)
- pUC 19 primer II (5' GTTTCGCCACCTCTGACTTGA 3'; Integrated DNA Technologies)
- Nuclease-free H_2O (Ambion, cat. no. AM9932)

Equipment

- Glass staining jar (Wheaton, cat. no. 900570)
- Cover glass slides (Corning, cat. no. 2947-3x1)
- Ultrasonic cleaner (Branson)
- Imaging glass slides (22x30mm, 0.16-0.19mm thick; Ted Pella, cat. no. 260150)
- Propane torch (Aldrich, cat. no. 318574)
- Parafilm (Pechiney Plastic Packaging, cat. no. S37441)
- Heat block (Fisher Scientific)
- Microcentrifuge tubes (Costar, cat. no. 3620)
- Microcentrifuge (Fisher Scientific)
- Milli-Q H_2O (Millipore)
- Quartz slide (Ted Pella, cat. no. 2601)
- Aluminum foil
- Vacuum centrifuge (Eppendorf)
- C8 HPLC column (Agilent Technologies, cat. no. 990967-906)
- AKTA purifier (GE Healthcare)
- Nanodrop UV-Vis Spectrophotometer (Thermo Scientific)

- PCR Thermal Cycler (Bio-Rad)
- Sterile disposable syringe (BD, cat. no. 309659)
- Filter (Millex-GV, cat. no. SLGV013SL)
- Plasma cleaner (Harrick, cat. no. PDC-3xG)
- Magnetic separation rack (New England Biolabs, cat. no. S1506S)

Single-molecule objective-type total internal reflection fluorescence (TIRF) microscope

- Inverted microscope (Olympus, cat. no. IX711F5)
- 100x oil objective (NA=1.4, Olympus, cat. no. 1-U2B836)
- Piezo positioner (Mad City Labs, Inc. cat. no. Nano-F100 with USB201 controller)
- CCD detector (iXon EMCCD camera; Andor Technologies, product code. DU-860E-C50-#BV)
- Green Laser (532 nm; Laserglow Technologies, model no. LRS-0532-CFM-00200-10)
- Red Laser (630 nm; Uniphase, model no. 1135)
- Neutral density filters (Thorlabs, Inc. part no. NE03B, NE05B, NE10B, NE20B, NE30B, NE40B)
- Shutter (Vincent Associates, part no. LS6Z2)
- Broadband mirrors (Thorlabs, Inc. part no. BB1-E02)
- Beam splitter (Thorlabs, Inc. part no. PBS101)
- Waveplate (Thorlabs, Inc. part no. WPMH05M-532)
- Slit (Thorlabs, Inc. part no. VA100/M)
- Dichroic mirror 1 (Omega Optical, part no. XF2009)
- Dichroic mirror 2 (Semrock, part no. FF560/659-Di01-25x36)
- Dichroic mirror 3 and 4 (Semrock, part no. FF662-FDi01)
- Band Pass Filter (Semrock, part. no. FF01-577/690-25)

- Lens 1 (Thorlabs, Inc. part no. AC254-300-A1)
- Lens 2, 3, and 4 (Thorlabs, Inc. part no. AC254-150-A1)
- Standard lever pinholes (Thorlabs, Inc.)

Magnetic tweezers (MT)

- Collimated LED (Thorlabs, Inc. part no. M470L2-C1)
- Magnets (K&J Magnetics, Inc. part no. B444-N52)
- Miniature linear stage LDC-25 (Pacific Laser Equipment, part no. LDC-25)
- DC servo controller (Pacific Laser Equipment, part no. DSP-21)
- Rotational stage (Pacific Laser Equipment, part no. PRD-20)
- Special DC brushless controller (Pacific Laser Equipment, part no. DSP-23K)
- OWIS XY stage KT 65 (Pacific Laser Equipment, part no. 16.362.0300 KT 65)

Reagent and Equipment Setup

Reagent Setup

- **1x PBS** 1x PBS is prepared by diluting 10x PBS with ddH_2O.
- **T50 Buffer** T50 buffer is prepared by mixng 10 mM Tris-HCl (pH 8.0) and 50 mM NaCl or by duliting a 1:1 molar ratio of 2x T50 and ddH_2O.
- **2x T50 buffer** 2x T50 Buffer is prepared by mixing 20 mM Tris-HCl (pH 8.0) and 100 mM NaCl.
- **Blocking buffer** Blocking buffer is prepared by mixing 5 mg/mL of BSA and T50 buffer.
- **Buffer A:** Buffer A contains 100 mM tri-ethylammonium acetate, pH 7.0 adjusted with glacial acetic acid.
- **Coupling buffer:** Coupling buffer contains 100 mM MES, pH = 6.0, adjusted with NaOH.
- **Equilibration buffer:** Equilibration buffer is prepared by mixing 50 mM Tris-Cl (pH = 8.0) and 100 mM NaCl.

- **Oxygen Scavenging System (Gloxy):** Gloxy solution is prepared by mixing 100 mg/mL of glucose oxidase, 4 mg/mL of catalase and T50 buffer. (**CRITICAL STEP**: Store the Gloxy solution in 4°C up to 7 days)
- **Imaging buffer:** Imaging buffer includes 50 mM Tris-HCl (pH 8.0), 100 mM NaCl, 0.4% w/v B-D-glucose, 1% v/v gloxy solution, and is then saturated with Trolox and filtered twice through a 0.2 micron syringe filter. (**CRITICAL STEP**: it is essential that all un-dissolved TROLOX is removed from the imaging buffer as it can lead to increased fluorescence background and may influence the mechanical properties of the SOI.)

Equipment Setup

- **Hybrid MT-smFRET microscope**

  We use a custom-built objective-type TIRF microscope for single-molecule imaging (**Fig. 5**). An Olympus IX71 inverted microscope is adapted to hold a custom-built magnet assembly together with a collimated blue LED illumination source for direct imaging of the magnetic beads. The magnet assembly is comprised of computer-controlled translation and rotation stages that precisely control the magnet height and angular displacement, which determines the degree of stretching force and twist applied to the DNA molecule. During initial screening for DNA tethers of the appropriate length, the blue LED light source is used to image the beads and the collected light is directed by a mirror toward a low magnification CCD camera connected to an external video monitor. After a candidate molecule is found at low magnification, this mirror can be removed from the path by a manual slider, so that the microscope may operate in smFRET mode. Excitation lasers (532 nm and 633 nm) for smFRET measurements are directed through an optical path that expands the beam diameter ten-fold prior to entering a lens which focuses the laser onto the back focal plane of an Olympus oil-immersion microscope objective (NA 1.4). The focusing lens is mounted on manually controlled linear translation stage, which

offsets the position of the entering laser to achieve the critical angle required for total internal reflection fluorescence (TIRF) microscopy. Excitation laser paths include computer-controlled shutters, neutral density filters for course grained power adjustments, and a combination of polarizing beam splitters with a wavelength matched half-wave plate for fine laser intensity adjustments. In addition, the paths of the red and green excitation lasers are combined using an appropriate dichroic mirror. The lasers entering the back port of the microscope are directed up toward the sample by a dual-band dichroic mirror and emitted fluorescence is collected by the microscope objective and passed through the appropriate dual-band emission filter for Cy3/Cy5 imaging. The emitted light is then passed through an imaging slit positioned at the image plane on the side port of the microscope, split into the donor and acceptor channels using appropriate dichroic mirrors, before being imaged onto a 128 x 128 Andor iXon EM-CCD camera. For force-calibrations, the magnetic bead is imaged directly using the collimated blue LED source with all of the dual band dichroic mirror and emission filters removed from the path. When imaged through an oil immersion objective with a collimated light source, the bead appears as a series of concentric diffraction rings which can be used to calibrate the distance of the bead from the coverglass as described elsewhere [17]. During calibration of the bead position, the objective is stepped in precisely defined increments using a piezo-driven objective positioning device.

- **Software**

  Raw movie files are captured in binary format using an Andor iXon 860 EM-CCD camera and custom camera control software written in Labview using the Andor software development. Post-processing of the data to extract the donor and acceptor dye intensities, or in the case of force calibration the x-,y-, and z-axis positions of the magnetic bead, is also performed using custom written Labview programs. All other hardware components, including the magnet assembly and laser shutters, are

controlled using a National Instruments PCI-6251 DAQ board and custom written Labview programs. The specific methods used to track the magnetic bead position during force calibration have been described elsewhere [17]. To analyze the smFRET data, the location of the donor and acceptor dye in the image is selected manually by the user. Based upon these user inputs, a 9x9 array of pixels is selected centered on each spot. At each frame, the most intense pixel within the 9x9 array was determined and correlated to previous positions to detect spurious peaks resulting from noise. In most cases the instrument noise did not shift the maxima more than a pixel. Once a local maximum was determined, a 3x3 array surrounding the maximum was summed as the dye intensity. Depending on user input, a region of varying size around the maximum pixel was used for background determination, typically a 12x12 pixel region was selected. Note array sizes will vary depending on the specific magnification of the microscope. Once the software extracts the numerical fluorescence signals, we calculate the FRET efficiency for each individual molecule as the acceptor intensity divided by the sum of the donor plus the acceptor intensity. Single-molecule FRET time trajectories are typically next processed using custom written Matlab programs, or are fit with the HaMMy software package [31] to generate idealized FRET traces used for subsequent data analysis. All custom Labview software is available upon request.

Procedure

Preparation of sample chambers

1. Place the coverglasses to be imaged in a glass staining jar.
2. Sonicate for 20 min in 10% w/v Alconox.
3. Decant all the Alconox out of the glass staining jar and rinse the coverglasses with excess Milli-Q H_2O.
4. Sonicate the imaging glass slides for 20 min in Milli-Q H_2O.

5. Decant all the Milli-Q H_2O out of the glass staining jar and rinse the coverglasses with excess Milli-Q H_2O.
6. Sonicate the coverglasses for 20 min in acetone. (**CAUTION**: Acetone is flammable and is a skin and eye irritant. Use it under a chemical fume hood.)
7. Discard the acetone from the glass staining jar.
8. Dry the coverglasses and the glass staining jar with nitrogen gas.
9. Sonicate the coverglasses for 20 min in sterile filtered1M KOH again. (**CAUTION**: KOH is corrosive and is a skin and eye irritant. Use it under a chemical fume hood.)
10. Discard the 1M KOH.
11. Sonicate the coverglasses for 20 min in fresh sterile filtered 1M KOH.
12. Rinse the coverglasses with excess Milli-Q H_2O.
13. Take out the coverglasses from the glass staining jar. (**CRITICAL STEP**: The coverglasses are fragile. A clean tweezers is recommended during coverglass handling). Store the cleaned coverglasses in Milli-Q H_2O covered up to 2 weeks.
14. To begin sample chamber assembly, start by drying one of the cleaned coverglasses with nitrogen gas.
15. Place coverglass on top of a clean quartz slide.
16. Quickly flame the top surface of the coverglass using a handheld propane torch to burn away any fluorescent organic molecules. (**CAUTION:** Use caution when handling the propane torch.) (**CRITICAL STEP**: The coverglasses are fragile under flame, therefore avoid excessive heating during this step).
17. Allow the coverglass to cool down to room temperature
18. Repeat steps 16 and 17 three times.
19. Plasma-clean microscope glass slide for 5 min.
20. Assemble sample chambers by sandwiching strips of parafilm between an microscope glass slide and a coverglass (**Figure 5-1A**)

21. Place the assembled slide in between two 95°C heat blocks for 15 s to adhere the parafilm to the glass.
22. Allow the assembled slide cool down to room temperature. **PAUSE POINT** The assembled sample chambers can be stored up to two weeks.
23. Pipette 35μL of 1mg/mL of biotinylated BSA into sample chamber, and incubate for 5 min (**Figure 5-1B**).
24. Wash the chamber with 100μL of T50 buffer, using a Kimwipe to draw liquid from pipette tip into sample chamber. (**CRITICAL STEP**: Avoid air bubbles during buffer exchange into the sample chamber).
25. Incubate 50μL of 0.2mg/mL streptavidin in sample chamber for 1 min.
26. Wash the chambers with 100μL of T50 buffer.
27. Equilibrate the chambers with 100μL of equilibration buffer.
28. Store the equilibrated slides in a humidity box to avoid evaporation. A humidity box can be made using an by filling the bottom of an empty pipette tip box with some water and covering tightly with lid.

Preparation of DNA molecules for MT-smFRET measurement

29. **Preparation of the structure of interest (SOI) segment (Figure 5-2A)**

    (A) Dye labeling DNA oligonucleotides

    (i) Dissolve amino-modified DNA oligonucleotides to be FRET labeled (50 nmol) in 30μL Milli-Q H_2O and transfer to a 1.5ml of microcentrifuge tubes. Precipitate the DNA with 3 μL of 3M NaOAc and 90 μL of -20 °C EtOH at -80 °C for 10 min in the Microcentrifuge tubes (**CAUTION:** EtOH is flammable and is a skin and eye irritant. Use it under a chemical fume hood.) Centrifuge the Microcentrifuge tubes at 17500 RPM for 30 min at 4 °C. Dry the DNA pellets in vacuum centrifuge for 5 min at room temperature and dissolve the pellets in 100 μL of Milli-Q H_2O.

(ii) Dissolve the mono-reactive dye packs (Cy3 or Cy5) with 50 µL of 0.2M $NaHCO_3$, combine with 50 µL of the appropriate resuspended DNA oligonucleotide, and incubate at 37 °C for 2 h. (**CRITICAL STEP**: Cy3 and Cy5 dyes are light sensitive, aluminum foil is recommended to cover the reaction tube to prevent photo bleaching of Cy5 dyes.)

(iii) Precipitate the dye labeled DNA handles with 10 µL of 3M NaOAc and 275 µL of -20 °C EtOH at -80 °C for 10 min in the microcentrifuge tubes. (**CAUTION:** EtOH is flammable and is a skin and eye irritant. Use it under a chemical fume hood.) Centrifuge the Microcentrifuge tubes at 17500 RPM for 30 min at 4 °C. Dry the pellets in vacuum centrifuge for 5 min at room temperature.

(iv) Redissolve the pellets in 60 µL of Buffer A and purify the dye-labeled DNA oligonucleotides using reverse-phase HPLC with a C8 column on an AKTA purifier as described [32].

(B) Annealing reaction for SOI segment

(i) Determine the concentrations of the dye-labeled DNA oligonucleotides and SOI oligonucleotide using a NanoDrop UV spectrophotometer. Make appropriate dilutions in Milli-Q H_2O to obtain a 1 µM concentration solution of each dye-labeled and SOI DNA oligonucleotide.

(ii) Mix the dye-labeled and SOI DNA oligonucleotide at a 1:1:1 molar ratio in T50 Buffer in 1.5 µL Microcentrifuge tube in a final volume of 30 µL, yielding a final concentration of 0.1 µM of each DNA oligonucleotide.

(iii) Anneal the SOI segment by heating the solution to 95°C for 4 min, followed by slow cooling to room temperature. (**CRITICAL STEP**: running a native gel is recommended for checking the annealing efficiency of the fluorescent labeled SOI segment (**Figure 5-2A, right**).

30. **Preparation of digoxigenin-modified DNA fragment (Figure 5-2B)**

(A) Prepare100 µL reaction in a microcentrifuge tube on ice (Table 5-1).

(B) Place the PCR tubes in a thermal cycler using the program shown in Table 5-2.

(C) Purify PCR products with QIAquick PCR purification kit, eluting the digoxigenin-modified DNA linker in Milli-Q H_2O.

(D) Digest the digoxigenin-modified DNA linker with BamHI at 37°C for 4 h, by preparing a 50 µL reaction in a microcentrifuge tube (Table 5-3).

(E) Separate the digested products from enzyme with the QIAquick PCR purification kit. (**CRITICAL STEP**: running a 1% agarose gel is recommended to check the enzymatic digestion efficiency (**Figure 5-2B, right**)).

31. **Preparation of DNA handle segment (Figure 5-2C)**

(A) Digest full-length lambda DNA at 37°C for 2 h with BamHI and EcoRI by preparing a 100 µL reaction in a microcentrifuge tube (Table 5-4).

(B) Purify the 15721 bp lambda BamHI/EcoRI digestion product on a 0.7% agarose gel using a QIAEX II Gel Extraction Kit and elute in Milli-Q H_2O.

32. **DNA ligation reaction for constructing MT-smFRET molecules (Figure 5-2D)**

(A) Make the final MT-smFRET molecule by setting up a DNA ligation reaction in a final volume of 20 µL and incubating overnight at 16°C (Table 5-5). Store molecules in ligation reaction mixture at 4°C. **(CRITICAL STEP**: To optimize ligation efficiency, the indicated concentrations of the SOI and DNA linker segments should be adjusted for annealing and BamHI digestion efficiencies. In addition, the efficiency of the final ligation reaction may be analyzed by comparing an ethidium bromide stained agarose gel with the same gel imaged by Cy3 and Cy5 fluorescence on a gel scanner (**Figure 5-2D, right**)).

Preparation of anti-digoxigenin-coated magnetic beads

33. Take 500 µL of carboxylated magnetic bead solution from the storage buffer.
34. Wash the beads using a magnetic rack with 1.5 mL of coupling buffer twice.
35. Dissolve the anti-digoxigenin in 200 µL of coupling buffer.

36. Mix the beads with the anti-digoxigenin solution.
37. Dissolve 10 mg of EDC in 1 mL of 4°C coupling buffer.
38. Add 50 µL of EDC solution to the beads and anti-digoxigenin mixture.
39. Tumble the reaction mixture at 4°C for 2 h.
40. Wash the beads with 500 µL of 0.2 M ethanolamine twice to quench the reaction and tumble at room temperature for 2 h.
41. Wash the beads with 1mL of 1xPBS buffer twice.
42. Store the anti-digoxigenin beads in 1.3 mL of 1X PBS + 0.02% w/v sodium azide at 4°C. (**CAUTION:** Sodium azide is toxic, therefore handle stock solution (2% w/v) in a chemical hood and wear protective equipment whenever handling any solutions containing sodium azide). (**CRITICAL STEP:** We find a single preparation of antibody coated magnetic beads is typically sufficient to last about one year).

Surface immobilization of DNA molecules for MT-smFRET measurement **TIMING** 2-3h

43. Mix anti-digoxigenin-coated magnetic beads with 750 µL 2x T50 buffer.
44. Place the DNA-magnetic bead and 2x T50 buffer mixtures on a magnetic separation rack.
45. Pipette out the supernatant, and repeat steps 43 - 45.
46. Block the anti-digoxigenin-coated magnetic beads with 500 µL of Blocking buffer at 4°C for at least 1 h.
47. Dilute the DNA ligation to 1:5 with 1X T4 DNA ligase buffer.
48. Incubate 6 µL of diluted DNA ligation with 3 µL of blocked anti-digoxigenin-coated magnetic beads at 4°C for 10 min. (**CRITICAL STEP**: We have found the efficiency of DNA binding to the anti-digoxigenin beads varies between batches, so it is necessary to empirically determine the DNA binding conditions for each preparation of MT-smFRET molecules and antibody-coated beads).
49. Gently agitate the DNA-magnetic bead mixture every 2 min.
50. Place the DNA-magnetic bead mixtures on a magnetic separation rack.

51. Carefully pipette out the supernatant (**CRITICAL STEP**: It is important not to disturb the pellet)
52. Resuspend DNA-bound magnetic beads with 200 µL blocking buffer, and repeat steps 50-52.
53. Store the DNA- bound magnetic beads in 15 µL blocking buffer at 4°C for up to one day.
54. Mix 6 µL of DNA-bound magnetic beads with 194 µL of equilibration buffer.
55. Deposit 100 µL of DNA-magnetic bead in equilibration buffer to the streptavidin-coated chamber.
56. Incubate the DNA-magnetic mixture at room temperature for 30 min in a humidity chamber with the coverglass side faced down to allow the DNA-bound magnetic beads to settle to the surface by gravity.
57. Wash the chamber with 100 µL of equilibration buffer by gravity to remove the unattached DNA-linked magnetic beads (**CRITICAL STEP**: Avoid rapid exchange of buffers, as the hydrodynamic drag on the magnetic bead can remove the DNA-bound magnetic beads from the surface. To control the rate of flow we set the sample chamber at a slight angle on the bench top and pipette a small volume onto one side of the flow cell, allowing the liquid to enter by gravity).
58. Flow 100 µL of imaging buffer to the chamber by gravity.

MT-FRET measurement

59. Prepare imaging buffer with oxygen scavenging system by mixing 2 µL of gloxy solution with 200 µL of imaging buffer.
60. Gently flow 100 µL of imaging buffer plus oxygen scavenging system into the chamber by gravity.
61. Place a drop of index-matched low fluorescence immersion oil (Type DF) on the microscope objective, and then place the sample chamber on the microscope with the coverglass side down.

62. Turn on the blue LED light.
63. Move the magnet several few millimeters above the slide to apply sufficient stretching force to extend the DNA molecule (~2-4 pN). Then use the low magnification side port CCD camera and video monitor to locate a bead that appears to be fluctuating the expected distance from the surface. Since the DNA tethers for our MT-smFRET experiments are long (~5 microns) this qualitative screening step is readily achieved by eye.
64. Next, rotate the magnets to positive 200 turns (counter-clockwise) to check if the bead is anchored by a single DNA molecule. The extension of a single MT-smFRET DNA tether that is not torsionally constrained should not change as turns are introduced. Again, changes in the z-position of the bead are readily detected by eye during this step. In the case of an experiments utilizing a torsionally constrained DNA tether, this same check can be performed. However in this instance, one can use the differential response of positively and negatively supercoiled DNA to stretching force as a check for the presence of a single DNA tether (**CRITICAL STEP**: This first quality control step is very important to ensure that the magnetic bead is not tethered by multiple DNA molecules, which will confound the measurement since the stretching force will be shared between the molecules.)
65. Next, use the manual slider to remove the mirror that directs the image to the low magnification CCD camera, so that the microscope can operate in smFRET mode. We note that although the emission filters and dichroic mirrors we use should nominally block the blue LED light source, a small amount of the blue light leaks through the system and can be imaged in the donor channel of the smFRET detection optics when the EM-CCD camera is operating with single-molecule sensitivity. This course bead image is useful in deciphering whether the smFRET dyes are coaxially positioned with the magnetic bead in the following steps.

66. Use the red (633 nm) laser to verify the presence of an active Cy5 dye located directly under the magnetic bead bead. Since the dye molecule is located ~5 microns away from the magnetic bead, it is necessary to focus the objective down toward the surface to observe the fluorescence signal.
67. Next, use the green (532 nm) laser to verify the presence of an active Cy3 molecule located directly under the magnetic bead.
68. Once the presence of an active smFRET pair has been verified, set the magnet assembly to a desired linear position, acquire movie (typically 10-30 frames per second) until dyes bleach. (**CRITICAL STEP**: It is important to exchange the oxygen scavenging system in the chamber after every hour of data collection, because it will gradually cause a drop in pH over time. The rate of pH change will be dependent on the choice of buffer used in the imaging buffer, therefore it is useful to characterize the timescale of stable pH for each experimental system).

Data analysis

All data is written in raw binary format directly to disk. To analyze the data, and extract the donor and acceptor intensities, we use programs written in Labview. These programs read in the movie file and allow the user to specify the location of the donor and acceptor dyes, as well as to input the size of the window to be used in calculating the background levels. Once the data are run through these programs, the data is then analyzed using custom written scripts written in Matlab. If the experiment requires dwell time distributions to be constructed from multi-state smFRET data, the individual traces are typically fit with the HaMMy [31] software to generate idealized smFRET tragectories.

Timing

Steps 1 – 28: Preparation of sample chambers: 3 – 4 h

Steps 29 – 32: Preparation of MT-smFRET molecules: 3 days

Steps 33 – 42: Preparation of anti-digoxigenin-coated magnetic beads: 5 h

Steps 43 – 58: Surface immobilization of DNA molecules for MT-smFRET measurement:2 h

Steps 59 – 68: MT-FRET measurement: various

Step 69: Data analysis: at least 30 min.

Anticipated Results

In the absence of stretching force, smFRET experiments performed with the telomere DNA GQ in the presence of 100 mM NaCl revealed conformational dynamics indicative of transient folding and unfolding transitions (**Figure 5-6B**). Using the integrated MT-smFRET assay described in this protocol we investigated the impact of stretching force on telomere DNA GQ folding and unfolding (**Figure 5-7**) [28]. A representative smFRET trajectory of a telomere DNA GQ molecule held under three different stretching forces in the MT is shown in **Figure 5-7A**. The effect of applied tension is immediately obvious: when held under high tension (5.2 pN) the DNA molecule spends the majority of the time in the unfolded (low FRET) state , whereas at lower tension (0.4 pN) the DNA molecule is predominantly in the folded GQ conformation (high FRET) (**Figure 5-7A and 5-7C**). At intermediate tension (2.6 pN) the DNA molecule samples both the folded and unfolded conformations. The data were fit with a hidden Markov model using the HaMMy software package to produce an idealized smFRET trajectory [31], which can then be used to extract quantitative information about the mechanical unfolding pathway for a telomere DNA GQ. The MT-smFRET approach should be readily adapted for biophysical studies of the mechanical properties of a wide variety of biomolecules including DNA and proteins.

Table 5-1

Preparation of digoxigenin-modified DNA PCR reaction

	Volume (μL)
pUC19 plasmid (10 ng/μL)	1
10X Taq reaction Buffer	10
Standard Taq DNA polymerase	1
pUC19 primer I (100 μM)	1
pUC19 primer II (100 μM)	1
dATP (10 mM)	5
dCTP (10 mM)	5
dGTP (10 mM)	5
dTTP (10 mM)	4
Digoxigenim-11-dUTP (1 mM)	1
Nuclease-free H_2O	66

Table 5-2

PCR thermal cycler for Preparation of digoxigenin-modified DNA

Step 1	3 min at 95 °C
Step 2	45 s at 95 °C
Step 3	30 s at 55 °C
Step 4	1 min at 72 °C
Step 5	Repeat Step 2 to Step 4 30 times
Step 6	10 in at 72 °C

Table 5-3

Digest reaction for the digoxigenin-modified DNA linker with BamHI

	Volume (µL)
Digoxigenin - modified DNA linker	x
10X NE Buffer 3	5
BSA (10 mg/ml)	5
BamHI (100,000 U/mL)	5
Milli-Q H_2O	35-x

Table 5-4

Digest reaction for the lambda DNA with BamHI and EcoRI

	Volume (µL)
Lambda DNA (500 µg/ml)	30
10X NEBuffer 3	20
BSA (10 mg/ml)	20
BamHI (100,000 U/mL)	5
EcoRI (100,000 U/mL)	5
Milli-Q H_2O	20

Table 5-5

Ligation reaction for the final MT-smFRET molecule

	Volume (µL)
SOI segment (0.3 µM)	2
DNA linker segment (0.3 µM)	2
DNA handle segment (0.3 µM)	2
10x T4 DNA ligase buffer	2
ATP (10 mM)	2
T4 DNA ligase (5,000 U/mL)	2
Milli-Q H_2O	8

Table 5-6

Troubleshooting

Step	Problem	Reason	Solution
30	Low digestion efficiency	High density of digoxigenin-modified nucleotide in the PCR fragments	• Increase the Enzyme digestion time or increase the enzyme concentration; • Lower the concentration of digoxigenin-dUTP in DNA linker PCR mixture
48	Too many braided molecules	Multiple DNA molecules attached to a single magnetic bead	• Further dilute the DNA ligation or increase the concentration of magnetic beads
48	No DNA tethers on surface	Low concentration of DNA molecules	• Increase the incubation DNA-magnetic bead incubation time • Increase the DNA concentration or reduce the magnetic beads concentration. • If the problem still persists, the DNA ligation may need to be optimized.
68	High fluorescence background	Surface impurities during slide preparation or insufficient elimination of unligated SOI segment	• Prepare fresh slides • Wash the DNA–magnetic bead mixture with larger volume of blocking buffer to eliminate the unligated dye-labeled SOI segment
68	Rapid photobleaching of smFRET dyes	High laser power; Insufficient oxygen scavenging system pH is too low	• Reduce the laser intensity • Prepare a fresh gloxy solution and imaging buffer • Check pH of imaging buffer and make sure the experiment has not been incubating for longer than ~ 1 hour.

Figure 5-1

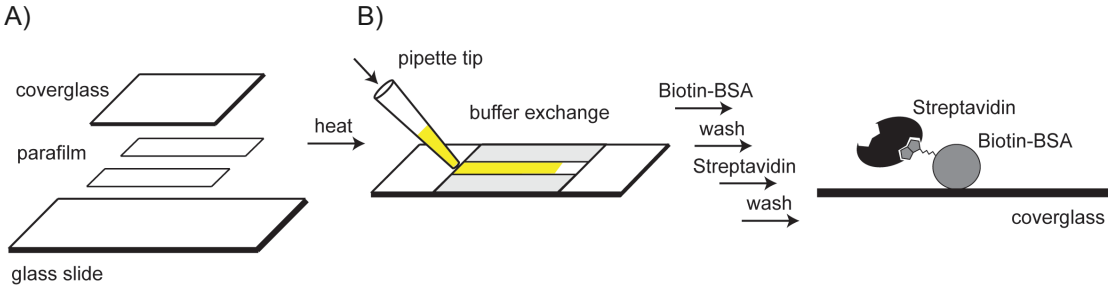

Preparation of sample chambers. (A) Sample chambers are assembled by sandwiching two strips of parafilm between a coverglass and a glass slide. To adhere the parafilm to the glass, the sample chamber is briefly heated and then allowed to cool to room temperature. (B) To prepare the cleaned and assembled sample chamber for an experiment, a series of buffer exchange steps are performed using a pipette. First a solution is of biotinylated-BSA is introduced which adheres non-specifically onto the coverglass. After washing away the unbound biotin-BSA, a solution of streptavidin is flowed over the surface. Following a final wash step to remove excess streptavidin, sample chambers are stored in a humidity chamber to prevent evaporation.

Figure 5-2

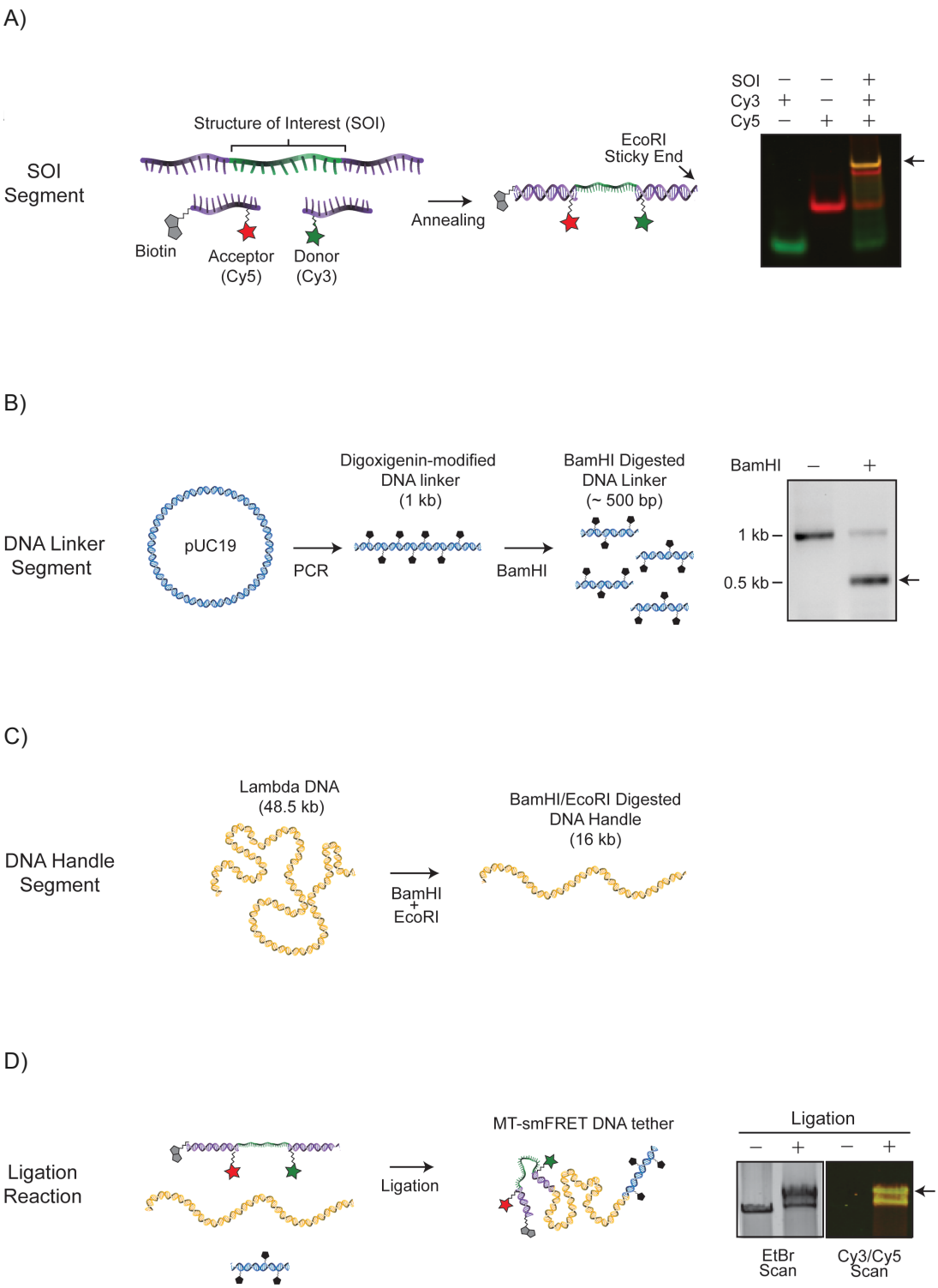
A)
SOI Segment
Structure of Interest (SOI)
Biotin
Acceptor (Cy5)
Donor (Cy3)
Annealing
EcoRI Sticky End
SOI – – +
Cy3 + – +
Cy5 – + +
B)
DNA Linker Segment
pUC19
PCR
Digoxigenin-modified DNA linker (1 kb)
BamHI
BamHI Digested DNA Linker (~ 500 bp)
BamHI – +
1 kb
0.5 kb
C)
DNA Handle Segment
Lambda DNA (48.5 kb)
BamHI + EcoRI
BamHI/EcoRI Digested DNA Handle (16 kb)
D)
Ligation Reaction
Ligation
MT-smFRET DNA tether
Ligation
– + – +
EtBr Scan
Cy3/Cy5 Scan

Preparation of DNA molecules for MT-smFRET measurement. The DNA molecule for MT-smFRET measurement is constructed from three different DNA segments. (A) The segment harboring the structure of interest (SOI), smFRET dyes, and a biotin modification is assembled via an annealing reaction by heating a mixture containing a 1:1:1 molar ratio of three different DNA oligonucleotides. (right) The efficiency of the annealing reaction is determined by run some of the sample on a native polyacrylamide gel and taking a fluorescence scan for the donor (Cy3) and acceptor (Cy5) dyes. The yellow band (small black arrow) represents the target product of the annealing reaction possessing all three oligonucleotides. (B) The DNA linker segment is prepared by PCR reaction with a pUC19 template using primers flanking the multiple cloning site in the presence of digoxigenin-11-dUTP. (right) The digoxigenin modified 1 kb PCR reaction product is digested with BamHI to obtain ~500 DNA linker segment (small black arrow) and analyzed on a DNA agarose gel. (C) The DNA handle segment is prepared by BamHI and EcoRI digestion of lambda DNA. The desired 15721 basepair segment is purified on an agarose gel. (D) To assemble the final MT-smFRET DNA molecule, a three segment DNA ligation reaction including the SOI, DNA linker, and DNA handle segments is performed. (right) Ligation efficiency is determined by comparing the ethidium bromide (EtBr) stained gel image of the ligation products with a fluorescence scan for Cy3 and Cy5. The largest band that is yellow (small black arrow) represents the target product possessing a DNA linker, DNA handle, and SOI segment.

Figure 5-3

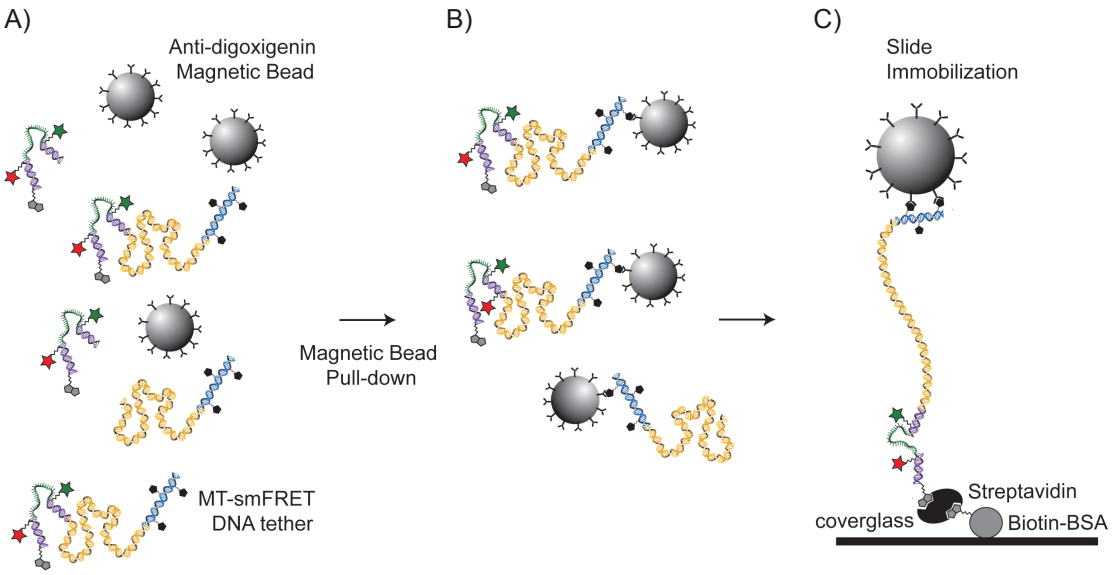

Surface immobilization of DNA molecules for MT-smFRET measurement. (A) Products of DNA ligation reactions are diluted and incubated with pre-blocked anti-digoxigenin coupled magnetic beads. (B) The DNA-magnetic bead mixture is placed on a magnetic separation rack to pull-down only those DNA tethers attach specifically to the antibody coupled magnetic beads via a digoxigenin moiety, while non-digoxigenin modified DNA is washed away at this step. (C) The washed DNA-magnetic bead mixture is introduced into a sample chamber and immobilized on the coverglass via a biotin-streptavidin linkage. The sample chamber is then gently washed with imaging buffer using gravity controlled buffer exchange to remove any unbound beads. This process greatly enriches for DNA tethers that are site-specifically oriented between the coverglass and magnetic bead.

Figure 5-4

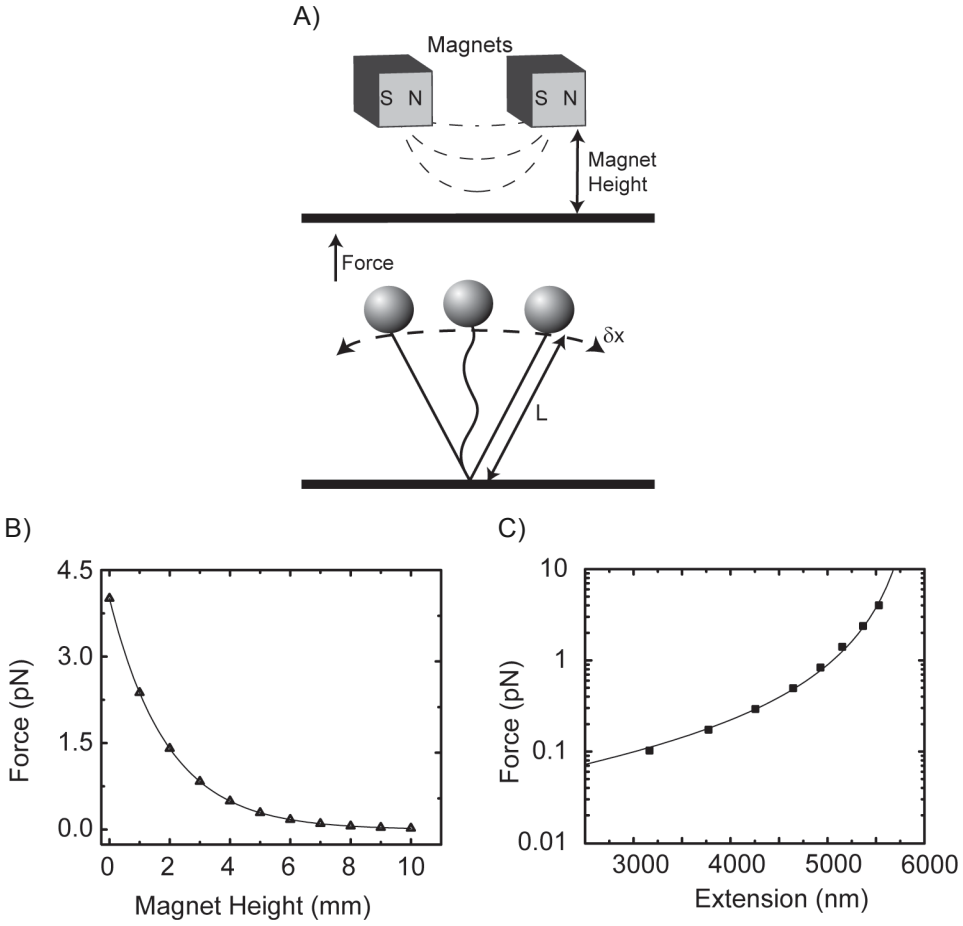

Magnetic tweezers force calibration. (A) Schematic illustration of a DNA molecule tethered between a coverglass and a magnetic beads. Forces are measured according to the expression $F = kTL/\langle dx^2 \rangle$, where F is the stretching force, k is Boltzman's constant, T is temperature, and dx is the amplitude of the bead fluctuation in the x-plane. The stretching force can be changed by varying the position of the magnet assembly held above the sample chamber. (B) Measured stretching forces in pico-Newtons (pN) as a function of magnet position in millimeters (mm) are plotted and fit by a single exponential decay function. The parameters of the exponential fit are then used to convert magnet position to force values across different experiments. (C) Experimental verification of force cablibration by fitting a force-extension plot of a DNA molecule with the worm-like chain model, yielding the expected persistence length of 45 nm for DNA under our experimental conditions.

Figure 5-5

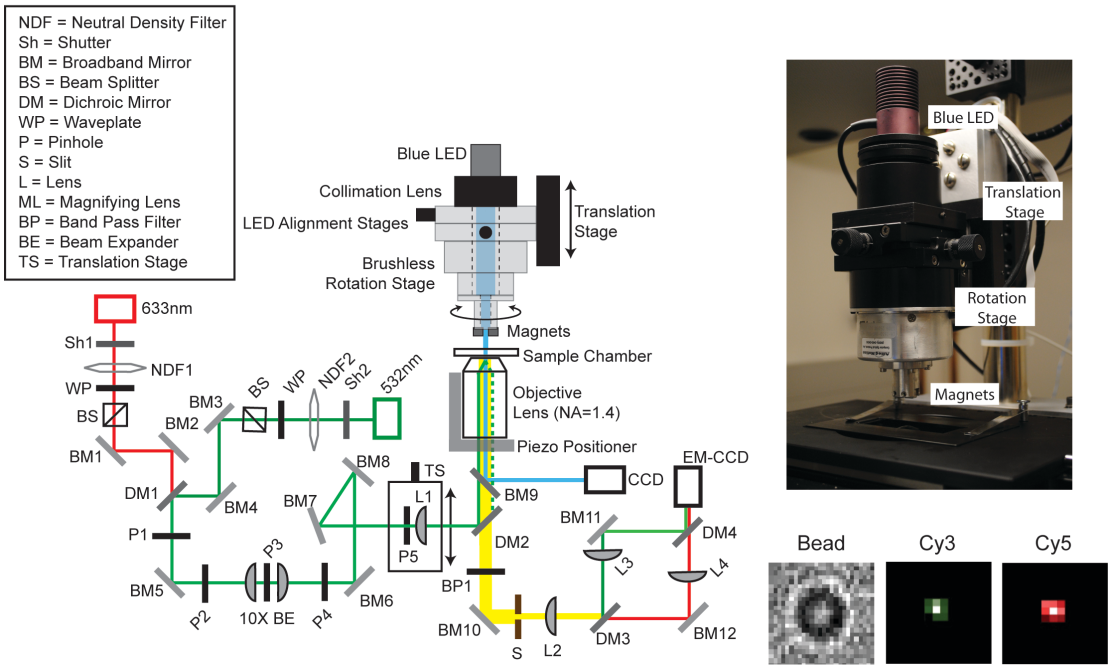

Hybrid MT-smFRET microscope setup. Schematic diagram of the MT-smFRET instrument. The MT-FRET instrument consists of a custom-built objective-type TIRF microscope, an Olympus IX71 inverted microscope, custom-built smFRET detection optics, and an EM-CCD camera. The excitation lasers are coupled through the back port of the microscope and guided to the sample through an oil-immersion objective. The custom-built magnetic tweezers apparatus, which controls the linear and angular positions of the magnets, is mounted above the sample chamber. The collimated blue LED light source is mounted directly onto the magnet assembly and is used for direct imaging of the magnetic beads (image of magnet assembly is shown on right). Detailed descriptions for all parts used in the microscope are listed in the main text. Representative images of a DNA molecule during a MT-smFRET measurement under blue LED, green laser and red laser illumination are shown.

Figure 5-6

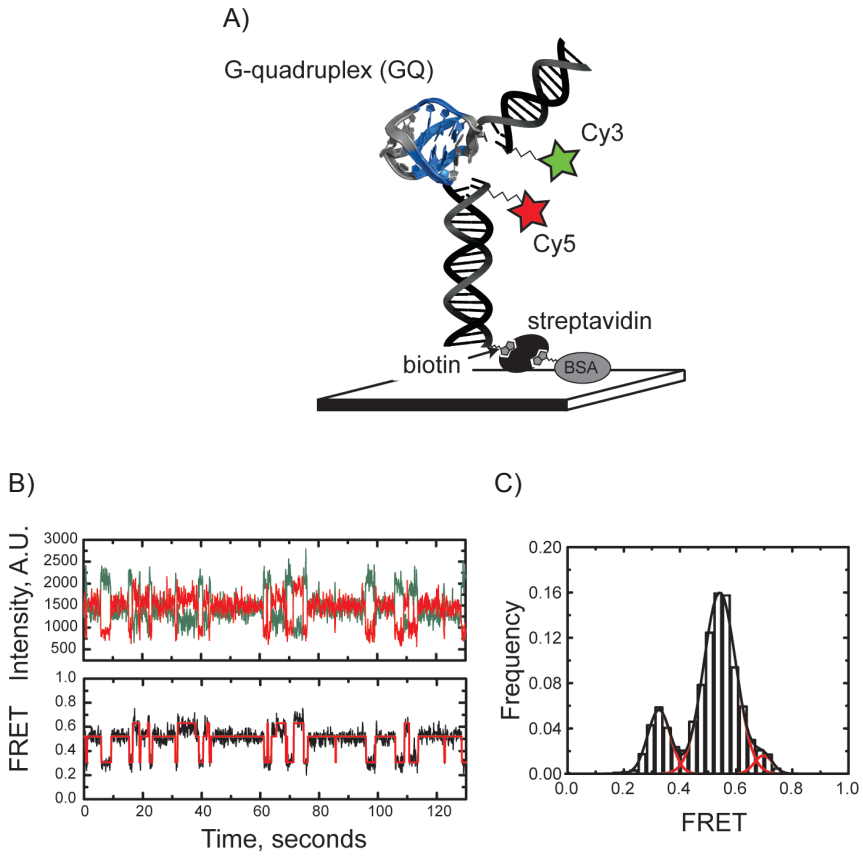

Single-molecule FRET analysis of telomere DNA GQ folding in the absence of force. (A) Schematic diagram of smFRET experimental setup. G-quartets highlighted in blue are flanked by two duplex DNA handles labeled with Cy3 and Cy5 dyes. The molecules are surface immobilized via a biotin-streptavidin linkage. (B) A representative smFRET trajectory taken in imaging buffer containing 100 mM NaCl shows individual Cy3 (green) and Cy5 (red) dye intensities (top) and calculated FRET ratio (bottom) according to the expression FRET = I_A / (I_A + I_D) where I_A and I_D are the background corrected intensities of the acceptor and donor dyes, respectively. Single-molecule FRET trajectories are fitted with a hidden Markov model yielding idealized FRET traces (magenta). (C) Single-molecule FRET histogram derived from data collected on >100 molecules is fitted with Gaussian functions centered at 0.33, 0.54 and 0.70.

Figure 5-7

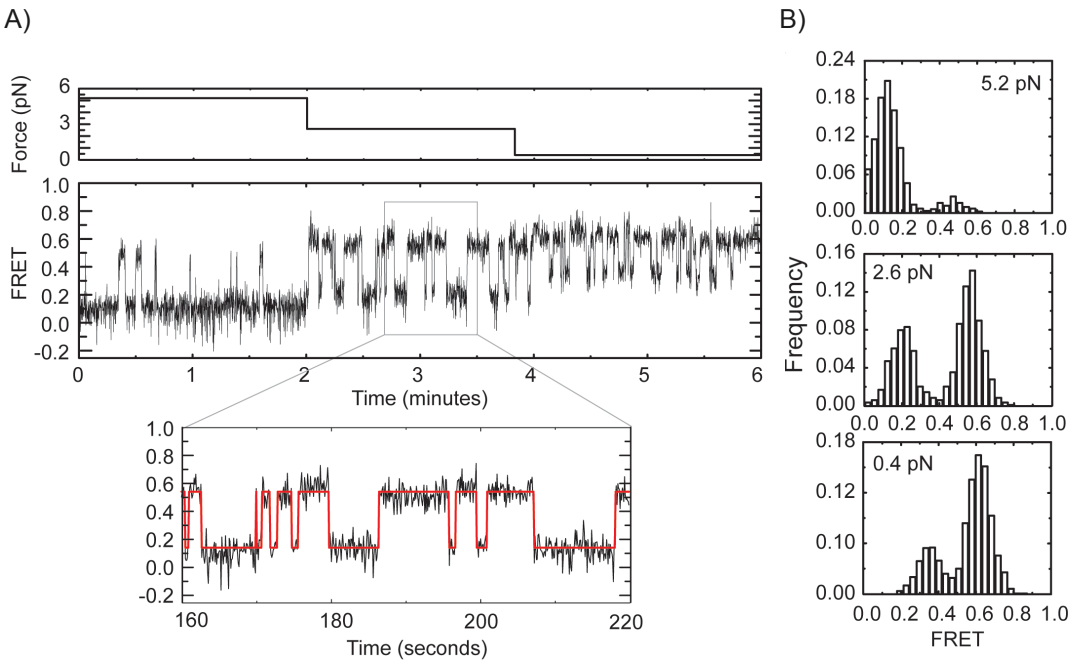

Mechanical unfolding of a human telomere DNA GQ probed using integrated MT-smFRET. (A) smFRET trajectory of a single human telomere DNA GQ held under three different stretching forces (5.2, 2.6, and 0.4 pN) taken in imaging buffer with 100 mM NaCl. (top) The force set point as a function of time. (bottom) The calculated FRET ratio for the telomere DNA GQ as a function of time. An enlarged region of the smFRET trajectory is plotted together with the idealized FRET trace (red) generated by hidden Markov modeling using HaMMy fitting software. (B) Single-molecule FRET histograms for data obtained at each stretching force demonstrate the impact of stretching force on the telomere DNA GQ folding/unfolding equilibrium.

References

1. Bustamante C, Chemla YR, Forde NR, Izhaky D (2004) Mechanical processes in biochemistry. Annu Rev Biochem 73: 705-748.

2. Dulin D, Lipfert J, Moolman MC, Dekker NH (2013) Studying genomic processes at the single-molecule level: introducing the tools and applications. Nature reviews Genetics 14: 9-22.

3. Brenner MD, Zhou R, Ha T (2011) Forcing a connection: impacts of single-molecule force spectroscopy on in vivo tension sensing. Biopolymers 95: 332-344.

4. Bustamante C, Bryant Z, Smith SB (2003) Ten years of tension: single-molecule DNA mechanics. Nature 421: 423-427.

5. Neuman KC, Nagy A (2008) Single-molecule force spectroscopy: optical tweezers, magnetic tweezers and atomic force microscopy. Nature methods 5: 491-505.

6. Bryant Z, Oberstrass FC, Basu A (2012) Recent developments in single-molecule DNA mechanics. Current opinion in structural biology 22: 304-312.

7. Woodside MT, Behnke-Parks WM, Larizadeh K, Travers K, Herschlag D, et al. (2006) Nanomechanical measurements of the sequence-dependent folding landscapes of single nucleic acid hairpins. Proceedings of the National Academy of Sciences of the United States of America 103: 6190-6195.

8. Sheinin MY, Forth S, Marko JF, Wang MD (2011) Und erwound DNA under tension: structure, elasticity, and sequence-dependent behaviors. Physical review letters 107: 108102.

9. Strick T, Allemand J, Croquette V, Bensimon D (2000) Twisting and stretching single DNA molecules. Progress in biophysics and molecular biology 74: 115-140.

10. Liphardt J, Onoa B, Smith SB, Tinoco I, Jr., Bustamante C (2001) Reversible unfolding of single RNA molecules by mechanical force. Science 292: 733-737.

11. Abbondanzieri EA, Greenleaf WJ, Shaevitz JW, Landick R, Block SM (2005) Direct observation of base-pair stepping by RNA polymerase. Nature 438: 460-465.

12. Moffitt JR, Chemla YR, Izhaky D, Bustamante C (2006) Differential detection of dual traps improves the spatial resolution of optical tweezers. Proceedings of the National Academy of Sciences of the United States of America 103: 9006-9011.

13. Carter AR, Seol Y, Perkins TT (2009) Precision surface-coupled optical-trapping assay with one-basepair resolution. Biophysical journal 96: 2926-2934.

14. Smith SB, Finzi L, Bustamante C (1992) Direct mechanical measurements of the elasticity of single DNA molecules by using magnetic beads. Science 258: 1122-1126.

15. Strick TR, Allemand JF, Bensimon D, Bensimon A, Croquette V (1996) The elasticity of a single supercoiled DNA molecule. Science 271: 1835-1837.

16. De Vlaminck I, Dekker C (2012) Recent advances in magnetic tweezers. Annual review of biophysics 41: 453-472.

17. Lipfert J, Hao X, Dekker NH (2009) Quantitative modeling and optimization of magnetic tweezers. Biophysical journal 96: 5040-5049.

18. Hohng S, Zhou R, Nahas MK, Yu J, Schulten K, et al. (2007) Fluorescence-force spectroscopy maps two-dimensional reaction landscape of the holliday junction. Science 318: 279-283.

19. Lang MJ, Fordyce PM, Block SM (2003) Combined optical trapping and single-molecule fluorescence. Journal of biology 2: 6.

20. Hards A, Zhou C, Seitz M, Brauchle C, Zumbusch A (2005) Simultaneous AFM manipulation and fluorescence imaging of single DNA strands. Chemphyschem : a European journal of chemical physics and physical chemistry 6: 534-540.

21. Lee M, Kim SH, Hong SC (2010) Minute negative superhelicity is sufficient to induce the B-Z transition in the presence of low tension. Proceedings of the National Academy of Sciences of the United States of America 107: 4985-4990.

22. Shroff H, Reinhard BM, Siu M, Agarwal H, Spakowitz A, et al. (2005) Biocompatible force sensor with optical readout and dimensions of 6 nm3. Nano letters 5: 1509-1514.

23. Tarsa PB, Brau RR, Barch M, Ferrer JM, Freyzon Y, et al. (2007) Detecting force-induced molecular transitions with fluorescence resonant energy transfer. Angewandte Chemie 46: 1999-2001.

24. Zhou R, Ha T (2012) Single-molecule analysis of SSB dynamics on single-stranded DNA. Methods in molecular biology 922: 85-100.

25. Zhou R, Schlierf M, Ha T (2010) Force-fluorescence spectroscopy at the single-molecule level. Methods in enzymology 475: 405-426.

26. Comstock MJ, Ha T, Chemla YR (2011) Ultrahigh-resolution optical trap with single-fluorophore sensitivity. Nature methods 8: 335-340.

27. Axelrod D, Burghardt TP, Thompson NL (1984) Total internal reflection fluorescence. Annu Rev Biophys Bioeng 13: 247-268.

28. Long X, Parks JW, Bagshaw CR, Stone MD (2013) Mechanical unfolding of human telomere G-quadruplex DNA probed by integrated fluorescence and magnetic tweezers spectroscopy. Nucleic acids research 41: 2746-2755.

29. Bustamante C, Marko JF, Siggia ED, Smith S (1994) Entropic elasticity of lambda-phage DNA. Science 265: 1599-1600.

30. Bouchiat C, Wang MD, Allemand J, Strick T, Block SM, et al. (1999) Estimating the persistence length of a worm-like chain molecule from force-extension measurements. Biophysical journal 76: 409-413.

31. McKinney SA, Joo C, Ha T (2006) Analysis of single-molecule FRET trajectories using hidden Markov modeling. Biophys J 91: 1941-1951.

32. Akiyama BM, Stone MD (2009) Assembly of complex RNAs by splinted ligation. Methods Enzymol 469: 27-46.

CHAPTER 6

Guide for using magnetic tweezers to manipulate single DNA molecule

Summary

In the past decades, the magnetic tweezers (MT) technique has emerged as a powerful method to probe the mechanical properties of nucleic acids and other biological systems. The basic design of this apparatus consists of a standard objective-type total internal reflection (TIRF) microscope, a pair of magnets located just above the sample chamber and a collimated LED light. In these experiments, we manipulate a molecule of interest, which is tethered in between a magnetic bead and a glass surface by changing the linear position and the angular displacement of the magnets. The DNA extension is used to monitor the response of the molecule of interest under stretching forces and torques. A protocol for using MT to manipulate a single DNA molecule is described in this chapter.

Materials and Setup

Reagents

- 10 x Phosphate-buffered saline (PBS; Mediatech, cat. no. 46-013-CM)
- NE Buffer 2.1 (New England Biolabs, cat. no. B7202S)
- Acetone (Fisher Scientific, cat. no. A929SK-4)
- Agarose (Thermo Scientific, cat. no. 17852)
- Alconox (VWR International, cat. no. 21835-032)
- Anti-digoxigenin (Roche, cat. no. 11333089001)
- KpnI (New England Biolabs, cat. no.R0142)
- Bovine serum albumin (BSA; New England Biolabs, cat. no. B9001S)
- Dynabeads MyOne Streptavidin magnetic bead (Invitrogen, cat.no. 650.01)
- DNA ligase (New England Biolabs, cat. no. M0202S)
- Digoxigenin-11-dUTP (Roche, cat. no. 11558706910)
- Biotin-11-dUTP (Roche, cat. no. 11093070910)
- XbaI (New England Biolabs, cat. no. R0145)
- Molecule of interest

- Nitrogen gas (Praxair Gas)
- QIAquick PCR Purification Kit (Qiagen, cat. no. 28106)
- Potassium chloride (KCl; Fisher Scientific, cat. no. P330)
- Taq DNA polymerase with standard Taq buffer (New England Biolabs, cat. no. M0273S)
- Tris-HCl (Fisher Scientific, cat. no. BP153)
- dNTP (New England Biolabs, cat. no. N0446S)
- pUC19 (New England Biolabs, cat. no. N3041S)
- pUC 19 primer I (5' ACATTTCCCCGAAAAGTGCCA 3'; Integrated DNA Technologies)
- pUC 19 primer II (5' GTTTCGCCACCTCTGACTTGA 3'; Integrated DNA Technologies)
- Nuclease-free H_2O (Ambion, cat. no. AM9932)

Equipment

- Glass staining jar (Wheaton, cat. no. 900570)
- Microscope glass slides (3"x1", 0.96-1.06mm thick; Corning, cat. no. 2947)
- Ultrasonic cleaner (Branson)
- Imaging glass slides (22x50mm, 0.16-0.19mm thick; Ted Pella, cat. no. 260150)
- Microcentrifuge tubes (Costar, cat. no. 3620)
- Milli-Q H_2O (Millipore)
- PCR Thermal Cycler (Bio-Rad)
- Sterile disposable syringe (BD, cat. no. 309659)
- Double-sided tape (Scotch)
- Needle (BD, 18G, ref. no. 305195)
- Epoxy (Devcon)
- Polyethylene Tubing (Becton Dickinson, I.D. 0.86mm, O.D. 1.52mm)

- Diamond drill bits (Starlite, no. 115010)
- TIRF microscope
- Magnetic tweezers

Equipment and Reagent Setup

- TIRF microscope and MT setup is described in Chapter IV
- 1x PBS is prepared by diluting 10x PBS with ddH_2O.
- T50 Buffer T50 buffer is prepared by mixing 10 mM Tris-HCl (pH 8.0) and 50 mM NaCl or by duliting a 1:1 molar ratio of 2x T50 and ddH_2O.
- 2x T50 Buffer is prepared by mixing 20 mM Tris-HCl (pH 8.0) and 100 mM NaCl.
- Blocking buffer is prepared by mixing 5 mg/mL of BSA and T50 buffer.
- Imaging buffer: Imaging buffer includes 10 mM Tris-HCl (pH 7.4), 150 mM KCl and 0.2% BSA

Software

A detailed description of software is described in Joseph Parks' Ph.D thesis

- **LabView Software for operating MT**

  Andor_887_beta.vi: controls the CCD camera

  BeadPanelTracker.vi: tracks the bead image (Determine the X,Y and Z position of the bead)

  BeadPanelTracker-Math.vi Front Panel: outputs the data to dax file

  Beadposition.vi Front Panel: reports real-time image analysis

  MotionControl.vi: controls linear and rotational position of the magnets, and the position of piezo stepper

- **LabView Software for Calibration of stretching force offline**

  LoadVedio128.vi: loads the offline movie

  BeadPanelTracker.vi: tracks the bead image (Determine the X, Y and Z position of the bead)

BeadPanelTracker-Math.vi Front Panel: outputs the data to dax file

- **MatLab program for Force Extension**

  readmtFileAndCrop.m: reads the dax file; selects the region of data for analysis

  getextensionsandforces1_manual.m: determines the forces; calculates the average DNA extensions at various forces

  fitWLC_weighted.m: fits the data with WLC model

- **MatLab program for Rotation Extension**

  ReadMTFile5.m: reads the dax file

  ScatterBellPlot1.m: plots the rotation extension curves

Procedure

Preparation of DNA molecules for MT measurement

1. Prepare the molecule of interest segment by setting up the 50 µL reaction in a microcentrifuge tube as described in Table 6-1
2. Incubate the reaction at 37°C for 2 h
3. Separate the digested products from enzyme with the QIAquick PCR purification kit
4. Prepare the Digoxigenin or Biotin modified DNA linkers (the protocol is described in Chapter IV).
5. Digest the digoxigenin-modified DNA linker with KpnI; Digest the biotin-modified DNA linker with XbaI (the protocol is described in Chapter IV)
6. Separate the digested products from enzyme with the QIAquick PCR purification kit.
7. Construct the final MT molecule by setting up the DNA ligation reaction in a final volume of 20 µL as described in Table 6-2 incubating overnight at 16°C. Store molecules in ligation reaction mixture at 4°C.
8. Heat inactivate the DNA ligase before measurement

Construction of flow cell (Figure 6-1)

9. Drill two 0.8mm diameter holes 40mm apart in the microscope glass slide

10. Sonicate the microscope glass slide in a glass staining jar for 20 min in 10% w/v Alconox, 20 min in Milli-Q H_2O, 20 min in acetone and 20 min in 1M KOH.
11. Rinse the microscope glass slide with excess Milli-Q H_2O.
12. Take out the microscope glass slide from the glass staining jar
13. Dry the cleaned microscope glass slide with nitrogen gas
14. Attach a tube to one of the holes on the microscope glass slide and seal it with epoxy
15. Cut the tip of 1000uL pipette tip, attach it to the other holes on the microscope glass slide and seal it with epoxy
16. Wait 30 minutes for epoxy to dry
17. Assemble a flow cell chamber by sandwiching two strips of double sided tape between an imaging glass slide and the microscope glass slide
18. Use a 20μL pipette tip to press the imaging glass slide onto the microscope glass slide to ensure proper adherence
19. Seal the flow cell with epoxy and wait a minimum of 30 min for epoxy to dry

Preparation of antibody covered surface

20. Pipette 50μL of anti-digoxigenin to the flow cell and incubate overnight at room temperature
21. Wash the chamber with 200μL of 1xPBS buffer

Fixation of reference beads

22. Incubate 100μL of polystyrene beads for 10-15 min
23. Wash the chambers with 200μL of 1xPBS buffer
24. Add 100μL of blocking buffer to the chamber and incubate for 1 hour

Preparation of blocked magnetic beads

25. Add 2μL of MyOne magnetic beads to 398μL of blocking buffer
26. Place the mixture on a rocker and allow it to tumble for at least 1 hour at 4°C

Surface Immobilization of the DNA molecule for MT measurement

27. Dilute the DNA ligation with blocking buffer

28. Add 100μL of diluted DNA ligation to the sample chamber
29. Incubate for 30-40 min at room temperature
30. Wash the sample chamber with 200μL of blocking buffer
31. Add 100μL of blocked magnetic beads to the sample chamber
32. Incubate for 40-60 min at room temperature
33. Wash the chamber with 500 μL of blocking buffer with minimum flow rate to remove the unattached magnetic beads. To control the flow of the blocking buffer, set the clamp to allow minimum flow rate
34. Flow 300 μL of imaging buffer to the sample chamber

Identification of single torsionally constrained DNA molecule

35. Place a drop of index-matched low fluorescence immersion oil (Type DF) on the microscope objective, then place the flow cell on the microscope
36. Open all MT control software
37. Define the highest magnet position as “HOME”
38. Lower the magnet to 20.5mm away from “HOME”
39. Re-define current magnet position as “HOME”
40. Move the magnet upward by 4mm
41. Through the eyepiece of the microscope, search for the magnetic beads that have Brownian fluctuations and have smaller ring patterns than the polystyrene beads
42. Rotate the magnets to positive 50 turns (counter-clockwise) to check if the bead is anchored by a torsionally constrained DNA molecule. The extension of a DNA tether that is torsionally constrained should decrease as turns are introduced.
43. Rotate the magnets to negative 50 turns (clockwise)
44. Apply a high force to the molecule by lowering the linear position of magnet. This step ensures the bead is anchored by a single torsionally constrained DNA molecule. The extension of a single DNA tether is expected to increase due to the removal of the plectonemes by high stretching force (F>1pN).

Calibration of Z-position

45. Rotate the magnets to positive 50 turns and lower the force by moving the magnet away from the sample chamber
46. Place the curses (red curse for the magnetic bead; yellow curse for the reference bead) on the center of the reference bead and the magnetic bead
47. Set the calibration range and the step increment for the piezo stepper to generate a stack of calibration images for the bead (also known as a look-up-table). The change of the concentric ring pattern surrounding the bead center depends on the relative distance between the bead and the focal plane. During the experiment, the current bead image is compared to the look-up-table to determine the length of molecule (Z-position).

Calibration of stretching force

48. Set the frame rate of CCD camera to 500Hz
49. Record movies while stepping through various magnet positions
50. Use LabView Software to determine the X and Y fluctuations of the magnetic bead at each magnet positions by analyzing the recorded movies
51. Calculate the stretching force for each magnet position based on following expression, where K_BT is the thermal energy, L is the contour length of the DNA molecule and X is the position of the magnetic bead.

$$Force = \frac{K_B T \times L}{\langle X^2 \rangle}$$

Measurement of force extension

52. Record the change of the Z-position as a function of force by changing the linear position of magnet
53. Fit the data with the Worm Like Chain (WLC) model, where K_BT is the thermal energy, L is the contour length of the DNA molecule, Z is the measured DNA extension and P is the persistence length of the DNA molecule.

$$Force = \frac{K_B \times T}{P}\left[\frac{1}{4}\left(1 - \frac{Z}{L}\right)^{-2} - \frac{1}{4} + \frac{Z}{L}\right]$$

49. Determine the contour length and the persistence length of molecule of interest

Measurement of rotation extension

54. Record the change of Z-position as a function of rotation by changing the angular displacement of the magnet at various stretching forces
55. Plot the Z-position as a function of turns

Anticipated Results

Stretching DNA

Under physiological salt conditions, a torsionally relaxed DNA molecule behaves like an ideal polymer chain at stretching forces between 0.02 pN and 2 pN. This phenomenon can be described by the WLC model. Fitting this model to the force extension curves allows us to extract the persistence length and the contour length of the DNA molecule. We expect the persistence length of the double stranded DNA molecule to be ~40-50nm (Figure 6-2). Extracting the persistence length from the WLC model also allows us to precisely check whether the tether between the magnetic bead and surface is a single tether. If two DNA molecules are attached between the magnetic bead and glass surface, we expect the persistence length to be half that of a single tether.

Twisting DNA

Under physiological salt conditions, at a low stretching force (Force<1pN), the DNA extension relates to rotation linearly (Figure 6-3). The symmetrical rotation extension curve demonstrates that the torsional stress applied to the molecule is being converted to plectonemes during both negative and positive supercoiling. However, at a high stretching force (Force>1pN), plectoneme formation in the negative supercoiling regime is forbidden. Instead, the torsional stress is transferred to denature the DNA molecule. Therefore, the DNA extension remains constant while the DNA is negatively supercoiled at a high force. In

contrast, plectonemes continue to form during positive supercoiling at a high force, which decreases the DNA extension.

Table 6-1

Preparation of the molecule of interest segment

	Volume (μL)
Lambda DNA (0.5 μg/μl)	10
10X NEBuffer 2.1	5
KpnI (100,000 U/mL)	2.5
XbaI (100,000 U/mL)	2.5
Milli-Q H_2O	30

Table 6-2

Construction of the MT DNA molecule

	Volume (μL)
Molecule of interest segment (0.3 μM)	3.5
Digoxigenin-modified DNA linker (2.4 μM)	1.5
Biotin-modified DNA linker (2.4 μM)	1.5
10x T4 DNA ligase buffer	2
ATP (10 mM)	2
T4 DNA ligase (5,000 U/mL)	2
Milli-Q H2O	7.5

Figure 6-1

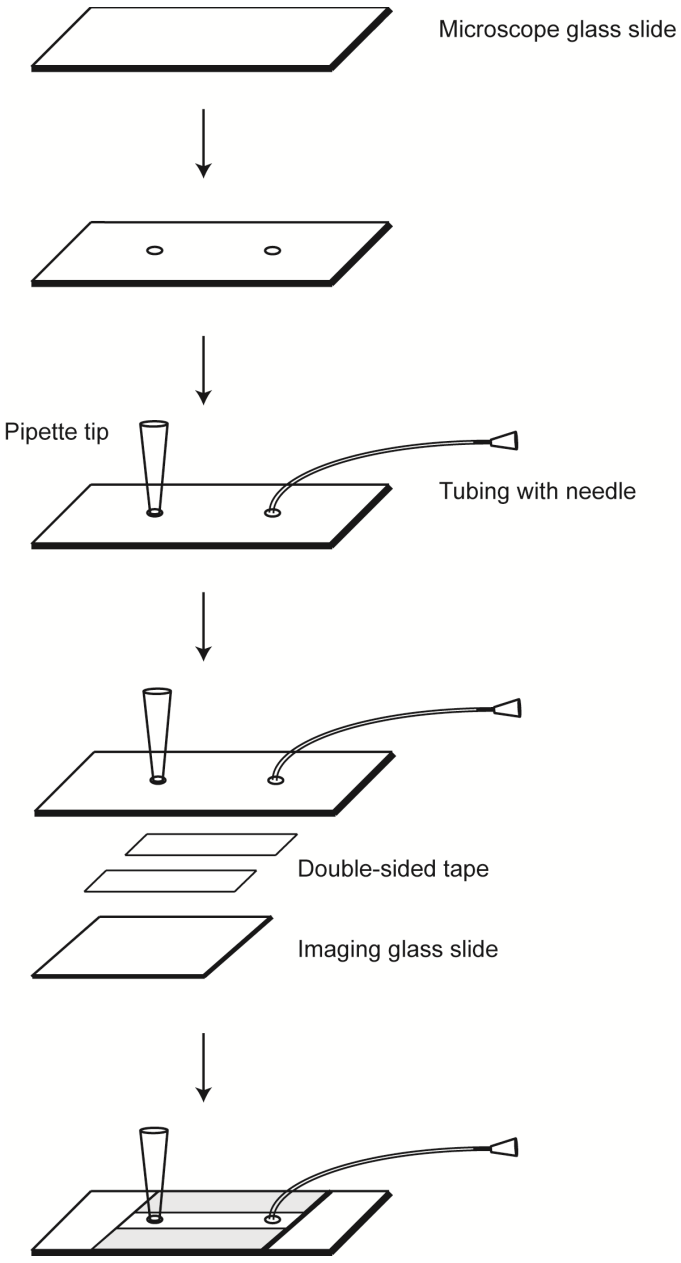
Microscope glass slide
Pipette tip
Tubing with needle
Double-sided tape
Imaging glass slide

Figure 6-2

Force vs. extension for a dsDNA with WLC model

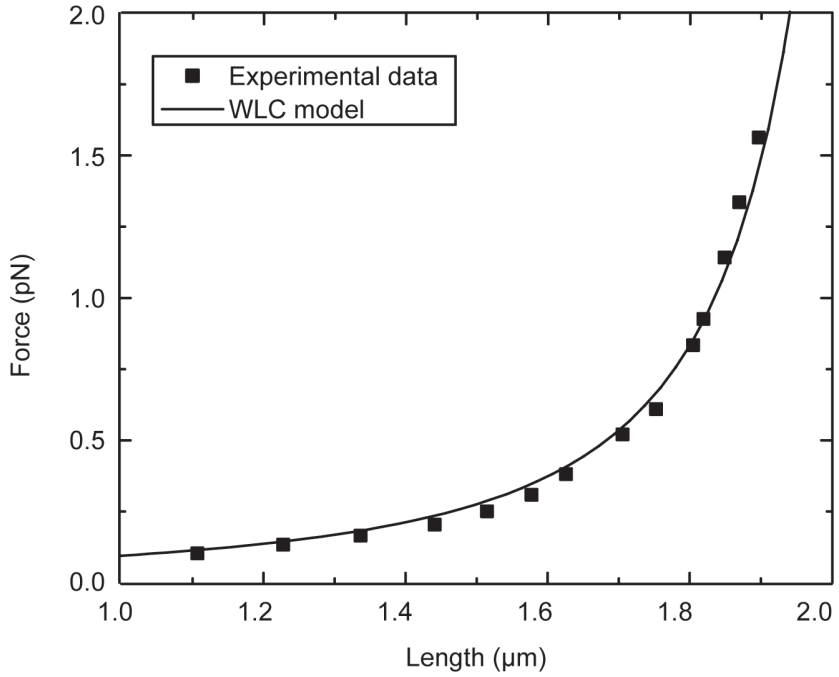

Force vs. extension plot for a single DNA molecule. The fitting with the WLC model yields persistence length=45nm and contour length=2.1μm for this molecule.

Figure 6-3

Rotation vs. extension for a dsDNA at various stretching forces. Negative rotations represent negative supercoiling, and positive rotations represent positive supercoiling.

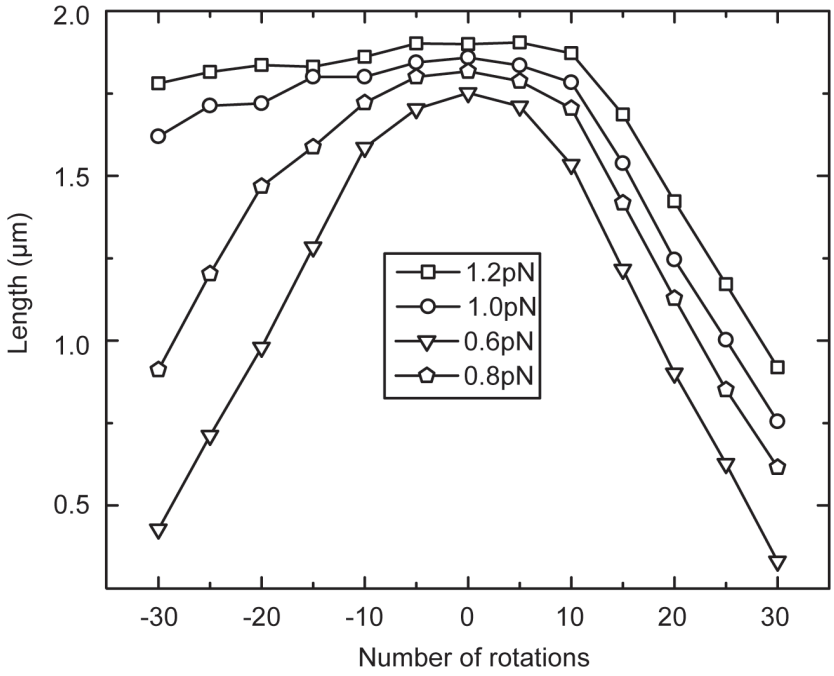

Chapter 7

Supporting Information

Figures

Figure S1-1

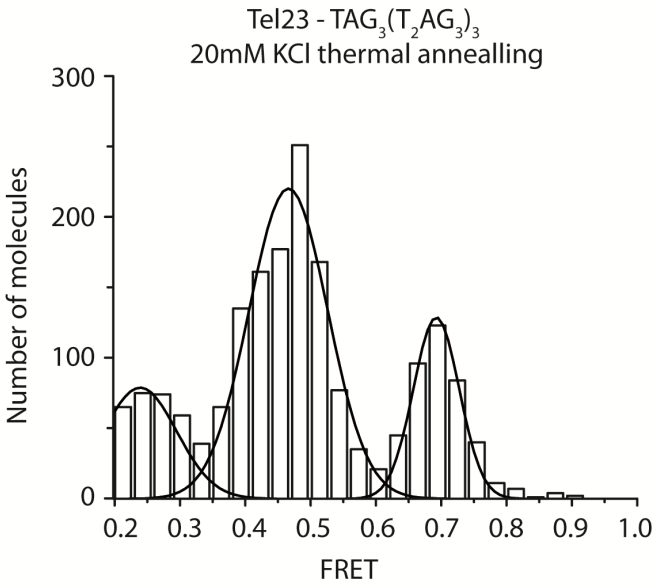

Gaussian fitting of smFRET distribution of Tel23 molecules thermally annealed and imaged in 20 mM KCl fit with three Gaussian functions centered at FRET = 0.25 (unfolded population), FRET=0.49 and FRET = 0.72 . The fit was performed using nonlinear least-squares curve fitting in Origin. Indicated R^2 values are adjusted for the number of free parameters used in the fit.

Figure S1-2

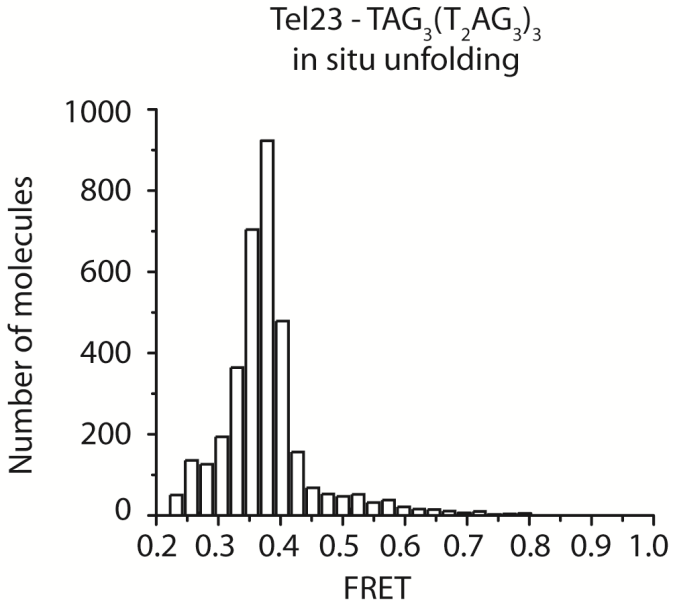

In situ unfolding of thermally annealed Tel23 molecules. Surface immobilized Tel 23 molecules that were thermally annealed and imaged in buffer T0 (10 mM Tris pH8, no salt). The unfolding treatment resulted in smFRET distributions that were centered at a value of FRET = 0.23, indicative of the unfolded state as described previously[1].

Figure S1-3

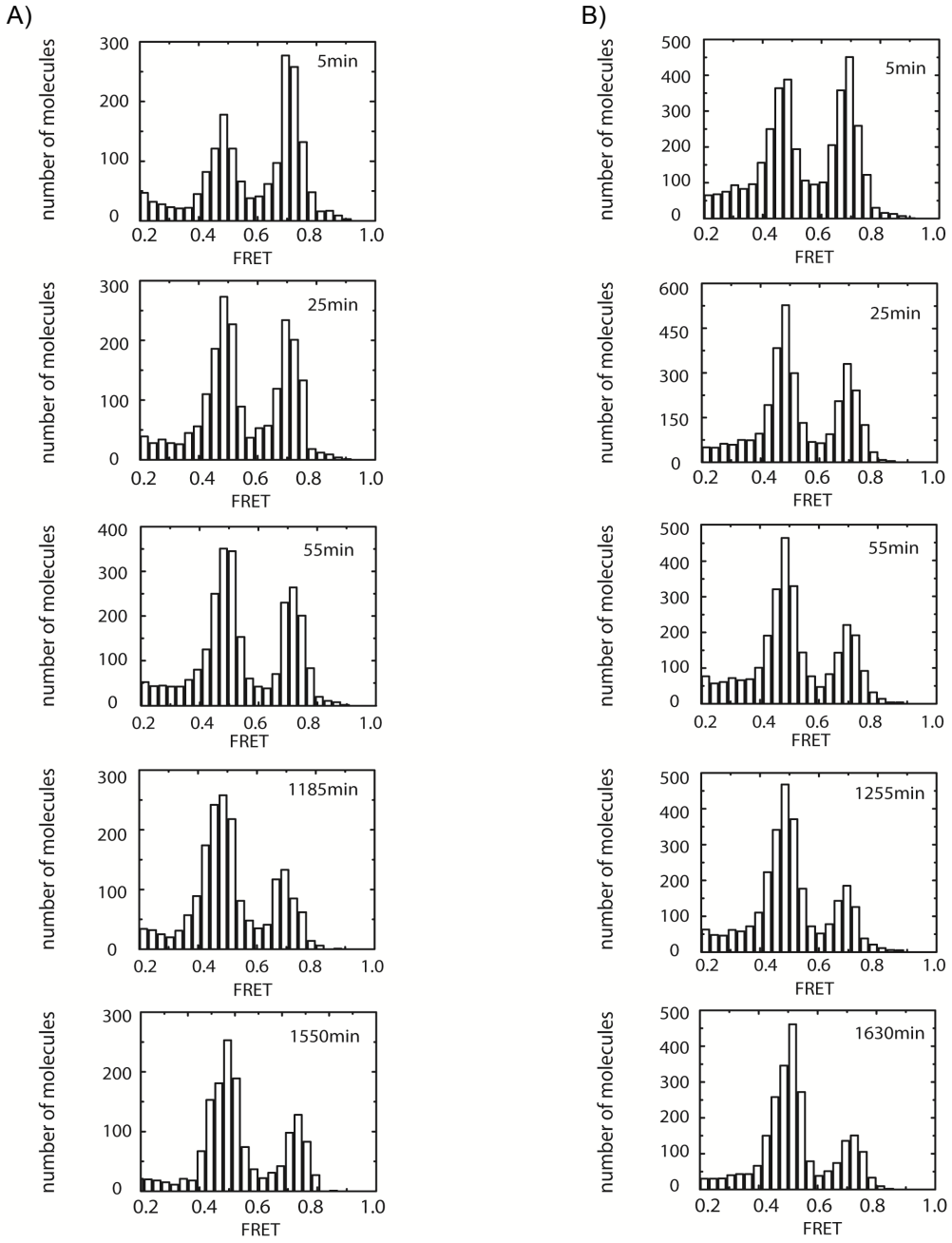

(A) Single-molecule FRET histograms of Tel23 *in situ* refolded in 60mM KCl for the indicated period of time. (B) Single-molecule FRET histograms of Tel23 *in situ* refolded in 20mM KCl for the indicated period of time.

Figure S1-4

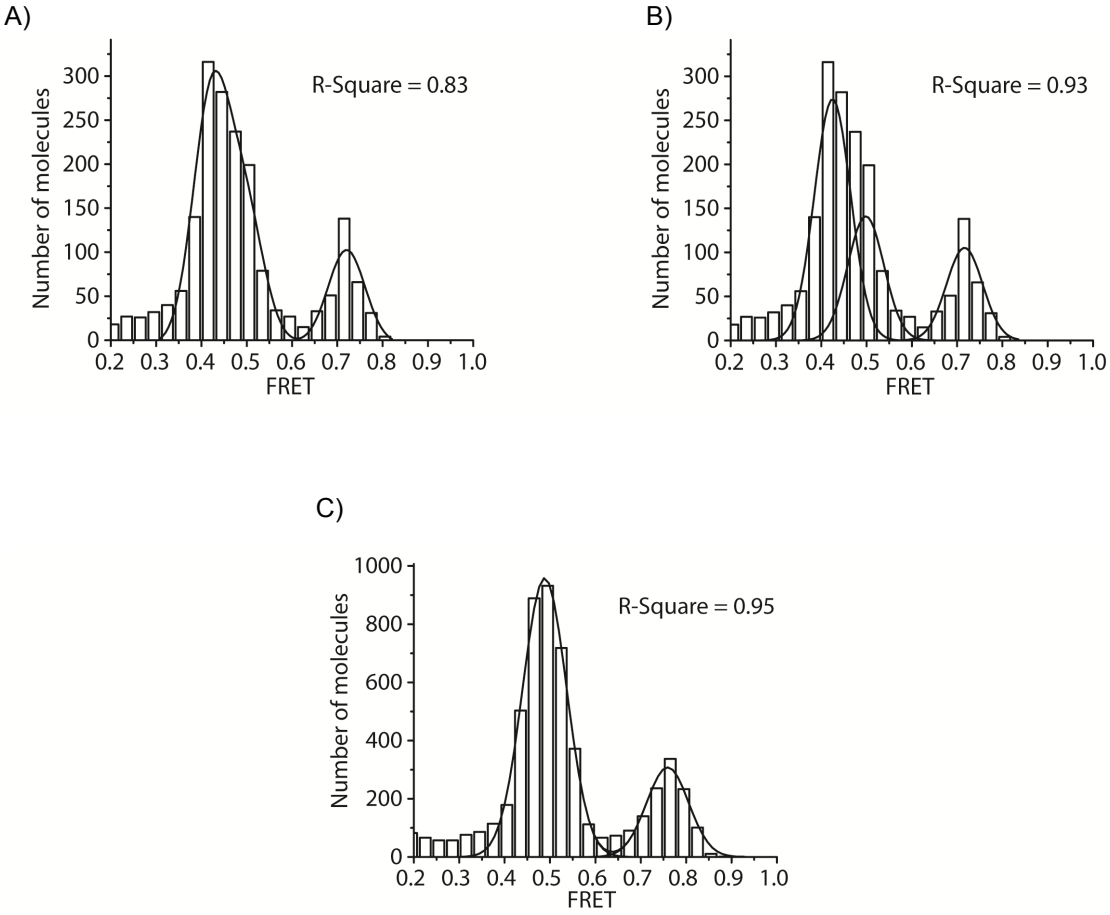

Gaussian fitting of smFRET distributions (A) Tel23 molecules thermally annealed and imaged in 100 mM KCl fit with two Gaussian functions centered at FRET=0.44 and FRET=0.72. (B) Tel23 molecules thermally annealed and imaged in 100 mM KCl fit with three Gaussian functions centered at FRET=0.42, FRET=0.50, and FRET=0.72. The addition of a third FRET population substantially improved the fitting results as indicated by the adjusted R^2 value. (C) In contrast, measurements of Tel22 molecules, lacking the 5' thymine, were well fit with only two FRET populations. This result highlights the effect of the 5' thymine in promoting the folding of the hybrid structure as has been previously reported by NMR analysis[2].

Figure S1-5

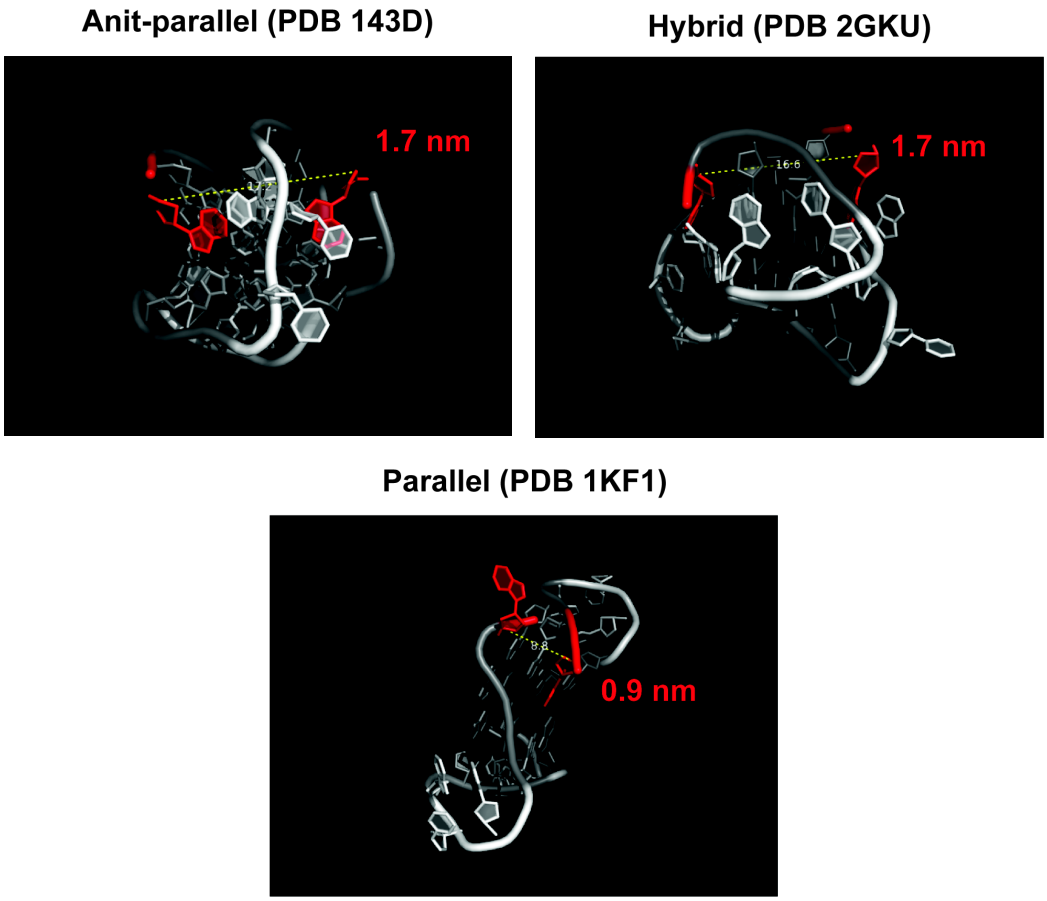

Atomic resolution structures of the parallel [3], anti-parallel [4], and a hybrid form [2] telomere DNA GQ conformation. Measurements between the terminal deoxyribose moieties are indicated in red. Although a these measurements cannot be quantitatively compared with our smFRET results, they nevertheless are in good qualitative agreement with the assignements of the high-FRET state to the parallel conformation and the mid-FRET states to a mixture of the anti-parallel and hybrid conformations.

Figure S2-1

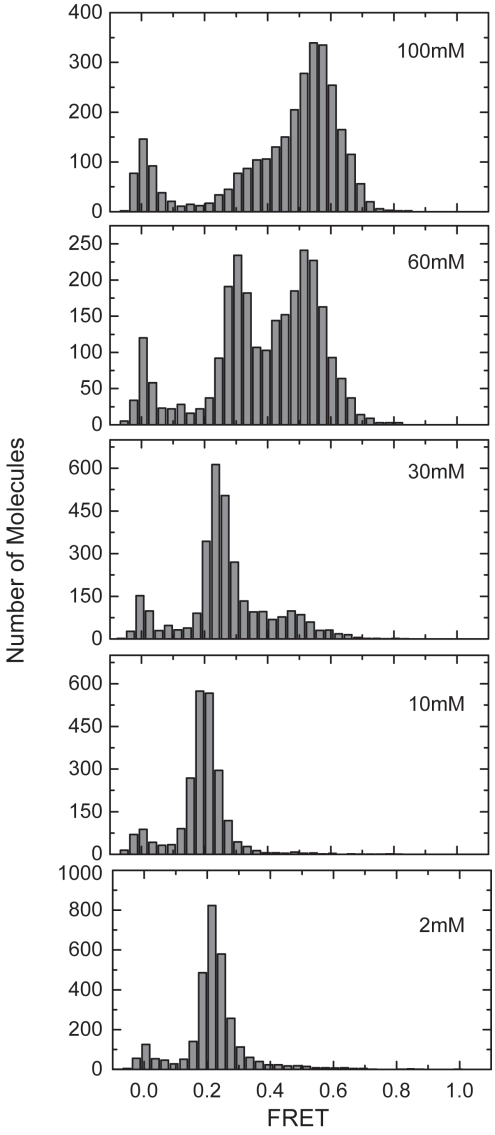

Single molecule FRET distributions for Tel24 molecules in the absence of force as a function of NaCl concentration. Increasing NaCl concentrations stabilizes the fraction of molecules in the folded FRET = 0.54 state. At low ionic strength Tel24 is unfolded as indicated by the FRET ~ 0.25 population. Histograms were compiled by averaging the FRET value for each molecule over a two second period (20 frames at 100 msec integration time). The peak centered on FRET = 0.0 corresponds to molecules that posses an inactive Cy5 dye.

Figure S2-2

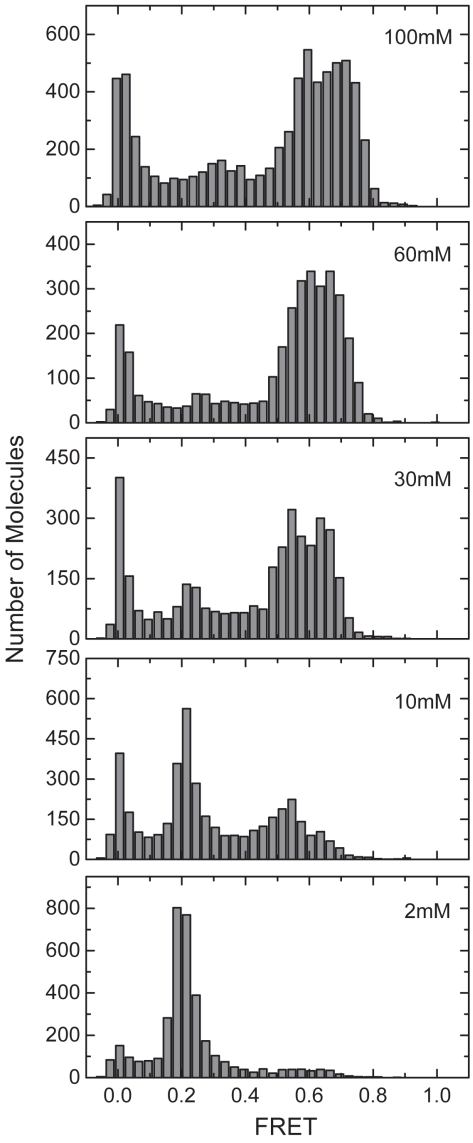

Single molecule FRET distributions for Tel24 molecules in the absence of force as a function of KCl concentration. Increasing KCl concentrations stabilizes the fraction of molecules in one of the higher FRET folded conformations. At low ionic strength Tel24 is unfolded as indicated by the FRET ~0.2 population. Histograms were compiled by averaging the FRET value for each molecule over a two second period (20 frames at 100 msec integration time). The peak centered on FRET = 0.0 corresponds to molecules that posses an inactive Cy5 dye.

Figure S2-3

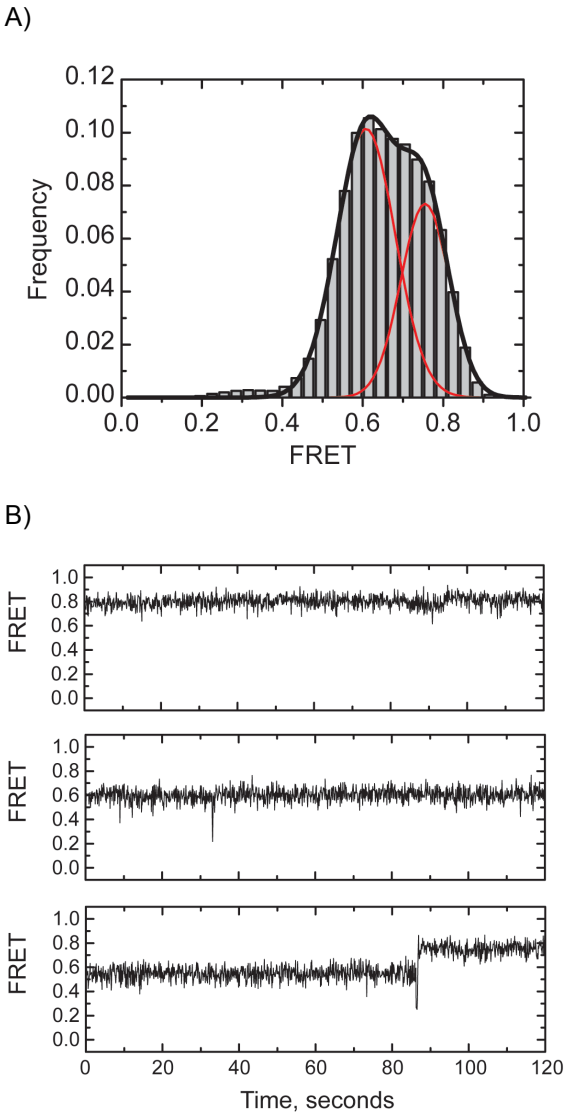

Increased complexity of Tel24 folding in the presence of 100 mM KCl. (A) Single molecule FRET histogram comprised from data taken on >100 molecules. Histogram was fit with two guassian functions centered at FRET = 0.61 and FRET= 0.76. (B) Representative smFRET trajectories demonstrating stable high FRET (top), mid FRET (middle), and occasional interconversion between the two FRET states (bottom).

Figure S2-4

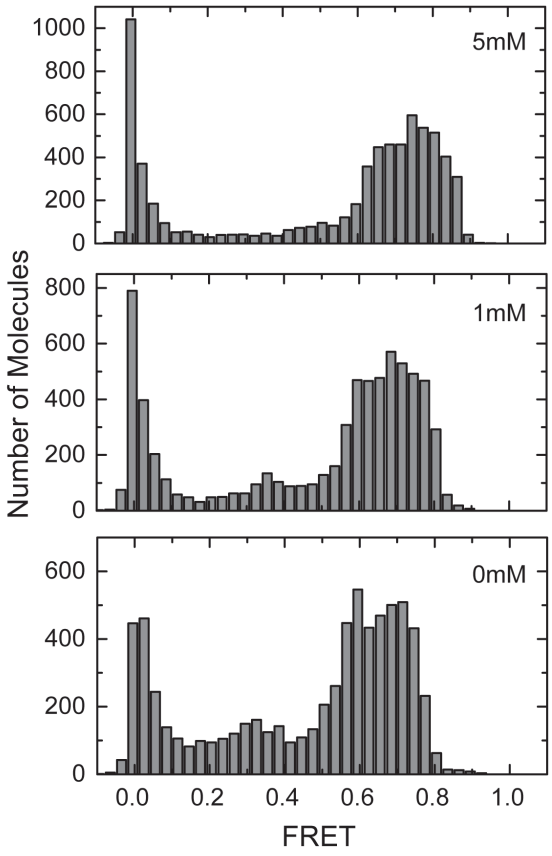

The effect of Mg^{2+} on the smFRET distributions of Tel24 in the presence of 100 mM KCl. To determine whether adding Mg^{2+} to the KCl folding buffer had any measurable impact on the FRET conformations observed in our assay, smFRET distributions were constructed for molecules folded in the presence of 100 mM KCl and the indicated amount of $MgCl_2$. The presence of physiological levels of Mg^{2+} appeared to have a slightly stabilizing effect on the Tel24 GQ fold, with fewer molecules occupying the unfolded low FRET state. However, the general behaviour of the Tel24 molecules was not substantially altered by the presence of Mg^{2+} in the reaction buffer.

Figure S2-5

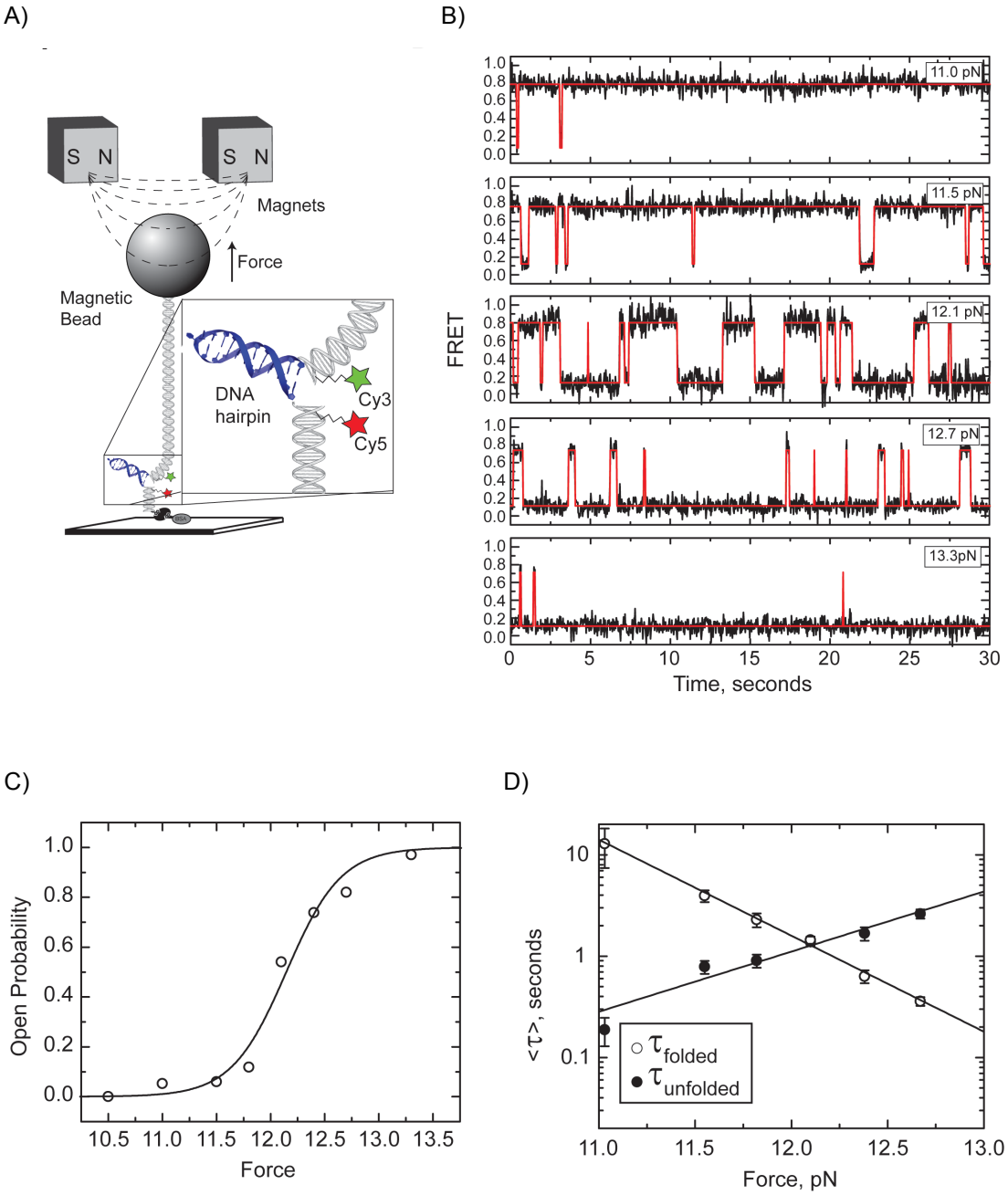

Integrated fluorescence and magnetic tweezers analysis of a model DNA hairpin (A) Schematic diagram of the experimental setup for measurements, which is similar to the setup described in the main text for Figure 2-2A. (B) Representative smFRET trajectories of a

single DNA hairpin molecule held under five different forces. The red line represents the model produced by fitting the smFRET trajectory to a Hidden Markov model. (C) Probability of unfolded state as a function of force fit with the two-state Boltzmann relation, $P_0(F)=\{1+\exp[((F_{1/2} - F)\bullet\Delta x)/k_BT]\}^{-1}$, yielding $F_{1/2}$ = 12.1pN and Δx = 16.2 nm. (D) Average lifetimes of the folded (high FRET) and unfolded (low FRET) states are plotted as a function of force. Plots are fit with exponential functions described in the main text, yielding $\Delta x^{\ddagger}_{unfolded}$ = 6.1 nm and $\Delta x^{\ddagger}_{folded}$ = 8.9 nm.

Figure S2-6

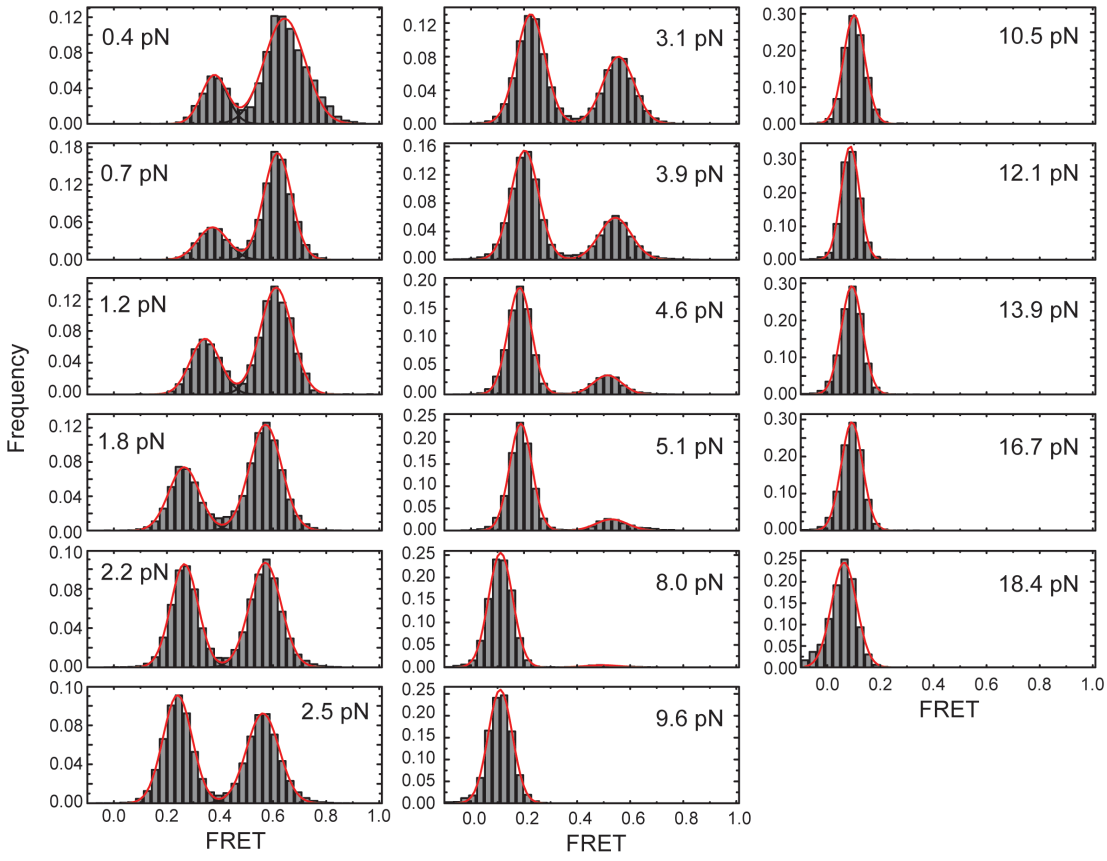

Complete data set for all Tel24 molecules analyzed in study. A total of 75 different molecules were analyzed. At each force, a minimum of five different molecules were studied. Each smFRET trajectory was fit with a Hidden Markov model using the HaMMy software, yielding an idealized FRET trace. Data corresponding to the rare transitions to the high FRET ~0.7 FRET state were removed prior to compiling the smFRET histograms, and each histogram was fit with either one or two Gaussian functions using the Origin software package.

Figure S2-7

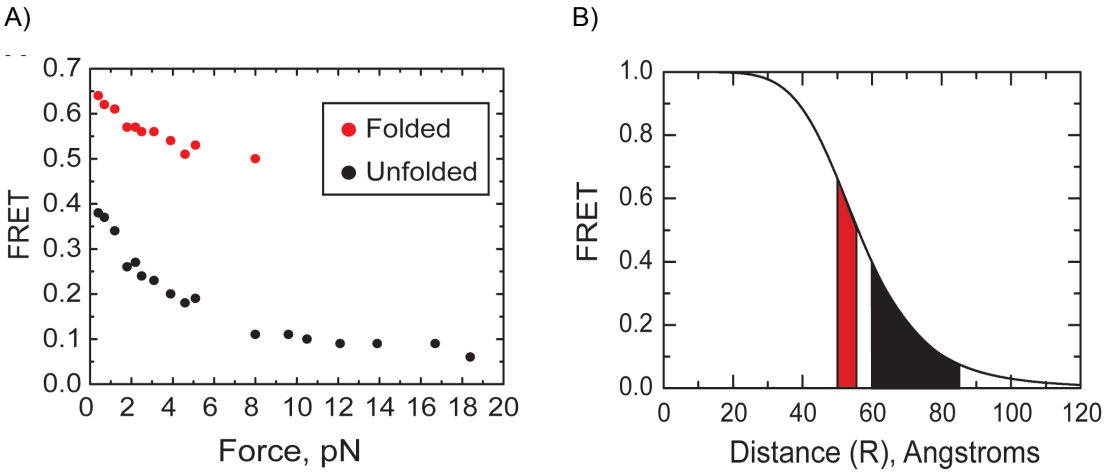

Analysis of the change in FRET observed for the mid FRET (folded, red) and low FRET (unfolded, black) states as a function of force. (A) Plot of the average FRET value derived from fits shown in Supplementary Figure 6 as a function of force. (B) Plot of the FRET response curve described by the equation, FRET = $1/[1+(R/R_o)^6]$, where R is the distance between the FRET dyes and R_o is estimated to be 56 angstroms. Note, since we have not determined the exact value of R_o under our specific experimental conditions, this plot is not intended to be interpreted as a precise conversion of our measured FRET values to absolute distances. Rather, we provide the plot to illustrate an estimate of the relative distance change that would correspond to the ΔFRET measured for the folded (red) and unfolded (black) states as a function of applied stretching force.

Figure S3-1

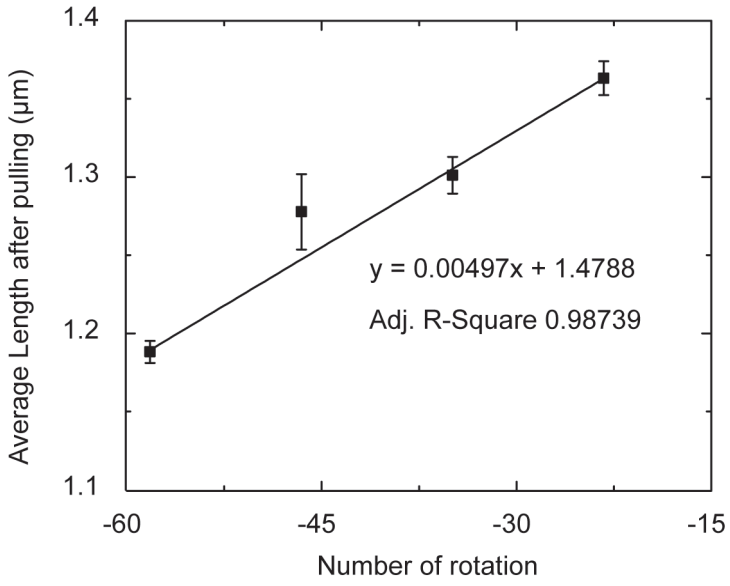

Linear regression fitting of average DNA extension after pulling as a function of number of rotation

Figure S3-2

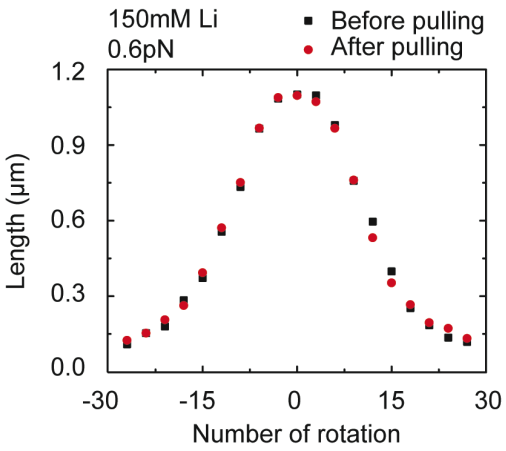

Rotation extension of telomere DNA before and after stretching in 150mM Li^+ buffers at 0.6pN

References

1. Jena PV, Shirude PS, Okumus B, Laxmi-Reddy K, Godde F, et al. (2009) G-quadruplex DNA bound by a synthetic ligand is highly dynamic. J Am Chem Soc 131: 12522-12523.

2. Luu KN, Phan AT, Kuryavyi V, Lacroix L, Patel DJ (2006) Structure of the human telomere in K+ solution: an intramolecular (3 + 1) G-quadruplex scaffold. J Am Chem Soc 128: 9963-9970.

3. Parkinson GN, Lee MPH, Neidle S (2002) Crystal structure of parallel quadruplexes from human telomeric DNA. Nature 417: 876-880.

4. Wang Y, Patel DJ (1993) Solution structure of the human telomeric repeat d[AG3(T2AG3)3] G-tetraplex. Structure 1: 263-282.